# Nanostructure, Self-Assembly and Friction in Confined Liquids


**Alexander M. Smith**

**Magdalen College**

**Physical & Theoretical Chemistry Laboratory**

**University of Oxford**

**Supervisor: Susan Perkin**

**Thesis submitted for the degree of**

***Doctor of Philosophy***

# CONTENTS

# ABSTRACT

The work presented in this thesis uses a custom-built surface force balance with extreme sensitivity and resolution to understand at the molecular level how the structure of confined liquid films relates to their frictional and lubricating properties. The experiments involve shearing two identical and atomically smooth mica surfaces past one another with sub-nanometer control of the film thickness and ultrasensitive force resolution. With this, molecular mechanistic details relevant to boundary lubrication are uncovered for several systems.

Friction modifiers are commonly used in engine oil formulations and adsorb as monolayers to surfaces, preventing surface contact and reducing friction between the surfaces. Here it is shown that the shape of additive surfactant molecules affects both the confined film structure and the lubricating behavior, with more upright monolayers exhibiting lower friction. Interestingly, mixing different surfactant molecules can give rise to friction much higher than for either molecule. This result is significant given that lubricant formulations typically contain many different types of additive molecules with different functions.

Measurements made with ionic liquids of varying alkyl chain length reveal a dramatic cross-over in the interfacial layering structure, from alternating cation- and anion-enriched monolayers for ionic liquids with short alkyl chains, to bilayer formation for more amphiphilic ions. Their structural and dynamic properties in confinement are pertinent to applications ranging from electrolytes in nanoporous electrodes to specialist lubricants in extreme environments. The ionic liquids show clear evidence for ‘quantized friction’, where multiple friction-load regimes with different friction coefficients are measured for different numbers of confined ion layers for the same ionic liquid. Most significantly, the results of these experiments allow elucidation of shear mechanisms and sliding interfaces for monolayer and bilayer-forming ionic liquids which differ markedly to those of molecular liquids.

# DECLARATION

This thesis is submitted for the degree of Doctor of Philosophy in Physical and Theoretical Chemistry at the University of Oxford. I confirm that the work presented here is my own. Where information has been derived from other sources, I confirm that this has been indicated in the thesis.

# ACKNOWLEDGEMENTS

I would above all like to thank my supervisor Susan Perkin for her continued support and encouragement and for providing expert guidance on this challenging experimental technique when I first joined the group. The advice, guidance and scientific freedom she gave me have contributed greatly to my development as a scientist over the last few years.

Thanks are also due to past and present members of the group, particularly to Kevin Lovelock for passing on his extensive knowledge and enthusiasm for ionic liquids, as well as taking the time to show me how to use Igor Pro. I would also like to thank Peter Dowding and Ken Lewtas at Infineum UK Ltd for all of their ideas, helpful discussions and insight into the lubricant additive industry.

I must also thank several people who in some way made my work easier. Dan Mitchell, Men Shuang, Andy Dolan, Tom Welton and Peter Licence provided most of the high purity ionic liquids used in these experiments, many of which are not available commercially. I am grateful to Michael Parkes for his help with image processing and analysis using LabVIEW software. Also a big thanks must go to lab services and the electronics and mechanical workshops who have been extremely helpful with solving equipment problems.

Funding for this studentship is gratefully received from EPSRC and Infineum UK Ltd.

*“If you want to have good ideas you must have many ideas.*

*Most of them will be wrong, and what you have to learn is which ones to throw away.”*

***Linus Pauling***

# PUBLICATIONS

The following published journal articles and manuscripts in preparation relate to the work conducted in this thesis:

Chapter 5.2
S. Perkin, L. Crowhurst, H. Niedermeyer, T. Welton, A.M. Smith, N.N. Gosvami, 'Self-assembly in the electrical double layer of ionic liquids'. ***Chemical Communications 2011***, ***47***, 6572-6574.

Chapter 5.2
A.M. Smith, K.R.J. Lovelock, N.N. Gosvami, P. Licence, A. Dolan, T. Welton, S. Perkin, 'Monolayer to bilayer structural transition in confined pyrrolidinium-based ionic liquids'. ***The Journal of Physical Chemistry Letters 2013***, *4*, 378-382.

Chapters 5.3, 5.4 & 6.2
A.M. Smith, K.R.J. Lovelock, S. Perkin, 'Monolayer and bilayer structures in ionic liquids and their mixtures confined to nano-films'. ***Faraday Discussions 2013***, *167*, 279-292.

Chapter 7.2
A.M. Smith, K.R.J. Lovelock, N.N. Gosvami, T. Welton, S. Perkin, 'Quantized friction across ionic liquid thin films'. ***Physical Chemistry Chemical Physics 2013***, *15*, 15317-15320.

Chapter 7.3
A.M. Smith, M.A. Parkes, S. Perkin, 'Molecular friction mechanisms across nanofilms of a bilayer-forming ionic liquid'. ***The Journal of Physical Chemistry Letters 2014***, *5*, 4032-4037.

Chapter 6.3
A.M. Smith, S. Perkin, 'Influence of lithium solutes on double layer structure of ionic liquids'. ***The Journal of Physical Chemistry Letters 2015***, *6*, 4857-4861.

Chapter 4
A.M. Smith, P.J. Dowding, K. Lewtas, S. Perkin, 'Molecular resolution studies of structure and lubrication for glycerol oleate-based organic friction modifiers in a base oil'. ***In preparation***.

Chapter 4.2
A.M. Smith, S. Perkin, 'Stick-slip friction across nano-confined dodecane films: shear melting, wall slip or interlayer slip?'. ***In preparation***.

Chapter 6.4
A.M. Smith, A.A. Lee, M.A. Parkes, S. Perkin, 'On the molecular ordering of supercapacitor electrolytes in slit pore geometry'. ***In preparation***.

# 1 INTRODUCTION

## 1.1 Surface Forces

### 1.1.1 Background

The study and direct measurement of forces at the solid-liquid interface is essential for providing insights into molecular mechanisms of many significant processes. These include everyday phenomena around us, ranging from the behaviour of biological systems to industrial processes, such as oil recovery techniques and ceramic processing. It is also beneficial to investigate the properties of surfaces and interfaces in relative motion, addressing the fundamentals of friction, lubrication and wear.

The development of a variety of experimental techniques enabling force measurements with extremely high resolution has led to a greater understanding of the typical range, magnitude and types of force that exist between surfaces. Particularly, the development of the surface force apparatus by Tabor, Winterton and Israelachvili[1,2] made possible the measurement of electrostatic and van der Waals forces between surfaces. In the early 1970s Israelachvili had extended the apparatus to operate with liquids between the surfaces, allowing determination of structural forces of confined liquid films. Since then, various modifications to the technique have been introduced which have allowed investigations into frictional and tribological properties of ultrathin liquid films.

### 1.1.2 DLVO Theory: van der Waals and Double Layer Forces acting together

DLVO theory, named after its originators Derjaguin and Landau[3] and Verwey and Overbeek[4], describes the force between two charged surfaces interacting across a liquid medium. DLVO theory states that the force between two particles (such as colloidal particles) or surfaces is made up of the combined effect of van der Waals attraction and repulsive electrostatic (or double-layer) forces. These repulsive double-layer forces often arise due to dissociation of surface ions, leaving a charged surface. Figure 1 shows a schematic plot of classical DLVO interaction energy against surface separation for two flat surfaces.

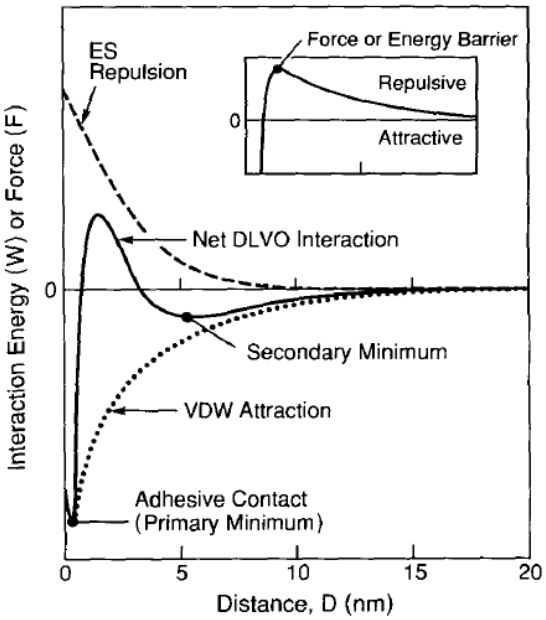


**Figure 1**

DLVO interaction energy as a function of surface separation between two surfaces in an electrolyte solution[5]

The van der Waals attractive potential has an inverse power law dependence on distance, while the double-layer repulsive force is roughly exponential in its distance

dependence. As a result the van der Waals attraction always dominates the double-layer repulsion at close enough separations, resulting in a force that is attractive at molecular contact and giving rise to adhesion. At larger separations, the medium may be considered as a continuum, and is well characterised by macroscopic quantities such as its refractive index, dielectric constant and density. In this case continuum theory gives a good description of the forces acting between the surfaces; Lifshitz theory for the attractive van der Waals force[6,7] and the Poisson-Boltzmann equation for the repulsive double-layer force[7-8] if present.

### 1.1.3 Structural Forces

Upon approach of the surfaces to very small separations on the order of nanometres, continuum models break down, and the observed force law differs from that predicted by continuum theories. The liquid can no longer be considered simply as a structure-less continuum, and must instead be treated as a collection of finite-sized molecules with packing constraints and possible directional interactions. Ordering of molecules can lead to a range of interactions not predicted by mean-field approaches, now frequently referred to as ‘structural’ or ‘solvation’ forces. These can provide very useful insights into structural behaviour of liquids confined between solids at a molecular level.

These structural forces generally oscillate between repulsion and attraction with thickness of the confined film, with a periodicity related to the dimensions of the molecules[9-10]. The oscillatory nature of the force law is related to the density distribution function; layers of molecules are energetically favoured and correspond to the free energy minima, whereas any distances which correspond to non-integral numbers of layers are energetically unfavourable and correspond to the energy maxima[11-12]. These oscillatory forces are general for liquid molecules sufficiently symmetric in shape confined between rigid, smooth surfaces.

### 1.1.4 Hydration Forces

While measurements of the force between mica surfaces across dilute electrolyte solutions generally agree excellently with DLVO theory[3-4], for more concentrated electrolyte solutions (specific to each electrolyte) there is an additional strongly repulsive force at very small surface separations, typically <4 nm[13-14].

For small or multivalent ions in highly polar solvents, ion-dipole interactions cause the solvent molecules to orient around the ions. When water molecules are involved, they are called hydrated ions, and the typical number of water molecules around an ion represents its hydration number. This first primary 'shell' of water molecules immediately around such a strongly solvated ion is the most structured and restricted in terms of position and orientation, whereas water molecules in subsequent shells are less tightly bound. When the hydration shells of ions or surfaces overlap, short range repulsive forces arise, known as hydration forces, arising from the energy required to de-hydrate the ions. Above a critical hydration concentration, this energy can be sufficient to prevent attraction of the surfaces or particles into adhesive contact from van der Waals forces[13-15].

Early force measurements between mica surfaces across aqueous electrolyte solutions by Pashley[14] attributed the strong measured monotonic repulsion to be due to adsorption of hydrated ions to the mica surfaces. The repulsive force corresponds to the work done to transfer water molecules from hydrated ions into the bulk liquid, with considerable energy required to de-hydrate the cations bound to the surface. Subsequent careful measurements found the force to in fact be oscillatory for separations <1.5 nm[16-17] which was attributed to water layering. However more recent high resolution measurements have shown that the oscillatory forces measured for aqueous salt solutions can in fact have periodicities closer to hydrated-ion layering[18-19].

### 1.1.5 Hydrophobic Forces

Hydrophobic forces may be interpreted as nanoscale manifestations of the hydrophobic effect, where hydrophobic solutes such as hydrocarbons and fluorocarbons tend to aggregate in aqueous solutions in order to minimise contact with water. An example of this is oil and water forming two distinct macroscopic phases even after thorough mixing. If amphiphiles – which contain both hydrophilic and hydrophobic parts in the same molecule – are added to water they can form microscopic stable structures to segregate the non-polar parts of the molecules away from water. Such self-assembled aggregates of different shapes can include micelles, vesicles and bilayers, in which the hydrophilic parts of the molecules are exposed to water[7, 20]. Hydrophobicity manifests differently depending on whether small molecules or large clusters are involved[21]; the self-assembly process is driven by the difference between the entropically-dominated solvation free energy for small hydrophobic molecules and the enthalpically-dominated solvation free energy of an extended hydrophobic surface.

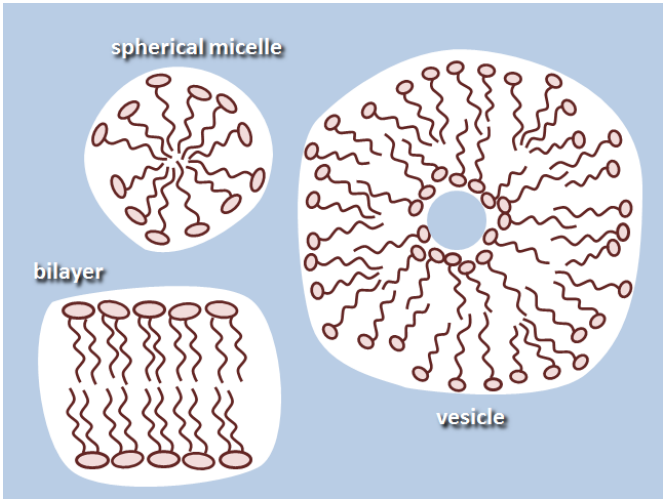


**Figure 2**

Examples of possible self-assembled structures of amphiphiles in aqueous media

If two extended surfaces are hydrophobic, they can experience an attraction much greater than that expected simply from van der Waals forces. Force measurements attempting to measure the range and magnitude of this hydrophobic force vary hugely and seem to depend on the particular hydrophobic surface used and its measurement method[22-23]. Surfaces rendered hydrophobic by deposition of a surfactant monolayer can show a long range exponential attraction, although this could be explained by instability of the surface under water with patches of monolayer overturning to form bilayer regions, exposing the hydrophilic moieties and even areas of bare mica. Such heterogeneous surfaces could experience attraction due to the interaction asymmetry between equally and oppositely charged surfaces[24]. Other complications can arise due to surface nanobubbles present which are surprisingly stable, difficult to detect, and also cause long-range attractive forces obscuring any real hydrophobic force[25-27].

The most stable hydrophobic surfaces show only a short range attraction, although even after several decades of measurements a clear understanding is still lacking. It is however clear that any true and intrinsic hydrophobic force should be very short range given that it must be determined by the orientation of water molecules closest to the surface, with the loss of water's hydrogen bonding network at a non-polar surface resulting in attraction between the surfaces at small separations. Indeed, very short-ranged attractive forces have recently been measured between pure, inert, hydrophobic oil droplets (a few microlitres) across water prior to coalescence[28].

## 1.2 Techniques For Measuring Surface Forces

### 1.2.1 Surface Force Apparatus/Balance (SFA/SFB)

Since its invention in the 1970s, the Surface Force Apparatus (SFA) has been used to directly measure forces between molecularly smooth surfaces as a function of

separation across air and in liquid media with high resolution. The work conducted in this thesis was carried out using a version of the apparatus – the Surface Force Balance (SFB) - modified by Jacob Klein to enable measurement of lateral forces between the surfaces with ultra-sensitive resolution[29]. Since the results shown in the present work are exclusively surface force measurements, the technique is described separately with much greater detail in Chapter 3.

### 1.2.2 Atomic Force Microscopy (AFM)

The atomic force microscope (AFM) was developed by Binnig, Quate and Gerber[30] in 1986, shortly after the first scanning tunnelling microscope (STM)[31] experiments. These powerful microscopes use atomically sharp tips to resolve features on surfaces at the atomic scale. In particular, the use of AFM allows imaging of insulating surfaces and of soft matter, whereas STM must operate with a conductive surface.

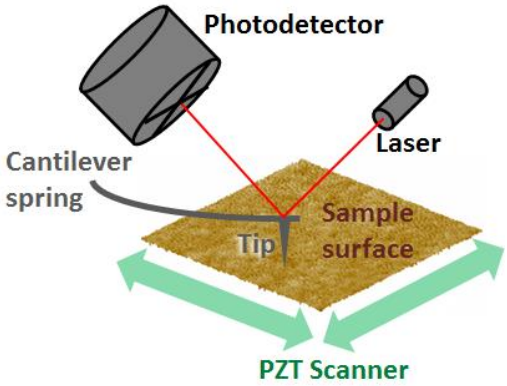


**Figure 3**
Schematic showing the basic principles of an AFM

The AFM setup consists of a tip made of Si or $Si_3N_4$ mounted on the end of flexible cantilever. A laser is reflected off the back of the cantilever and detected using a quadrant photodetector, and any deflection of the cantilever due to forces between the tip and sample is measured with Ångstrom resolution. Gluing a colloidal particle to a tip-less cantilever also allows measurement of colloidal forces between a colloidal

probe and a surface in sphere-plane geometry. Measurements can be made in air or under a liquid environment. Contamination is often less under liquid, and capillary forces are eliminated which allows better imaging of soft materials.

The AFM can be used in contact mode, where the cantilever is 'dragged' along the surface and its deflection is used to determine topography directly. More commonly, a feedback loop is used to keep the cantilever at a fixed height above the surface. In non-contact modes, the amplitude or frequency of an oscillating cantilever is used as a feedback mechanism and the tip does not contact the sample surface. Intermittent contact – known as tapping mode – can also be used.

### 1.2.3 Computer Simulations

Measurement of surface forces provides direct experimental evidence on the behaviour of liquids confined to thin films, but there are limitations regarding lengthscales, timescales and specific surface chemistries. Theoretical approaches can provide additional molecular insights.

Numerous studies based on molecular dynamics simulations[32-35], density functional theory[36-37] and theoretical methods[38-39] were used to study the interfacial liquid density profile for Lennard-Jones fluids, showing an oscillatory nature due to liquid structure at the solid interface. Later investigations focussed on the effect of molecular shape[40] and surface roughness[41-42] on the structure of the molecular films. Real liquid molecules are often non-spherical and interact via anisotropic orientation-dependent potentials both with each other and with the surfaces. As a result the oscillations can in some situations be 'softer' and more sinusoidal.

## 1.3 Single Asperity Contact Mechanics

### 1.3.1 Derjaguin Approximation

The measured force law, $F(D)$, from the crossed-cylinder arrangement of surfaces in the SFA/SFB can be directly related to the interaction free energy per unit area, W(D), between two flat surfaces through the Derjaguin Approximation[7]:

$$F(D)_{\text{curved}} = 2\pi R W(D)_{\text{planar}}$$

In this equation, $R$ is the radius of curvature for the crossed cylinders. This approximation is valid for any type of force (attractive, repulsive or oscillatory) as long as the separation distance is much smaller than the radius of curvature. In the apparatus used, $R$ is typically ~1 cm, and the separation distance for the forces of interest is typically less than a few hundred nanometers, rendering the approximation valid. Usefully, it relates the force measured between crossed cylinders with theory for the interaction energy between parallel plates. It also provides a normalisation method allowing comparison of data from different contact spots and between different experiments using surfaces with different curvature.

### 1.3.2 Adhesion Mechanics

Surfaces are said to adhere when energy is required to separate them. The attractive forces between them may be caused by one or several types of intermolecular force. Real surfaces are however not completely rigid, and can deform elastically under the influence of an external load or due to an attractive adhesive force.

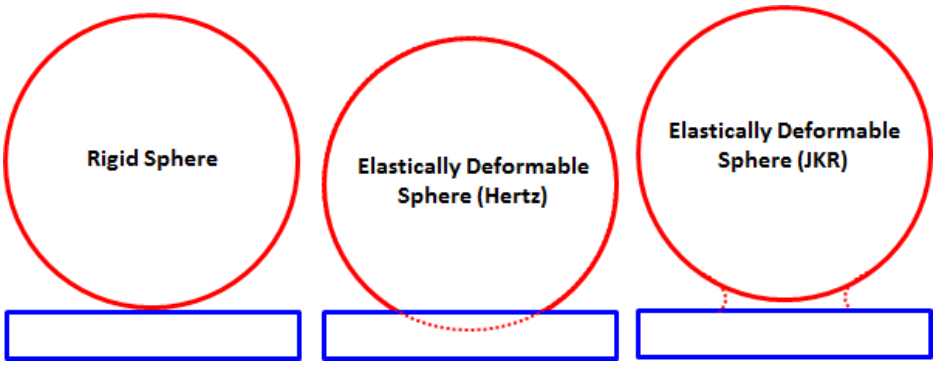


**Figure 4**

Schematic representations of contact mechanics models for a single asperity. For the Hertz model, the contact radius increases as the surfaces deform elastically. In the JKR model a neck forms between the surfaces upon retraction, such that there is a finite contact area even at zero and negative loads.

The first model was derived by Hertz[43], which shows that in the absence of adhesion, the contact area increases with load, $L$, as $L^{2/3}$. In this model the contact radius between two elastic spheres is equal to zero when there is no external force.

Johnson, Kendall and Roberts[44] later took into account cases where attractive surface forces are present between surfaces, and developed what is known as JKR theory. The dependence of contact radius, $r$, on the external load, $L$, between two spheres of curvature, $R$, bulk elastic modulus, $K$, and surface energy, $\gamma$, is given as:

$$r = \left(\frac{R}{K}\left[L + 6\pi R\gamma + \sqrt{12\pi R\gamma L + (6\pi R\gamma)^2}\right]\right)^{1/3}$$

JKR theory is applicable for large, deformable surfaces with high surface energy. DMT Theory[45] (proposed by Derjaguin, Müller and Toporov) also takes into account the

adhesive forces outside the contact region but better describes small and hard surfaces with low surface energy.

# 2 ACCOUNT OF PUBLISHED WORK

## 2.1 Surface Forces Across Liquids

### 2.1.1 Non-polar Liquids

The simplest systems investigated using the surface force apparatus involve the measurement of forces between smooth mica surfaces in non-polar organic liquids. Horn and Israelachvili[10] chose octamethylcyclotetrasiloxane (OMCTS) as an initial starting point for investigating possible structural effects due to its spherical shape and relatively large size; larger molecules would allow single-molecule resolution with the 0.2-0.3 nm resolution of the instrument. The molecules are approximately spherical in shape and of diameter ≈ 0.9 nm.

There is some slight variability of force magnitudes from one experiment to the other but provided there is no contamination, the normal forces always oscillate between distinct maxima and minima for very small surface separations. Figure 5 shows measurements of these oscillatory forces, alternating between attraction and repulsion. The magnitudes of the forces increase exponentially as the surfaces approach each other, as shown by the peak-to-peak amplitudes, until a final steep drop into an attractive well when the mica comes into contact. The peak-to-peak amplitudes show a roughly exponential decay with distance, until the oscillatory force merges with the continuum (non-oscillatory) van der Waals force.

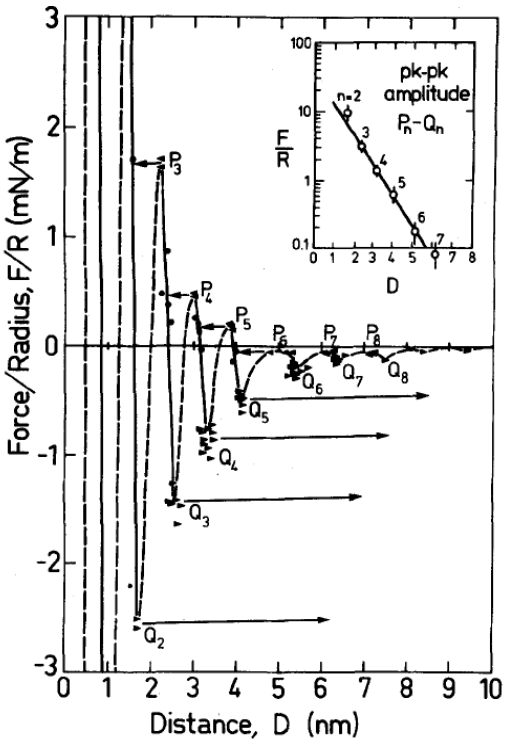


**Figure 5**

Experimental results of normalised force, F/R, as a function of separation, D, for two curved mica surfaces (of radius $R$ =1.65 cm) in OMCTS at 22°C.[10]

The nature of these structural forces is due to changes in the ordering of the molecules as they are squeezed out, with a periodicity equal to the mean molecular diameter of OMCTS. It is more energetically favourable to have an integral number of molecules confined between the mica and energetically unfavourable for the mica to be at intermediate separations. This explains why the energy, and hence the force, oscillates as a function of distance. The range of measurable forces corresponds to about ten molecular diameters. Interestingly, the first four or five layers have a slightly smaller periodicity than at larger separations where it remains unchanged. This is most likely due to the molecules at the surface lying with the short axis perpendicular to the surface, but another possibility is that the molecules simply pack more efficiently near a surface.

It is important to note the regions inaccessible to measurement (represented by dashed lines as a guide to the eye in Figure 5) in the force curves, where the force gradient

exceeds the spring constant. As a result the surfaces are brought towards each other to an unstable region they jump to the next stable region. Similarly there are large jumps outwards from the force minima as the surfaces are brought away from each other. The arrows pointing to the left and right from the maxima and minima show the inward and outward jumps that occur as the number of molecular layers changes.

The effect of foreign molecules is to disrupt the layering and packing, hence it is important that the liquids are carefully distilled and thoroughly dried. It has been shown that as water activity is increased, there is a reduction in the magnitudes of the structural forces[46]. In addition to this the innermost oscillations tend to become experimentally inaccessible when water is present. This is due to a sudden attraction which replaces the solvation force. At contact there is often much greater adhesion, reflecting the presence of condensed water at the surfaces.

Amplitudes of structural forces were also found to be reduced when making measurements for a binary mixture of non-polar liquids[47]. At equimolar concentrations of cyclohexane and OMCTS, there is less structure than for either of the pure liquids. The addition of some fraction of smaller molecules tends to reduce packing efficiency at separations equal to the number of layers of larger molecules, but it facilitates packing at intermediate separations. As a result it is not surprising that the amplitudes of the forces decrease, given that there is a reduction in the magnitude of the free energy at both the maxima and minima.

The general conclusions of Horn and Israelachvili[10] are strongly supported by subsequent work[48] by Christenson et al. studying other non-polar liquids. The experiments were repeated using cyclohexane, benzene and n-octane, and the force was again found to be an oscillatory function of distance. The authors note that the heights of the innermost repulsive barriers are most likely overestimated. This can be attributed to the fact that large repulsions close to contact can elastically deform the glue

underneath the mica, and the resulting flattening of the surfaces makes it difficult to squeeze out the last layer or two of confined molecules. While with experiments using OMCTS[10] the authors concluded that when confined to only a few layers the molecules lie with their short axis perpendicular to the surface, the results for cyclohexane do not indicate a change in periodicity of oscillations. This is perhaps surprising given that cyclohexane molecules are also oblate. The authors speculate on possible reorientations or rearrangements in the packing structure without removing a whole layer.

Although it was found that these solvation forces are not strongly temperature dependent, the presence of even trace amounts of water has a dramatic effect; the adsorption of water onto the surfaces disrupts the packing and generally shifts the force curve to lower, more attractive energies. A drying agent such as $P_2O_5$ should be placed in the apparatus chamber to keep the atmosphere as dry as possible.

When liquids are confined to narrow gaps, new dynamic behaviour emerges which differs greatly to that of bulk liquids. While macroscopically thick films exhibit fluid behaviour, decreasing the gap to molecularly thin films results in a transition to solid-like behaviour[29, 49-50]. This liquid to solid phase transition is reversible and occurs due to confinement alone**.** Figure 6 shows direct recordings of the relative lateral displacement of one mica surface with respect to the other over time. The liquid used was OMCTS, and trace (a) shows the characteristic vibrational noise at large separation (1160 Angstroms) of the spring. The same random vibrations persist to ~62 Å, shown in trace (b).

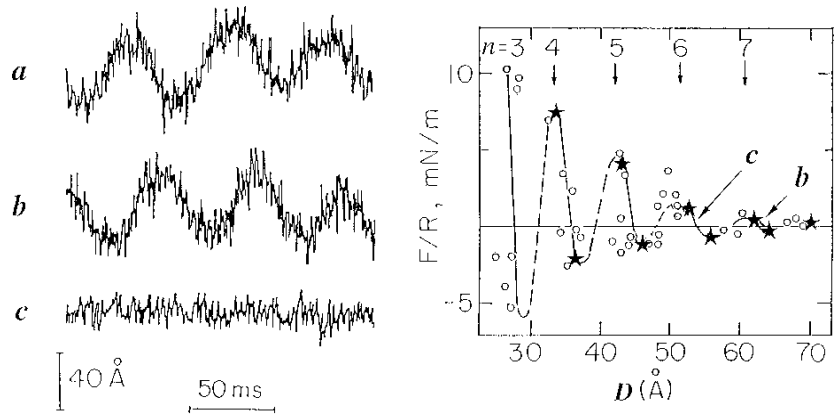


**Figure 6**

Shear traces for mica surfaces immersed in OMCTS with no applied lateral motion at three different separations[29]

Upon further reduction of the mica separation to ~54 Angstroms, the vibrations cease abruptly, shown in trace (c). During this transition the film thickness has been reduced from seven to six molecular layers, and is now able to resist the random shear motion induced by ambient noise; a fundamental signature of a solid. The exact separation where this transition occurs depends on the particular liquid used and its water content, and may also depend on the ambient noise itself. A likely scenario is for the transition to be observed at a very slightly larger separation if the noise is especially low.

Similar results are observed with different non-polar molecules and even linear alkanes, which further suggests that the phase transition is due to confinement and packing alone, and does not depend on any coincidental commensurability that may occur between the confined liquid structure and the mica lattice[51].

The shear force can be directly measured by applying a controlled voltage to the piezoelectric tube, such that one surface moves laterally relative to the other. As seen in Figure 7, there is an initial elastic regime where the shear stress rises to a yield point, followed by a region where the two surfaces slide past each other. The variation of shear stress with sliding velocity is very different in liquids or solids, so it is interesting to

look at this variation in confined films following this liquid to solid phase transition. Given that such a huge increase in shearing velocity, as shown in the different traces, makes such little change to the magnitude of the shear response, the shear stress must be only very weakly dependent on the shear velocity. For a liquid one would expect a relationship between the shear stress and shear velocity, so this further reinforces that the observed behaviour is more like that of a ductile solid confined between the surfaces. The presence of a 'yield point' itself is indicative of a solid-like film, whereas a liquid by comparison shears immediately with infinitesimal stress. The solid-like response is also not induced by shear itself, since it does not degrade with time even after the motion has stopped.

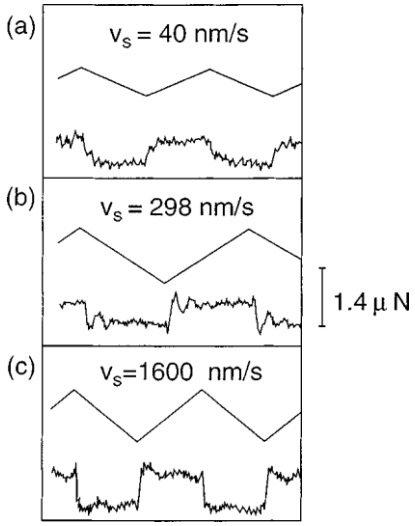


**Figure 7**

Traces of the back and forth motion applied to the upper mica surface as it slides across the lower surface, together with their corresponding shear forces at three different shearing velocities, across a film of $n$ = 6 OMCTS monolayers[29]

However Granick[52] showed that the effective viscosities decay with shear rate when dodecane is immersed between mica surfaces. It was found that the rate of the shear thinning follows an empirical power law, but varies depending on the thickness of the film. Yoshizawa[53] found that at low shearing rates, chain-type molecules produce low

friction forces because the molecules have enough time to rearrange and disentangle themselves. This would explain the higher friction forces observed at higher speeds.

A solid-like thin film is capable of sustaining a maximum shear force before yielding, and this is the frictional force opposing the sliding. When such solid-like thin films are sheared under moderate stress, a characteristic stick-slip behaviour is observed[53,54], where as long as the shear force applied is low enough, the two surfaces are coupled together. This is the 'stick' part of the stick-slip process. During this 'stick', the shear force increases due to the surface moving laterally and bending the shear springs. A critical point is reached where the surfaces slide across each other, the 'slip' part of the stick-slip process. At the end of the slip, the film solidifies and this stick-slip cycle repeats itself as long as the surfaces are still moving laterally relative to each other.

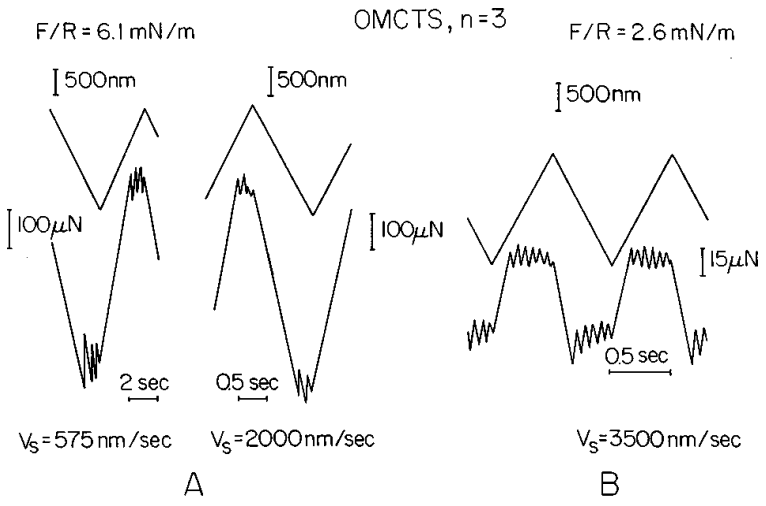


**Figure 8**

Traces of the back and forth motion applied to the upper mica surface, together with the corresponding shear responses for different shear velocities and normal loads showing stick-slip motion[50]

This stick-slip behaviour has been investigated as a function of shear velocity[50] for different film thicknesses. The variation of shear stress required to slide the surfaces is predominantly independent of shear velocity, and the stick-slip behaviour persists over a

wide range of shear velocities. Shear traces for the film at much lower film compressions also show stick-slip behaviour. The exact mechanism of this behaviour is not very well understood[55,56], however some studies suggest that in order for stick-slip to occur there must be some geometric compatibility between the shape of the liquid molecules and the structure of the confining walls[57]. It is also unclear whether the molecules behave like a liquid or a plastically deforming solid via dislocations or disclinations during this motion.

Measurements of solvation forces between mica with even-numbered alkanes from hexane to hexadecane show that the spacing between repulsive walls does not increase with carbon number[58]. The periodicity of the oscillations of ~0.5 nm is instead related to the width of the linear alkane molecules, implying that the molecules orientate themselves with their long axis parallel to the surface. The next molecule away from the mica will also tend to lie in the same direction, but this likelihood decreases as the distance from the mica surface increases. This picture is consistent with earlier thermodynamic measurements of the adsorption of ordered alkane monolayers onto graphite[59] and $NiCl_2$ surfaces[60]. However, the chain-like molecules need not lie rigidly, and it is extremely likely that different segments of the longer molecules may occupy different layers in the confined film.

Such interdigitations in confined films of chain molecules are a significant source of friction[61]. The first layer of molecules is adsorbed to the mica surface and tends to move laterally with it. The molecules with segments in different layers resist the 'ironing-out' caused by the shearing and these entanglements are thought to generate friction. The friction force is generally low for slow shear velocities, since the molecules have enough time to rearrange by thermal fluctuations and diffusion. Consequently higher shear velocities cause an increase in the friction force.

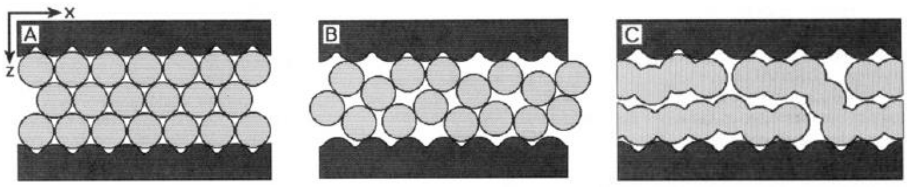


**Figure 9**

A schematic view of interfacial films under a compressive pressure between two solid crystalline surfaces, composed of: (A) spherical molecules such as OMCTS; (B) spherical molecules that are not free to adjust their dimensions; and (C) chain molecules[53]

The critical velocity at which stick-slip disappears to give way to smooth sliding is affected by load, and affects molecules differently according to their shape. If the two surfaces are free to move so as to attain the lowest energy states, they will adjust their dimensions such that trapped spherical molecules become epitaxially ordered into a solid-like film. In this case the two lattices shift to accommodate the molecules in the most commensurate way.

On the contrary, if the solid surfaces are not free to equilibrate the structure would be disordered. This is the case for the rigid walls of capillaries. If the confined molecules are chain-like, they are less likely to become commensurate with the lattices even if the surfaces are free to adjust their position. This explains why load increases the critical velocity for spherical molecules such as OMCTS but decreases it for chain-like molecules. For this reason chain-like molecules make better lubricants than simple isotropic liquids.

There has been much debate in the literature amongst experimentalists about the nature of solidification in confined liquids[62-64], with some studies simply showing a gradual viscosity increase as the film thickness decreases and so contradicting the liquid-solid phase transition. It was thought that platinum nanoparticles from the surface preparation

procedure were causing contamination, and experiments investigating the structure of confined branched alkanes have also been controversial[65-67] for similar reasons. It has been shown using different surface preparation methods that the effect of such platinum nanoparticles (if present) can be ruled out as a source of the discrepancies[68]. Even with the increased fidelity and rigour of more recent computer simulations over the past decade[69], their conclusions remain the same and agree with a many-order-of-magnitude increase in viscosity for a certain number of confined non-polar molecules, demonstrating the existence of phase transitions induced by confinement.

### 2.1.2 Double Layer in Polar Liquids and Electrolyte Solutions

A surface can become charged by ionization or dissociation of surface groups, such as proton dissociation from surface carboxylic acid groups to leave behind a negatively charged surface. Previously uncharged surfaces may also adsorb or bind ions from solution, making them charged. One of the earliest and simplest double layer models was proposed by Helmholtz[70], who envisaged that the excess charge on the surface would be neutralized by an adjacent monolayer of counterions. This simplistic concept of two layers of opposite charge is the origin of the term ‘double layer’, but nowadays it is still the general term for the interfacial structure.

Gouy[71] and Chapman[72] independently proposed a diffuse double layer model where the ions are free to move and subject to thermal motion. The concentration of ions is greatest next to the surface and progressively decreases with distance to that of the homogeneous bulk ionic concentration. However this theory neglects the finite size of the ions, and Stern’s model addresses this by combining both the Helmholtz and Gouy-Chapman models. More recent approaches consider two possible planes of closest approach: one for specifically adsorbed ions and one for other non-specifically adsorbed ions. Grahame refined Stern’s model by considering the adsorbed layer to be composed

either of solvated ions (such as small positive ions) or unsolvated ions (such as large negative ions). The distance from the surface to the centre of the unsolvated or solvated ions is different, and these are called the outer Helmholtz plane (OHP) and inner Helmholtz plane (IHP) respectively. This interface structure is of great importance to electrode kinetics since this is where electron transfer takes place.

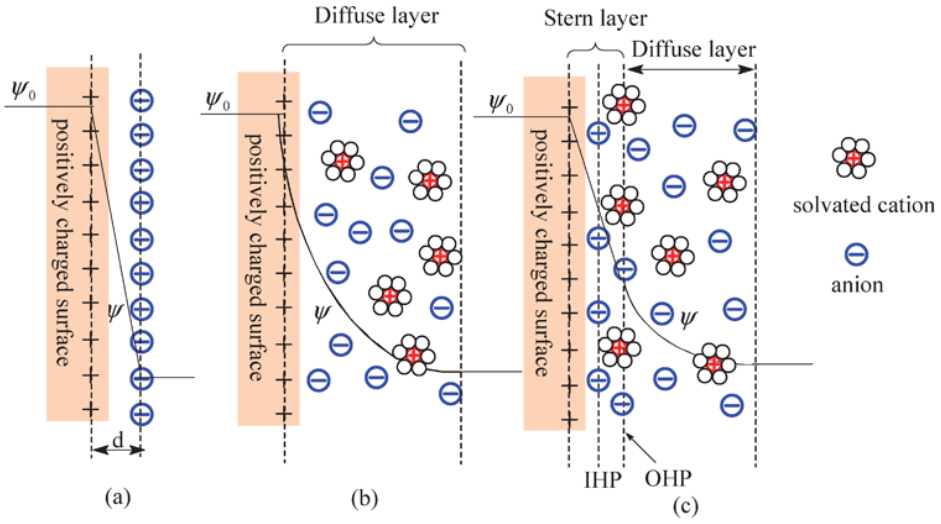


**Figure 10**

Models of the electrical double layer: (a) the Helmholtz model, (b) the Gouy-Chapman model, and (c) the Stern model[73]

When two surfaces approach each other, the diffuse parts of their double layers start to overlap, resulting in a measured repulsive force for surfaces of the same charge. This force can be understood in terms of the osmotic pressure which arises due to differences in ion concentration in the region between the surfaces compared to the bulk electrolyte. The earliest force measurements between mica surfaces across aqueous electrolyte solutions show excellent agreement with DLVO theory[13-14]. At large separations there is a repulsive double-layer force, the magnitude and range of which is dependent on the surface potential, $\psi_0$, and electrolyte concentration, $c$, respectively through the following expression:

$$F_{\mathrm{DL}}/R = 128\pi \mathrm{k_B} T c \kappa^{-1} \tan^2\mathrm{h}(\frac{e\psi_0}{4\mathrm{k_B}T})\exp(-\kappa D)$$

Where the Debye screening length, $\kappa^{-1}$, relies on the dielectric constant of the solvent, $\varepsilon$, as follows:

$$\kappa^{-1} = \sqrt{\frac{\varepsilon_0 \varepsilon_{\mathrm{rel}} \mathrm{k_B} T}{8\pi e^2 c}}$$

A small attractive jump between the surfaces is observed for very small separations due to the van der Waals forces dominating at short range (for higher concentrations this attraction is not observed due to repulsive hydration forces) depending on the Hamaker constant, $A_H$, for the system:

$$F_{vdW}/R = -\mathrm{A_H}/6D^2$$

However experiments with other non-aqueous polar liquids show marked differences compared to water[74-76]. While the measured long range repulsive forces are again in excellent agreement with DLVO theory, at short separations the force is oscillatory as a function of separation, even for very dilute concentrations. These short range forces are insensitive to electrolyte concentration, and like for non-polar liquids, the oscillation distances correspond to solidification and layering of the liquid molecules. The oscillatory structural forces appear to be superimposed on the background double layer force and as a consequence, some of the measured force minima occur at positive normal forces.

Water appears to be the only liquid where an attractive van der Waals force is measured to contact at low enough salt concentrations making any structural forces (if present) inaccessible to measurement. In fact, the measured attraction between surfaces across water for close surface separations instead of oscillatory structural forces must be related to water's ability to remain fluid-like in confinement[77-79], most likely due to

suppression of its highly directional hydrogen-bonded networks. This result is highly susceptible to contamination, which may act to solidify a nano-confined film of pure water. Molecular dynamics simulations[80-81] have also shown generally that materials with such expansive freezing properties are expected to have good boundary lubrication properties.

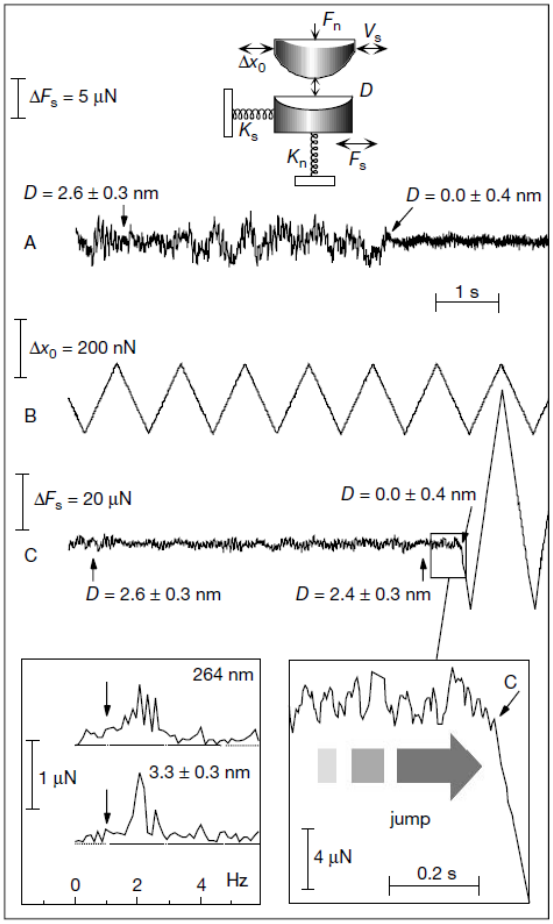


**Figure 11**

Shear forces between mica surfaces across pure water during approach to contact: (A) the noise in $F_S$ arising from ambient vibrations as the surfaces jump into contact under thermal drift, (B and C) the shear force $F_S$ transmitted across the film during a back-and-forth lateral motion, showing no shear response during the jump to contact[77]

Measurements of shear forces between mica surfaces across ultrathin films of salt-free water[77-78] reveal that no shear stress is sustained (within the sensitivity of the

instrument) right down to sub-nanometer film thicknesses during the attractive jump itself. With consideration of the time taken for this jump and the geometry of the confining surfaces, the effective shear viscosity is estimated to be within a factor of about 3 (in either direction) of that for bulk water.

While the hydration layers surrounding ions can be strongly attached and difficult to remove, at the same time they are able to relax very rapidly under shear. This mechanism, which has been termed 'hydration lubrication',[82-83] provides incredibly low friction at high normal loads between surfaces across trapped hydrated layers and has also been found to apply to sliding between surfactant monolayers[84-85] and charged polymer brushes[86-88] in aqueous media.

## 2.2 Surfactants as Friction Modifiers in Engine Oil Additives

By interposing a liquid lubricant between surfaces, friction and wear of surfaces moving relative to each other in close proximity can be reduced. Nearly all motor oils have an additive package, carefully balanced with different types of functional molecules used to improve the performance of the oil[89]. Anti-wear additives generate a protective film, protecting metal parts and hence reducing wear and scuffing. Detergents and dispersants are also commonly included to protect mechanical components and maintain the life of the oil by dispersing impurities and contaminants.

Almost a quarter of energy generated in an engine by burning fuel is lost through friction[90]. Friction modifiers are a particularly important additive to reduce boundary friction at points where surfaces contact each other. They are generally amphiphilic molecules which are attracted to surfaces through strong adsorption forces, with the

polar headgroup anchored to the surface and the hydrocarbon tail left solubilized in the oil. These layers are difficult to remove but easy to shear, reducing frictional heat, start-up torque and noise in engines. Common organic friction modifiers include long chain fatty amides such as oleylamide, and partial esters such as glycerol mono-oleate. Other additives in the oil such as detergents and dispersants may have an affinity for the surface and compete with friction modifiers, potentially increasing friction.

In order to develop new and improved lubricant formulations with better efficiency, it is necessary to gain a fundamental understanding at a molecular level of what mechanisms are taking place at the solid/liquid boundary. Simple model system experiments have involved surfactants of different headgroup chemistries dissolved in alkanes at different concentrations[91-92]. Even a very small amount of friction modifier as an additive removes the well established oscillatory force normally observed for confined linear alkanes. The repulsive hard wall for the surfactant solutions also corresponds to a thicker film than for the pure solvent, implying the adsorbed surfactant molecules lie perpendicular to the surface forming upright monolayers.

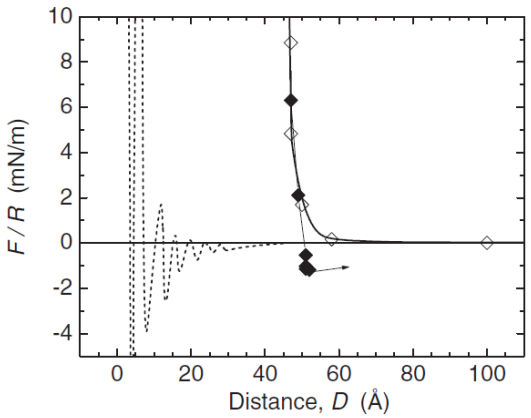


**Figure 12**

Force profile for 0.1 wt% hexadecylamine dissolved in tetradecane. Also shown as a dashed line is the expected force law for pure tetradecane[92]

The frictional properties appear to be a result of the adsorbed layers exposing the hydrocarbon chains rather than the particular type or chemistry of the surfactant headgroup. This result is consistent with the accepted mechanisms of boundary lubrication involving sliding at the interface between alkyl chains for non-aqueous media and not necessarily involving shear of the monolayers at the surfactant headgroup/solid interface.

More recent molecular dynamics simulations show semi-ordered monolayers perpendicular to the surface[93-94], in line with the interpretations from surface force measurements. By interpretation of the density profiles over a wide range of normal pressures, the monolayer structures were observed to remain largely unchanged, with changes in volume occurring in the gap between monolayers or between the monolayers and trapped liquid molecules.

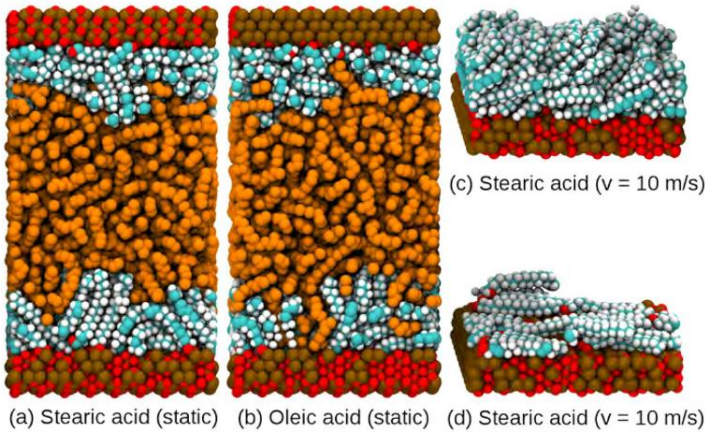


**Figure 13**

(a) and (b) Simulation snapshots of the stearic and oleic acid films at high coverage; (c) and (d) Stearic acid films of different surface coverages while sliding, with solvent molecules not shown[94]

The presence of a double bond in the alkyl chain of the friction modifier seems to affect both the structure of the adsorbed monolayer and the resulting friction. At low surface coverages in a squalane solvent, simulations show that the solvent appears to penetrate

further into stearic acid films than it does for oleic acid films[94]. The stearic acid film is more diffuse and the oleic acid film forms a more compact film that admits less solvent penetration. This is quite unexpected, given that in the bulk, unsaturated molecules usually pack less well in the solid phase which leads to a reduction in their melting point compared to their saturated analogues. However at higher surface coverages the monolayers are very similar. The surfactant film thicknesses do not change significantly under the application of shear, despite significant tilt of the molecules while sliding. This is because the molecules also elongate and the two effects cancel each other out, leading to the film thickness generally being insensitive to shear.

Surface force experiments with analogous fatty acids dissolved in hexadecane show a slightly lower friction coefficient for stearic acid compared to oleic acid[95]. At the macroscale with steel surfaces, it has been shown that in the boundary lubrication regime the friction coefficient increases with sliding velocity for stearic and elaidic acid, while it remains constant for oleic acid[96]. This suggests that the increase of friction with sliding speed originates from its ability to form close-packed layers, an idea put forward in early work[97]. As the surface coverage decreases, more solvent penetrates into the film and this increased order and structure gives rise to an increase in friction with sliding speed. This is a key requirement in preventing stick-slip friction which leads to noise and shudder as well as possible wear of the surfaces.

## *2.4 Ionic Liquids in Confinement: From Specialist Lubricants to Novel Electrolytes*

Ionic liquids are salts which are liquid under ambient conditions, and are composed entirely of cations and anions. Their history began with the discovery of ethylammonium nitrate, whose melting temperature (12 °C) is extraordinarily low

compared to that of a common salt such as sodium chloride (801 °C). Ionic liquids commonly consist of large molecular ions, which are often asymmetric in shape and with delocalized charge, all of which generally hinder crystallisation into an ionic solid. The cations are often amphiphilic: only part of the ion structure holds the charge whilst another part (or parts) of the ion is uncharged. This asymmetry results in more complex interactions than when compared with high temperature molten salts; certain preferred orientations of an ion relative to its neighbours cause meso-structure and order in the liquid, both in the bulk and at interfaces[98-104]. This complexity introduced by multiple and directional interactions – such as electrostatics, van der Waals, dipole interactions and hydrogen bonding – means that subtle changes in the environment can lead to dramatic switches in the preferred ion ordering in the liquid.

The mesostructure in ionic liquids is in some ways akin to the self-assembly observed for amphiphilic solutes in water, such as the aggregation of surfactants into micelles or lipids into bilayers. There is, however, an important difference: ionic liquids have the additional constraint that the whole of the volume of the liquid must be taken up by the ions themselves, with no solvent to 'fill the spaces'. The result must be a balance between the optimised inter-ion interactions and the space-filling requirement.[98-101]

By varying the chemistry of the ions and alkyl chain substituents, liquid salts with low melting temperatures, negligibly low vapour pressures and high thermal stability have been synthesized. They have many applications in a variety of fields, including heterogeneous catalysis, nanoparticle stabilisation and lubrication. In particular, their high ionic conductivity and wide electrochemical window render them exciting electrolytes for electrochemical applications such as in electrodeposition, batteries, solar cells and supercapacitors. In almost all of these novel applications, the solid/liquid interface plays a crucial role; hence an understanding of the structural arrangement and

dynamic properties of ionic liquids at solid interfaces is necessary for their development as electrolytes and would undoubtedly lead to significant progress.

X-ray reflectivity studies first revealed strong interfacial layering of ionic liquids at a charged sapphire substrate[105], starting with a cation layer at the surface and decaying exponentially into the bulk liquid. The charge density in the layers oscillates between positive and negative with distance from the surface, attributed to strong correlations between unscreened ions. This alternating cation-anion layering structure was later found to also be the case for ionic liquids at a mica surface[106]. However for uncharged graphene, the layering consists of mixed cations and anions, highlighting the importance of charge induced correlations on the ionic liquid nanostructure.

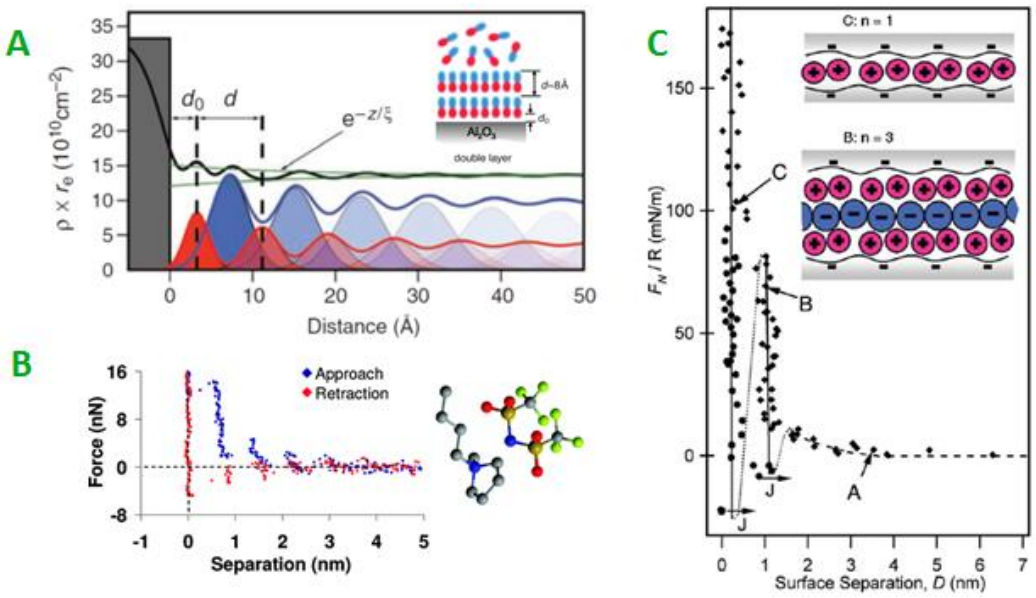


**Figure 14**

(A) Electron density oscillations for cations and anions from x-ray reflectivity[105] of an ionic liquid at a charged sapphire surface (B) Layering of an ionic liquid at a charged mica surface as observed with an AFM tip[107] (C) Layering of an ionic liquid confined between charged mica surfaces[108]

The structure of ionic liquids at a variety of surfaces has also been studied with AFM[107, 109-112]. With this setup, both positive and negative electrode potentials of different magnitudes can be used to investigate how surface charge affects the layering of the ions. A charge templating effect is again observed, where higher applied potentials lead to more layers due to stronger electrostatic interactions. However, the shape of the tip is hard to characterise, and hence magnitudes of forces are not particularly meaningful when comparing different experiments. The contact area between the AFM tip and surface is ~$10^6$ times smaller than that between two smooth surfaces in the surface force apparatus, which produces reduced signal-to-noise ratios. In contrast to surface force measurements, the absolute surface separation is not known throughout the experiment and unless the tip is able to penetrate the last molecular layer and image the surface with atomic resolution it is difficult to know exactly how many ion layers are confined due to problems with thermal drift. With ionic liquids, imaging the substrate is very difficult for charged surfaces since the first layer of ions is tenaciously held by electrostatic interactions.

Early pioneering work on structural forces of confined room temperature ionic liquids involved ethylammonium nitrate[113]. It is miscible with water in all proportions, hence enabling the study of an electrolyte up to unusually high concentrations. At low concentrations in water, the liquid behaves as a simple electrolyte and follows DLVO theory. The surfaces are however prevented from coming into contact, due to a strong repulsive barrier of cations adsorbing to the negatively charged mica surface and forming a Stern layer. Increasing the concentration to 50% results in an additional layer (containing both anions and cations) manifested as a second, weaker barrier at a slightly larger separation. Increasing the concentration further results in pronounced oscillatory forces with more layers being detected up to pure ethylammonium nitrate, where up to nine layers are observed. The nature of these forces is very similar to that of non-polar liquids, but here the layers being squeezed out must consist of equal numbers of cations

and anions so that electroneutrality of the ionic liquid film and mica surfaces is conserved.

In recent years, the theory of ionic liquid double layer structure has received considerable interest[114-118] from the electrochemical community, particularly since the discovery of the moisture- and temperature-stable ionic liquids. Understanding the charge and electric potential distribution, which is completely different to dilute electrolyte solutions, is of course crucial for their performance as electrolytes in devices. Much progress has been made in the theory, understanding and experimental

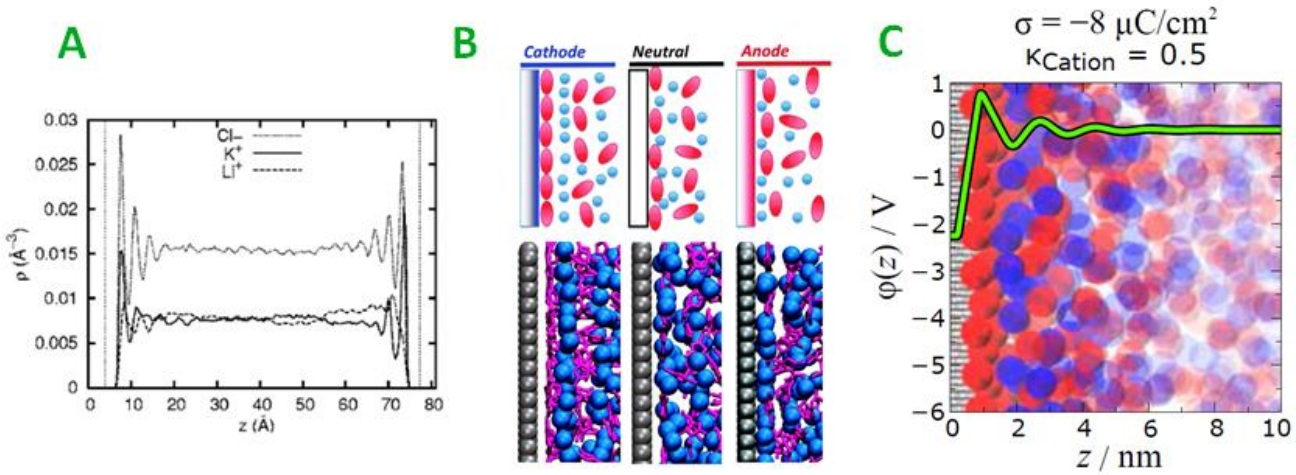


characterization of ionic liquids at flat electrodes, but this remains to be studied in nanoconfinement.

**Figure 15**

(A) Ionic densities for a molten salt-electrode interface at an applied potential of 1.63 V[114] (B) Cartoon and simulation snapshots representing the main structural changes of an ionic liquid near an electrode upon charging[117] (C) Electrostatic potential with an underlying simulation snapshot for an ionic liquid represented as charged spheres equal size[119]

While ionic liquids are expensive to manufacture in large quantities, of particular interest is their use as specialist lubricants in high vacuum or extreme temperature

conditions. With the ongoing miniaturisation of devices they are also prospective lubricants for nano/microelectromechanical systems (NEMS/MEMS), where lubrication must be achieved with ultra thin films, typically only a few molecular layers in thickness. At such small length scales, surface forces dominate and it becomes critical to understand molecular friction, adhesion and wear mechanisms at the nanoscale.

The shear properties of an ionic liquid, 1-ethyl-3-methylimidazolium ethylsulfate, have been characterised with surface force experiments[108], with measurements of the shear force at different mica separations as a function of normal force revealing low friction coefficients. This was attributed to irregular ion structures, resulting in some lateral disorder in the films and consequent absence of particular close packed alignments of the ions within the layers. The strong coulombic interactions between the ions however appear to play a role in maintaining a robust film under load while shearing. Similar investigations, although less direct, on the shear properties of ionic liquids have also been carried out using resonance shear measurements[120]. Although the effective viscosity of the ionic liquids studied under confinement was 1-3 orders of magnitude higher than that for their bulk equivalents, this was still low when compared to viscosities at the glass transition. This too suggests that the confined molecules maintain mobility, even though they are in a solid-like ordered arrangement in the direction normal to the surface.

While ionic liquids confined between charged surfaces such as mica, silica and metal electrodes exhibit pronounced layering, enhanced viscosity and eventually solid-like behaviour, this is not the case for methyl-terminated surfaces[121]. In the case of bare mica[108,122], an ion exchange process takes place where potassium ions initially present on the freshly cleaved mica surface are replaced by ionic liquid cations. This leads to a cation monolayer bound to each mica surface, playing a pivotal role in determining the near surface structure. With neutral, methyl-terminated surfaces[121], the absence of an adsorbed cation monolayer on the surface appears to hinder layering. The presence of

pronounced layering of non-polar OMCTS molecules confined between the same methyl-terminated surfaces alludes to the conclusion that inhomogeneities or possible surface roughness is not playing a role here. Instead, the absence of layering is related to interactions between ions and the surface as has been well described in the literature.

With charged surfaces, the strong ion layering in the direction normal to the surface induces dynamical slowdown and increased viscosity under confinement, as is the case for non-polar liquids. Somewhat surprisingly, the absence of pronounced molecular layering in the ionic liquid confined between methyl-terminated surfaces appears to result in the film retaining its bulk-like transport properties even for small surface separations.

# 3 EXPERIMENTAL METHOD

## 3.1 The Surface Force Balance

The work in this thesis primarily involves experimental measurements of normal and shear forces using a Surface Force Balance (SFB). The SFB is a high resolution force measuring instrument employing macroscopic surfaces in crossed cylinder configuration. In this chapter the experimental details of the SFB technique are discussed.

## 3.2 Mica Surface Preparation

The most commonly used substrate for surface force measurements is muscovite mica. Alternative substrates such as sapphire[123], silica[124] gold[125], graphene[126] and even a liquid mercury droplet[127] have also been implemented. Mica is however ideally suited because it is transparent, inert, and can be easily cleaved to give relatively large atomically smooth sheets (< 1 Å roughness) down to one micrometre in thickness.

Contamination of mica is often a problem[128], and preparing surfaces that are truly clean is not easy. Mica is a high-energy surface that readily adsorbs water and organic contaminants. It can also become charged on cleaving, making it prone to picking up oppositely charged particles or flakes of mica. Hence all surface preparation is carried out in a laminar flow hood to minimise particulate contamination, and freshly cleaved mica surfaces to be used in experiments are exposed to air for as little time as possible. All glassware is cleaned with piranha solution (a mixture of concentrated sulfuric acid and hydrogen peroxide in a 3:1 ratio), a strong oxidiser, to clean off organic residues.

Stainless steel parts and tools are passivated in nitric acid before rinsing and sonicating in ultrapure water (18.2 MΩ cm resistivity, <3 ppb TOC), toluene and absolute ethanol.

Single-facet mica pieces of ~1-3 micrometers in thickness are cut away using a hot platinum wire. Although this may cause platinum nanoparticles and solidified droplets of molten mica, characterisation by AFM has shown that their abundance can be significantly reduced by using thinner platinum wire at lower temperatures[129]. Larger pieces of cut mica are also preferable so that the contact region in the middle of the piece is far from any edge which has been melt-cut using platinum, when mounted in the apparatus[130]. It has been shown that identical normal and shear forces are obtained across a variety of liquids using mica which is torn off (and hence guaranteed to be free of nanoparticles) and that which is melt cut with careful consideration of laminar air flow, within experimental scatter[68].

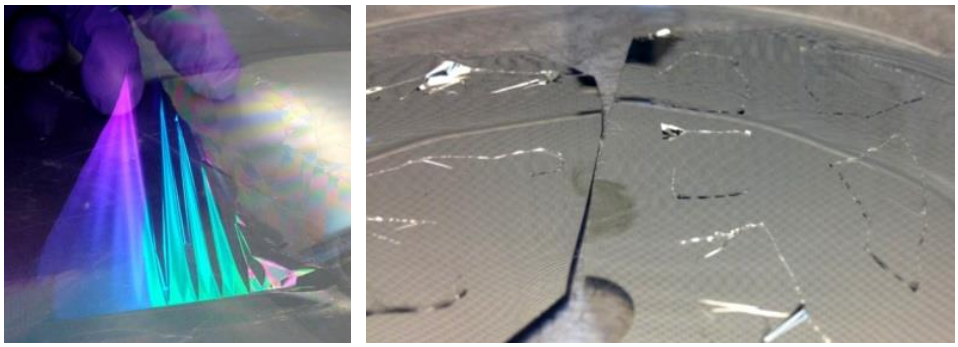

**Figure 16**

Mica cleaved to thin sheets (~1 μm), atomically smooth and free of steps over large areas, typically several $cm^2$ (left) and mica pieces adhered to a larger mica base sheet with evaporation of a semi-reflecting silver mirror (right)

Once cut away the mica pieces are adhered to a freshly cleaved base sheet of mica, with pieces from the same facet aligned according to their crystallographic orientation. The surfaces on the base sheet are then silvered on their back side by deposition of a thin film (40-65 nm) of silver at a base pressure of ~$10^{-6}$ mbar. The silver deposition rate is

controlled by the current supply to the heater and a mechanical shutter, with a quartz-crystal microbalance used to monitor the film thickness. A relatively low deposition rate of ~0.3 $Å s^{-1}$ is used to ensure a smooth and homogenous film. Subsequently the samples are stored under vacuum in a dessicator until required, no longer than a few months.

Once peeled off with tweezers, they are glued silver side down onto cylindrical lenses, such that the clean mica surfaces face upwards. The glue is chosen to be insoluble in the liquid to be studied[131,132]. The lenses are then mounted in the apparatus with their axes crossed in a crossed-cylinder configuration, resulting in the surfaces meeting at a particular contact spot.

**Figure 17**

Photograph of back-silvered mica pieces glued to cylindrical lenses (left), and when mounted in the inner section of the apparatus in a crossed-cylinder configuration (right)

The liquid of interest is typically injected with a clean syringe to form a droplet between the surfaces, though for liquids with higher volatility the lower lens holder can be filled with liquid. The crossed-cylinder arrangement of the surfaces is advantageous since it avoids edge effects and the difficulty of parallel alignment associated with two flat surfaces.

## 3.3 Liquid and Solution Preparation

Dry solvents were either used from freshly opened bottles (Sigma-Aldrich, anhydrous, ≥99%) or filtered (0.2 µm) after being stored over molecular sieves (3Å pore size) for several days. Molecular sieves were pre-dried at 250 °C for 24 hours immediately before use. Such a procedure reliably provides dry solvents with residual moisture in the sub-30 ppm range[133].

Ionic liquids used in the work described here were synthesized using modifications of existing literature procedures[134-135] in the groups of Prof. Tom Welton (Imperial College London) and Prof. Peter Licence (University of Nottingham). Due to their negligible vapour pressure they can be dried in vacuo ($10^{-2}$ mbar, 70°C), with Karl Fischer titration showing water levels below 50 ppm. However, the injection process between the surfaces in the apparatus is likely to introduce a small amount of water resulting in a final estimated water content below 200 ppm.

## 3.4 Determination of Surface Separation: Multiple-Beam Interferometry

The thin semi-reflecting silver layer on the back side of each mica surface serves as an optical interferometer, where collimated white light impinging normal to the surfaces passes through. Multiple reflection occurs between the two silver layers, and the emerging beam is focused into the slit of a grating spectrometer. Constructive interference at certain wavelengths leads to observable multiple beam interference fringes called ‘fringes of equal chromatic order’, FECO. These fringes are observed as a series of curved bright lines in the spectrogram.

When the surfaces are separated by air (or liquid), the region of closest approach has a fringe pattern consisting of a series of arcs arising from the crossed-cylinder geometry. As the surface separation is decreased, the fringes move to shorter wavelengths, and are further apart from each other in wavelength space when viewed through the grating spectrometer. The fringe wavelengths can be inferred by comparison with the known wavelengths of the spectral lines of mercury. Upon adhesive mica-mica contact, flattening of the fringes is observed due to elastic deformation of the glue underneath the silver mirrors. This flattening corresponds to the circular contact, and is typically 20-50 micrometres in diameter in air depending on the amount and type of glue used.

When the two pieces of mica are of equal thickness separated by a medium of thickness *D*, a general equation for a symmetrical three layer interferometer (of which each layer has its refractive index, $\mu_{\text{layer}}$) can be used[136]:

$$\tan(k\mu_{\text{medium}} D) = \frac{2\bar{\mu}\sin\theta}{(1+\bar{\mu}^2)\cos\theta \pm (\bar{\mu}^2 - 1)}$$

where $\bar{\mu}$ is the quotient: $\bar{\mu} = \frac{\mu_{\text{mica}}}{\mu_{\text{medium}}}$

and $\theta$ is the function: $\theta = \frac{n\pi\Delta\lambda_n}{\lambda}$

with the fringe order, *n*, given by: $n = \frac{\lambda_{n-1}}{\lambda_{n-1}-\lambda_n}$

This means the separation of the surfaces can be determined by comparing the difference of the FECO wavelengths when the surfaces are in contact in dry air (using two particular adjacent fringes of wavelength $\lambda_n$ and $\lambda_{n-1}$) and when there is a medium of thickness *D* between the surfaces. Since a crossed-cylinder configuration is used, the fringes are parabolic in shape, and the local (average) radius of the interacting surfaces

can be directly measured. The geometry of this configuration near the region of closest approach is equivalent to that of a sphere approaching a flat surface.

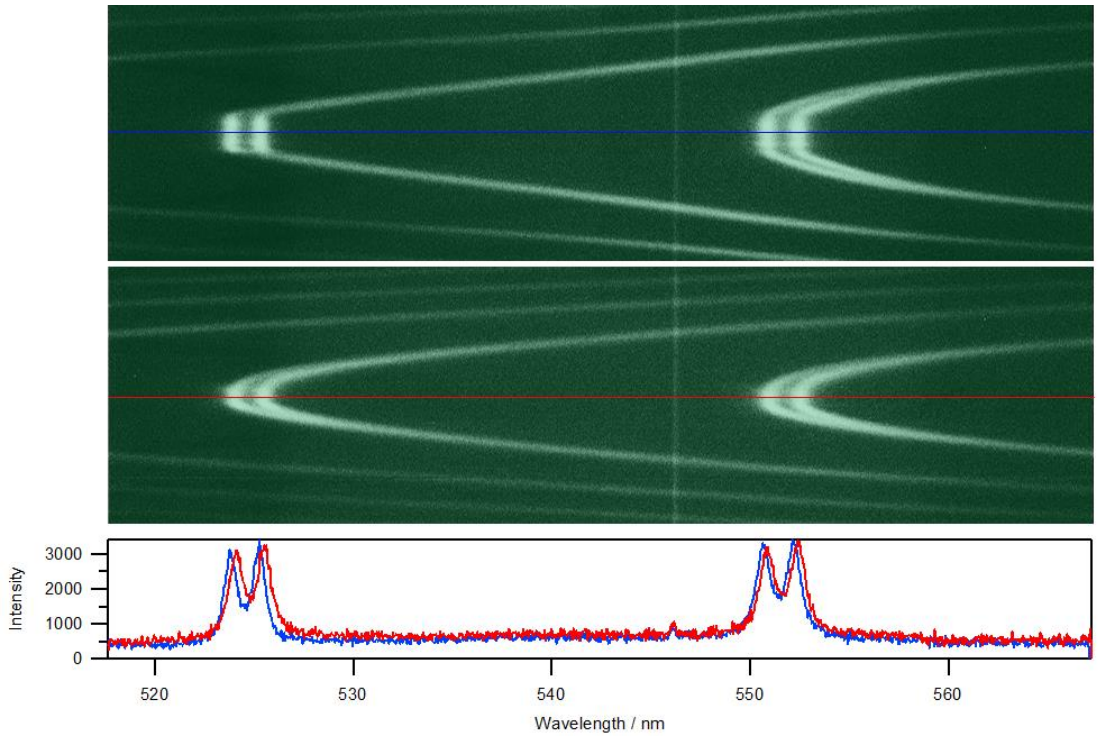


**Figure 18**

FECO patterns produced by two mica surfaces (each of thickness 1.7 μm) in a crossed cylinder configuration, photographed directly from the spectrometer. Doublets are visible on each fringe due to the birefringence of mica. Flattened fringes (above) are observed when the mica surfaces are in adhesive contact. Curved fringes (below) with some very small flattening are seen when the same mica surfaces are separated by 2.5 nm of OMCTS, corresponding to 3 confined molecular layers of the liquid. The profile of pixel intensity from the CCD as a function of wavelength shows clearly the wavelength shift relative to separation of the surfaces in air. The green spectral line of mercury (546.1 nm) is also shown as a reference wavelength.

In most experiments shown here, distance measurements were made manually using an eyepiece by aligning the grating of the spectrometer to record the position of closest approach of a particular fringe for each data point. Obtaining a resolution of 1-2 Å

requires a combination of delicately thin mica (~1 μm), high quality silver mirrors – which have a narrow window in thickness for optimum reflectivity – and correct crystallographic alignment of the mica surfaces in order to achieve widely spaced doublets. Collecting information from the fringes for a single distance measurement requires great care and patience, and as a result, profiles of force as a function of distance are rarely composed of more than a few tens of data points.

In other cases the fringes were recorded using a CCD camera for later analysis. This facilitates the acquisition of many more data points and also allows for measurements of dynamic processes. Cross sections of pixel intensity at the region of closest approach can be fitted to Gaussian or Lorentzian curves, and from these the intensity maxima converted to wavelengths. In both cases (experiments 'by eye' and by using the CCD camera) the resolution is often 1-3Å with optimum mica thickness and fringe quality, however use of the camera eliminates human error in the judgement of fringe position.

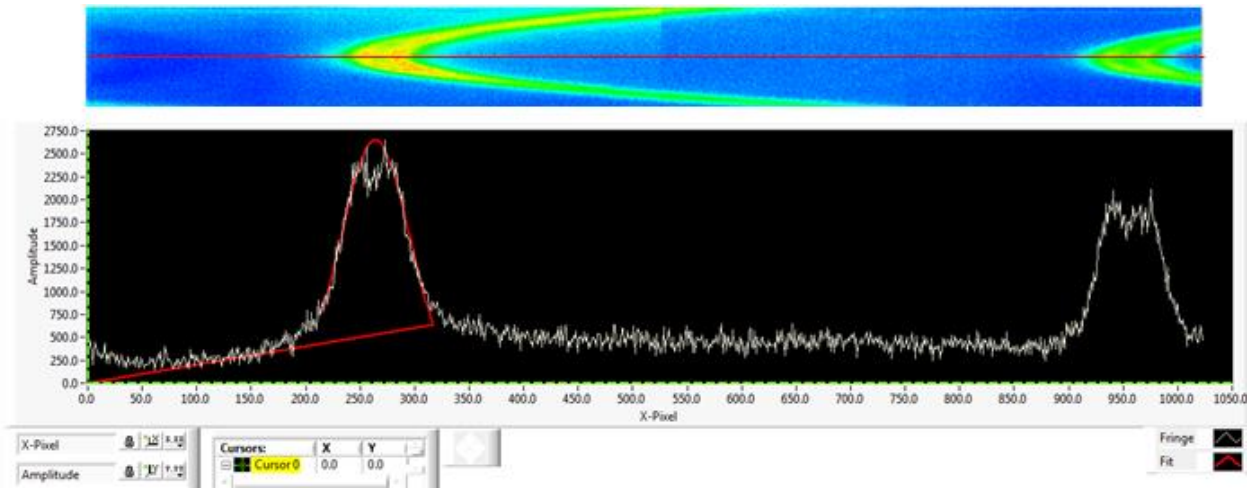


**Figure 19**

Automated analysis of successive fringe images as executed using LabVIEW software, to determine pixel positions of intensity maxima for an interference fringe.

## 3.5 Determination of Normal Forces

One of the lenses is mounted onto a horizontal leaf spring of known spring constant, $K_N$, and the deflection of this spring as the surfaces move towards or away from each other is used to calculate the force, the resolution of which is better than $10^{-7}$ N. The separation between the two surfaces is controlled using a three-stage mechanism; a coarse control motor allows positioning to about 1 μm, a fine control motor allows positioning to about 1 nm by way of a differential spring mechanism, and a rigid piezoelectric crystal tube can control the position to better than 1 nm.

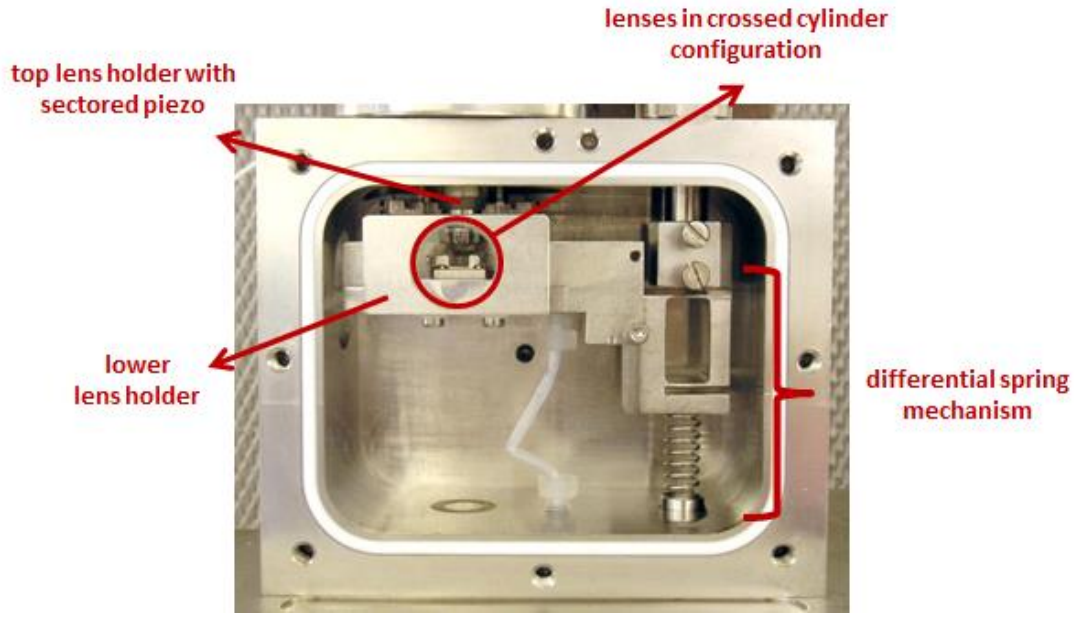


**Figure 20**

Photograph of the SFB used to measure normal and shear forces between two molecularly smooth mica surfaces across liquids with Angstrom resolution[137]

The fine control motor allows extremely linear motion at controlled velocities as low as 2-3 $Å s^{-1}$, allowing simultaneous quasistatic approach of the surfaces and acquisition of film thickness measurements with the camera. Faster approaches allow measurement of hydrodynamic forces although depending on the viscosity of the liquid, approaches much faster than 30 $nms^{-1}$ result in vibrations from the motor which add considerable

noise to the data. However the piezoelectric crystal tube allows motion over several micrometres without any added vibrations.

In a typical force profile, measurements begin at large separations where there is no force acting between the surfaces. The surfaces are brought towards each other from this large surface separation to contact. The spring deflection is measured as the difference between the measured film thickness and that expected with the linear motion in the absence of any forces. Repulsive forces result in compression of the force measuring spring, while attractive forces cause the spring to extend. Figure 21 shows an example of a force profile measured from ~300 nm, showing no measurable forces until confined on the order of several nanometers, where there is an onset of repulsion. The deflection of the spring can be multiplied by the spring constant to obtain the force for all of the measured film thicknesses. Consequently a force profile can be measured from large separations down to contact.

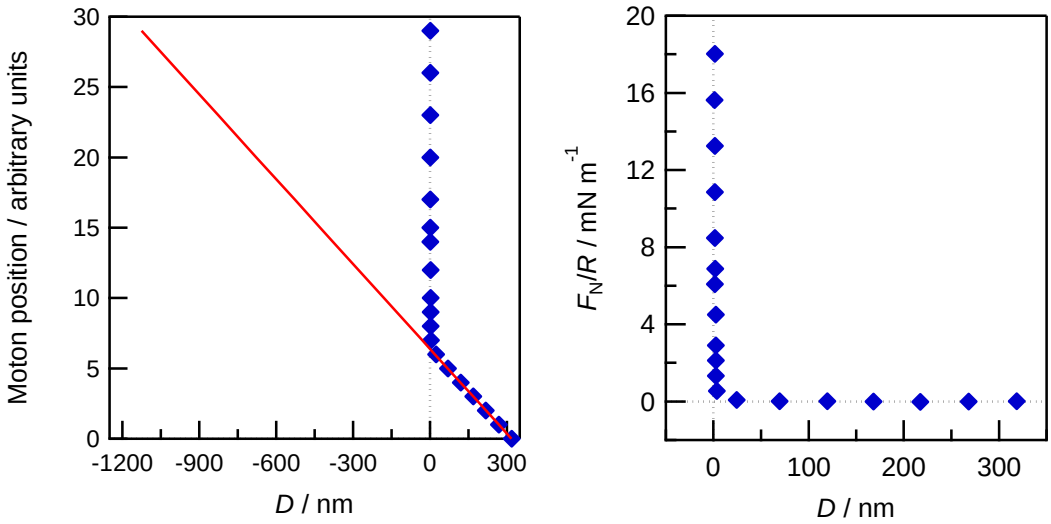


**Figure 21**

Film thickness measurements upon approach of the surfaces showing linear motion in the absence of force, and deviation due to repulsive forces. The measured $F_N$ is divided by $R$ for normalization between experiments.

Although the radius of curvature of the lenses, *R*, used in these experiments is constant at 10 mm, the actual curvature of the mica surfaces varies slightly due to the glue layer underneath. The equivalent *R* of the two mica surfaces can be directly measured from the fringe images using the resolution of the CCD in the direction parallel to the surfaces, which is 1 μm/pixel. Typical values for *R* are in the range 7-11 mm.

## 3.6 Determination of Shear Forces

Lateral motion of one surface with respect to the other over a range of velocities and frequencies is achieved using a piezoelectric tube to which the top mica surface is mounted. Parallel motion is possible since the piezoelectric tube is sectored; equal and opposite voltages are applied to the opposing outside sectors so that one expands while the other contracts[29]. However, this would result in an arc-like motion, so additional voltage is applied to the inner sector of the tube at appropriate rates to correct for this, resulting in parallel motion (typically several hundreds of nanometers shear amplitude are possible with <1 nm deviation in film thickness). It is important that the surface separation remains constant while making a shear measurement to ensure constant normal force between the surfaces.

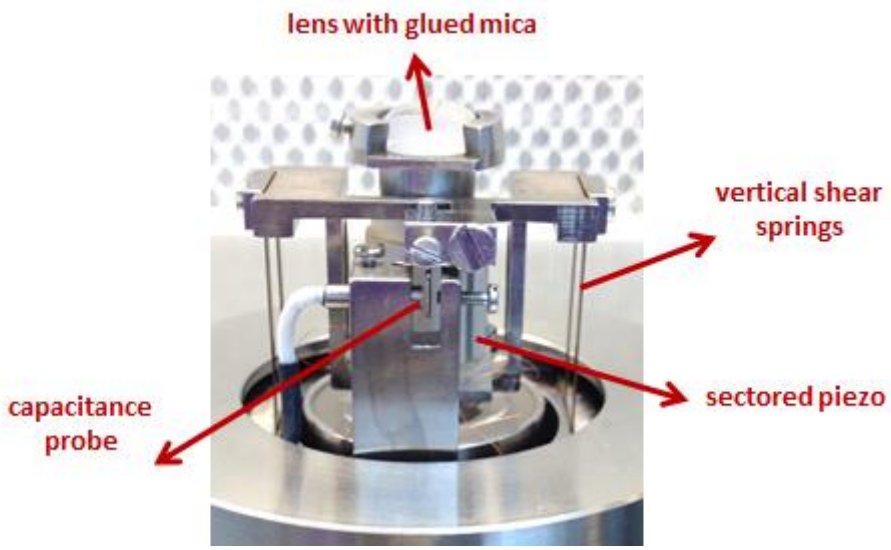


**Figure 22**
Photograph of the top lens holder with which shear measurements are made. When mounted in the apparatus it is place upside down above the lower lens

Any shear forces between the surfaces bend the vertical leaf springs, of known spring constant, $K_S$, and this bending can be measured with extreme precision via an air-gap capacitor as follows: changes in the capacitance of a small air gap between a capacitance probe and a polished flag coupled to the moving lens are used to deduce lateral movement of one lens with respect to the other. Temperatures in the measurement room are kept constant to reduce thermal drift in the apparatus, and ambient noise from random vibrations is minimised by placing the apparatus on a vibration isolation unit. The sensitivity and resolution of this method to determine shear forces is comparable to that achieved when measuring normal forces using interferometry. Simultaneous shear and normal motion is also possible, enabling the measurement of shear forces as the surfaces approach each other and at controlled normal load.

# 4 LUBRICATION MECHANISMS FOR GLYCEROL BASED ORGANIC FRICTION MODIFIERS IN BASE OILS

## 4.1 Introduction

Friction modifiers play a very important role in boundary lubrication conditions, where hydrodynamic and elastohydrodynamic lubrication is not present and the surfaces come to very close contact at their asperities. One common example is bearings, which normally operate with a thick lubricating film but experience boundary lubrication at low sliding speeds, particularly during routine start-up and shut-down. Machines are most susceptible to wear at these low speeds, so it becomes important to prevent surface contact to reduce friction and wear.

Glycerol mono-oleate (GMO), the structure of which is shown in Table 1, is an organic friction modifier commonly used in lubricant formulations. Commercially available GMO often contains small amounts of glycerol di-oleate (GDO) and glycerol tri-oleate (GTO) impurities. In this chapter, surface force measurements were carried out to examine the film structure and friction of each of these surfactants dissolved in dodecane, a model base oil. Some experiments with mixtures at different concentrations were also performed to investigate possible competition at the surface and the resulting effect on their overall lubricating properties. Before embarking upon the friction modifier experiments, the pure solvent, dodecane, was investigated.

**Table 1** A summary of the glycerol-based surfactants investigated here

| Name | Chemical Structure | Abbreviation |
|---|---|---|
| Glycerol mono-oleate | 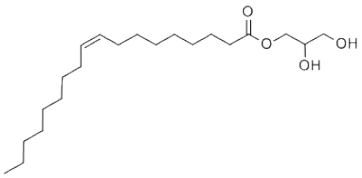 | GMO |
| Glycerol di-oleate | 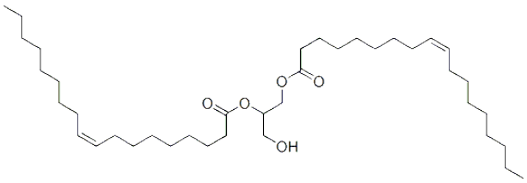 | GDO |
| Glycerol tri-oleate | 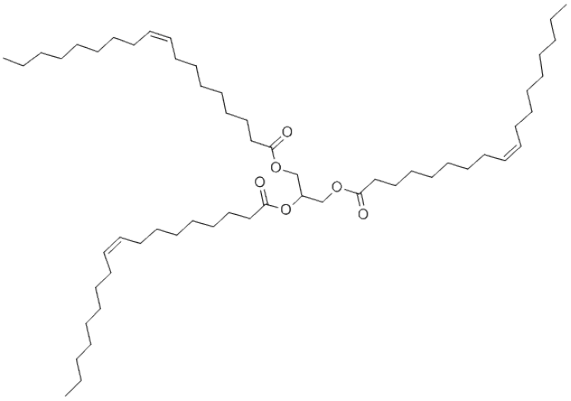 | GTO |

## 4.2 Pure Dodecane

The force profiles between mica surfaces across dodecane show both positive (repulsive) and negative (attractive) $F_N$ as $D$ is decreased, *i.e.*, oscillations in $F_N$ with respect to $D$ are observed as shown in Figure 23. Such oscillatory force profiles are observed for non-associating liquids when structured in ordered layers between two surfaces[10, 29]. The oscillatory forces are caused by the sequential squeeze-out of liquid layers, observed as repulsive walls at specific $D$ values which match a stable liquid

configuration – an integral number of layers – and attraction at intermediate thicknesses corresponding to unstable films.

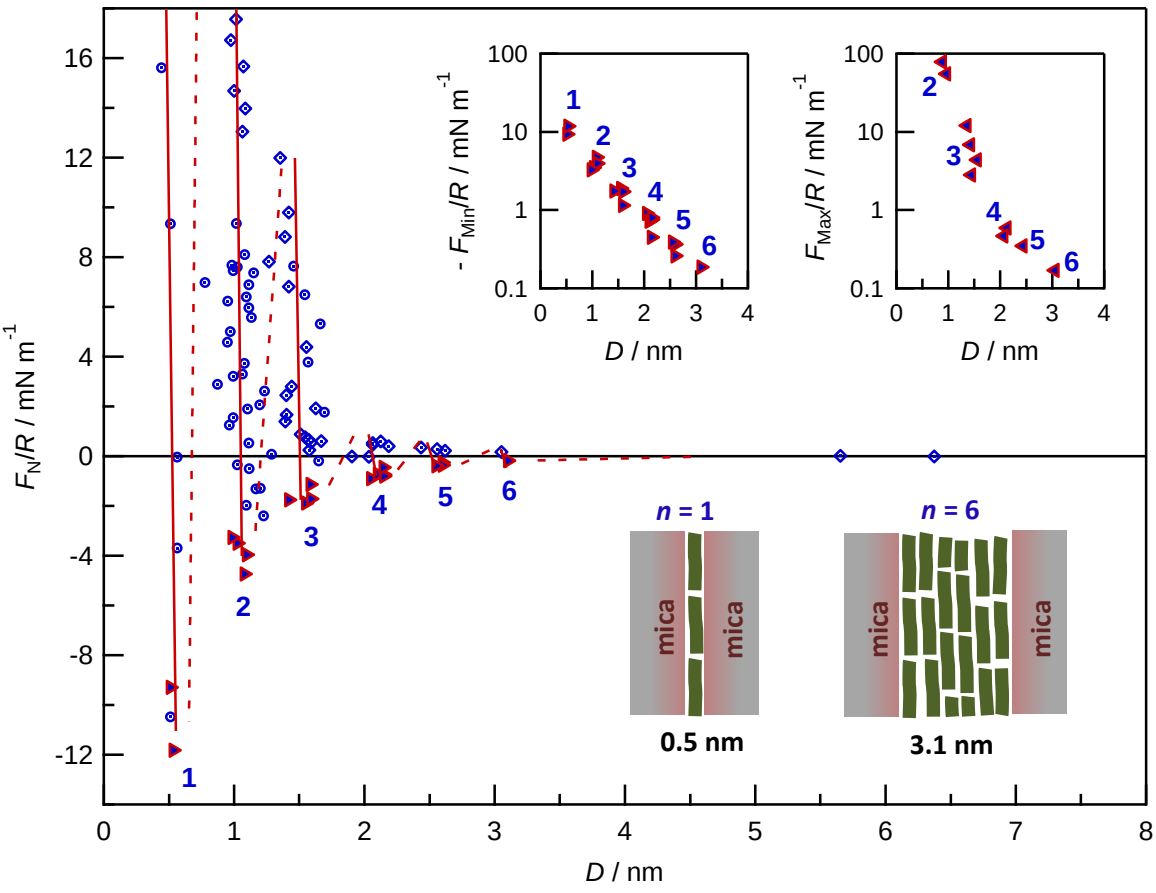


**Figure 23**

Experimental results for the force, $F_N/R$, measured between curved mica surfaces as a function of surface separation, $D$, across dry dodecane. Data points measured during approach and retraction of the surfaces (shown as diamonds and circles respectively) are represented by data from two separate experiments each using different pairs of mica pieces with particularly good distance resolution. Adhesive minima are shown as filled triangles and are from four separate experiments. The adhesive minima and repulsive maxima are also shown on logarithmic scales in the insets.

Retraction of the surfaces from any point on the force profile leads to a jump-apart of the surfaces from the nearest adhesive minimum (marked as filled triangles in Figure 23). These outward jumps are observed when using spring deflection to measure

attractive forces: on retracting the surfaces at a particular stable film thickness *D*, the spring will extend until the attractive force balances the elastic restoring force. Once the gradient of the attractive force $dF/dD$ exceeds the spring constant, *K*, the surfaces jump apart to large separations. This jump distance multiplied by *K* yields the force of adhesion at the minimum. Thus the positions of the repulsive walls in the oscillatory force profile, and in particular the location of these energy minima, can be used to determine the layering structure of the confined film.

The measured spacing between successive layers for dodecane, ~0.5 nm, corresponds to the width of the molecule rather than its length or any other average dimension, indicating a very parallel orientation near the surfaces and in agreement with previous surface force studies with even-numbered alkanes from hexane to hexadecane[58].

In these experiments six oscillations in the force profile can be measured, corresponding to up to six layers of dodecane molecules confined between the mica surfaces. The strong repulsive barrier at ~0.5 nm and resultant flattening of the surfaces prevented them from squeezing out the last molecular layer and approaching any further. In agreement with previous literature[10, 48, 58], the measured maxima in the force profiles were found to vary depending on the approach rate of the surfaces, with faster approaches resulting in higher measured forces required to squeeze out molecular layers. This suggests a kinetic barrier, most likely due to interlocking and entanglements of the chain molecules which hinder drainage of the liquid film from the gap in the contact zone. As a result of the flattening of the surfaces (due to elastic deformation of the glue behind the silver mirrors), the values of $F_N/R$ are overestimated for values above ~2 $mNm^{-1}$, shown clearly in the inset to Figure 23 as a deviation from simply exponential behaviour. The adhesive minima are on the other hand very reproducible, and vary exponentially down to one confined molecular layer.

At larger separations, a weak van der Waals attraction is measurable from ~6 nm. At a distance of ~3 nm there is an abrupt repulsion between the surfaces, corresponding to six confined molecular layers. This is accompanied by a reduction in the ambient vibration noise lateral to the surfaces shown clearly in Figure 24, in accordance with confinement induced liquid-to-solid phase transitions first observed for cyclohexane and OMCTS[49].

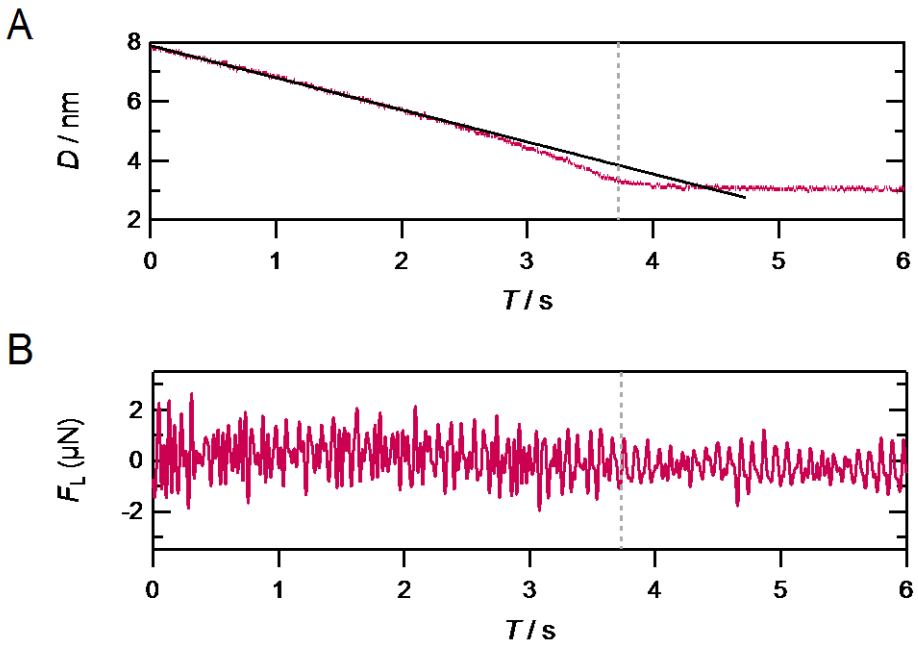


**Figure 24**

(A) A plot showing a thin film of dodecane confined initially to a film thickness of 8 nm then allowed to gradually approach under thermal drift. A weak attractive van der Waals force is observed at short range indicated by the deviation of the measured curve from the linear baseline, followed by a repulsive wall at 3 nm, which corresponds to 6 confined dodecane layers. (B) A direct recording from an oscilloscope showing the transition (marked by a grey dashed line) in ambient vibration noise in the direction lateral to the surfaces, for the distances shown in (A).

Shearing the surfaces laterally at this solidification distance (3 nm, $n$ = 6) results in stick-slip friction shown in Figure 25, as has been observed for molecularly confined films of hexadecane[53, 138]. A comparison of the kinetic friction forces for films of $n$ = 4, 5 and 6 are shown in Figure 26. For films of thickness $n \leq 3$, the kinetic friction force is too high to be measured with the spring constant and sliding distances used in these experiments, a problem exacerbated by much higher static friction forces required to initiate sliding for higher loads and thinner films. $F_{S,K}$ varies linearly with $F_N$, where the coefficient of friction, μ, is the proportionality constant.

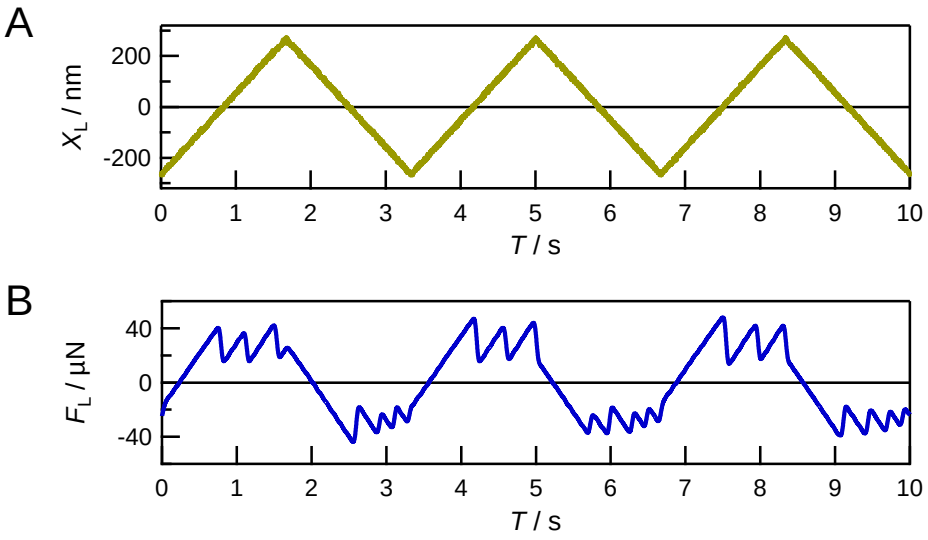


**Figure 25**

(A) Back-and-forth lateral displacement of one of the surfaces relative to the other at constant velocity ($v_S$ = 320 nms$^{-1}$) (B) Friction traces showing $F_L$ transmitted across a dodecane film at constant thickness ($n$ = 4) to the opposite surface at fixed load ($F_N$ = 6.1 μN).

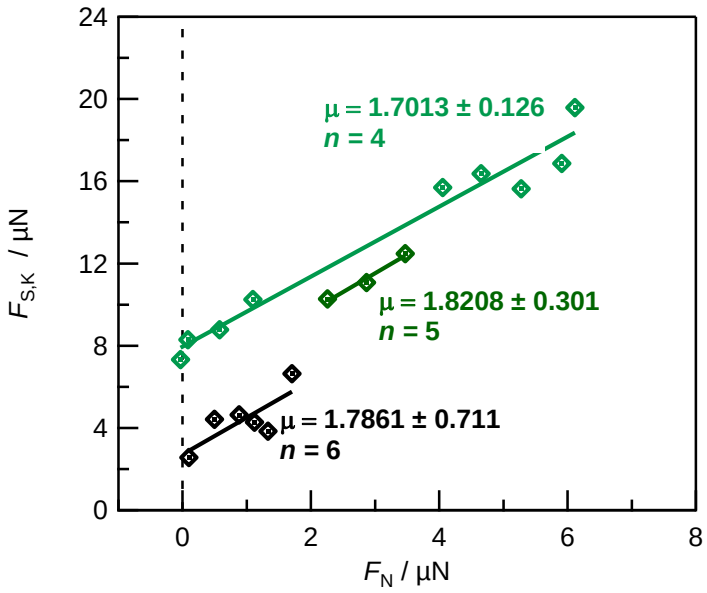


**Figure 26**

Normal and shear forces between mica sheets across different numbers of confined dodecane layers for one example experiment. The lines are linear fits to the data.

While friction forces across octane have previously been found to be both quantized and load dependent[139], tetradecane has a simple load dependence of friction regardless of the number of layers[140]. For dodecane, these friction measurements as a function of load suggest that the friction is load dependent but also quantized with respect to the number of confined molecular layers. Therefore dodecane seems to behave like octane in this regard. With longer chain hydrocarbons the molecules are less straight and rigid, and it is more likely for different segments of the same molecules to occupy different layers, and so the number of confined layers becomes less important in determining the friction.

The friction coefficients measured here for molecularly confined dodecane films appear to be constant irrespective of the number of confined layers, and only the adhesion contribution to friction is different. This is expected from the oscillatory nature of the

force profiles, with adhesive minima increasing in magnitude for thinner films (Figure 23 inset). These friction coefficients ($\mu \geq 1$) are comparable to several previous experiments with tetradecane and hexadecane[54, 141], however other contrasting studies have shown lower friction coefficients ($\mu \sim 0.1$) for the same molecules at similar sliding speeds[95]. Additionally, different quantized friction regimes have been shown for two and three layers of hexadecane[142] which is not expected from the above rationalisations. These discrepancies in the literature have not yet been properly explained but may be ascribable to differences in the confined film structure. This could perhaps be due to varying rate of confinement[143], sliding direction and twist angle of the confining surfaces with respect to crystallographic alignment[144], together with different in-plane ordering of molecules[145-146] contributing to the measured friction.

## 4.3 Glycerol-based Surfactant Solutions

Adding small concentrations of GMO to dodecane disrupts the layering adjacent to the surfaces. Instead of the oscillatory force for dodecane, a repulsive wall at a much larger thickness of ~5.1 nm is observed (Figure 27). By comparing with van der Waals dimensions of the molecules, this distance suggests a perpendicular alignment of the surfactant molecules forming an upright monolayer at each surface. A small adhesive force is measured – which is always the same magnitude and jumps out from this same distance even after large pressures are applied. Forces resemble those between surfactant coated mica surfaces across alkanes[147].

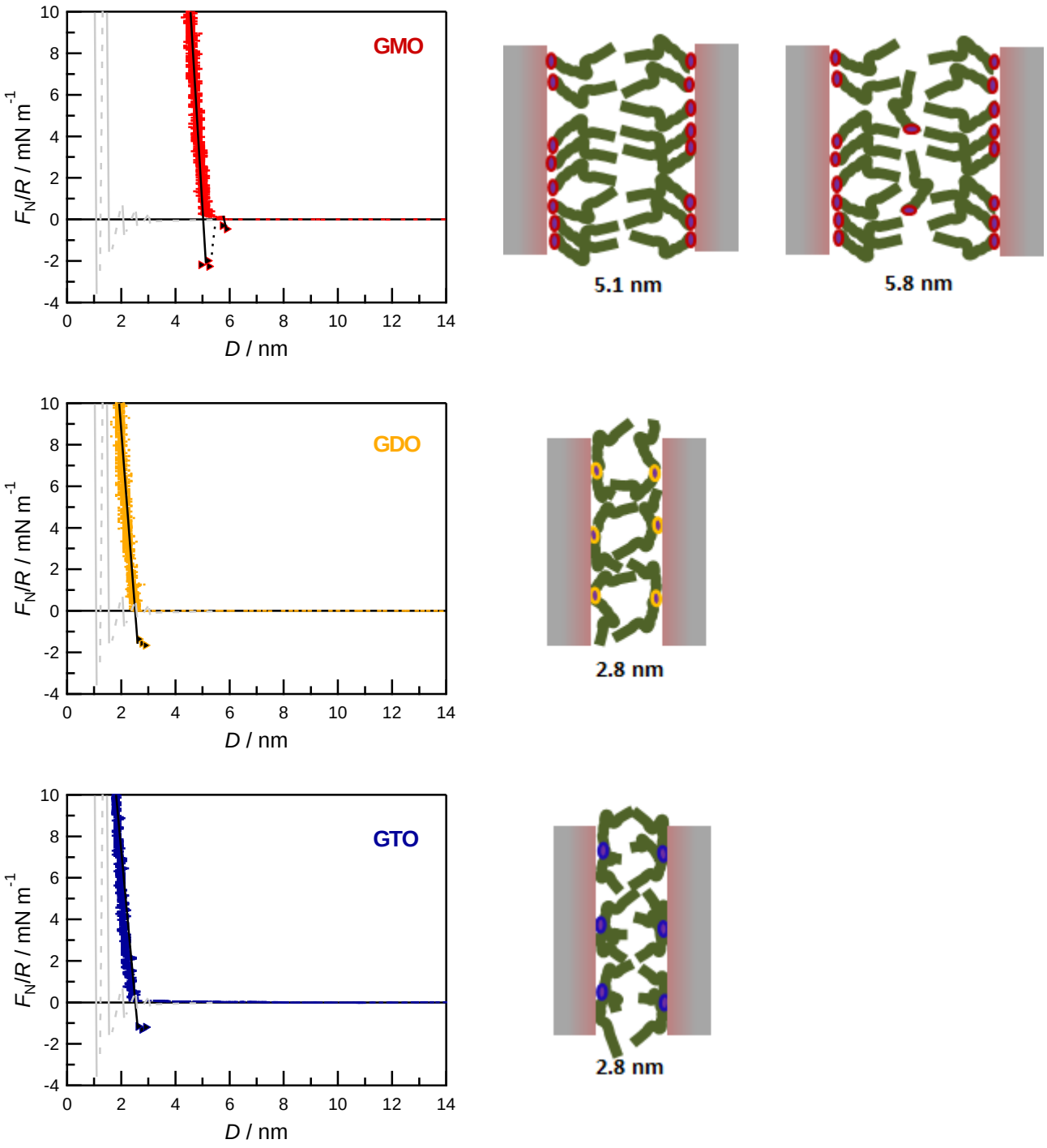


**Figure 27**

Experimental results for the force, $F_N/R$, between curved mica surfaces as a function of surface separation, $D$, across 1 wt% solutions of GMO, GDO and GTO in dodecane. The measured forces are reproducible to within 0.3 nm over different experiments and over different contact areas within an experiment, but for clarity the repulsive walls are represented by one particular approach. Adhesive forces shown are averages for several

different contact areas of the mica sheets. Also shown for comparison are the measured results for pure dodecane from Figure 23, represented by grey lines.

Also observed is a much weaker secondary adhesive minimum ~7Å larger than the film thickness for two monolayers contacting each other. This appears to be due to a thin layer of mixed GMO and dodecane molecules lying mostly parallel to the surface between the GMO monolayers. This adds further evidence to the suggested film structure consisting of adsorbed surfactant monolayers at the surfaces, since a possible film of confined reverse micelles would have comparable dimensions to two contacting monolayers. Reverse GMO micelles which must exist in the bulk liquid appear to be squeezed out from the film too easily to be detected in these measurements.

At the highest applied pressures (not shown on the scale of Figure 27), GMO solutions can be compressed to ~2.0 nm, while GDO and GTO solutions can be compressed to ~1.1 nm. The compressibility can be attributed to continuous tilting of the molecules with increasing force, however these thickness values may be slightly underestimated since the mica pieces themselves may have some compressibility at these large loads (although to a much lesser extent than the monolayers themselves[148]).

For GDO solutions, there is again no dodecane layering, but the film thickness is approximately half that for GMO. This suggests that the GDO molecules adsorbed at the surface lie with their hydrocarbon chains slightly more parallel to the surface compared to GMO. They are unlikely to lie completely flat, otherwise some molecular layering of both surfactant and solvent parallel to the surfaces would be expected. Such a disordered structure is akin to that of branched alkanes in confinement[149]. The different orientation of the GDO chains compared to GMO could be due to conformational restriction from having an extra hydrocarbon chain attached to the headgroup, but can also simply be explained by a lower surface coverage. In fact, the normal force measurements for GTO solutions are remarkably similar to those for

GDO, indicating similar molecular orientations and film structure when three hydrocarbon chains are attached to the headgroup.

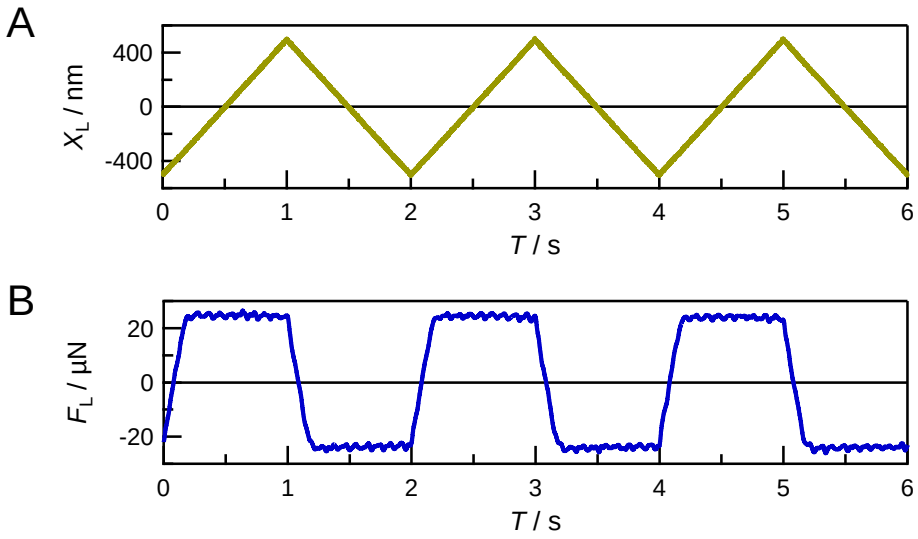


**Figure 28**

(A) Back-and-forth lateral displacement of one of the surfaces relative to the other at constant velocity ($v_S$ = 1001 nms$^{-1}$) (B) Friction traces showing $F_L$ transmitted across a 1 wt% solution of GMO in dodecane to the opposite surface at fixed load ($F_N$ = 4.2 mN, $D$ ~ 3 nm).

Recording high resolution traces of $F_L$ as a function of lateral displacement of the top surface for a range of $F_N$ and $v_S$ reveals smooth sliding (as shown in Figure 28) at the kinetic friction force, $F_{S,k}$. It is notable that $F_{S,k}$ is very low, and independent of $v_S$ over the range of $v_S$ investigated. Once the direction of applied lateral motion is reversed, similar smooth sliding behavior is observed in the opposite direction. Both the normal and shear forces measured 15 minutes after injection of the liquid remain unchanged after several hours, indicating that adsorption to the surfaces from solution occurs quickly. Additionally, no discernible changes in the normal force profiles occur after performing shear measurements, as long as there is no wear or re-cleaving of either surface. Similar normal and shear forces are in fact measured even for concentrations

as low as 0.05 wt%. This is much lower than the critical micelle concentration for GMO in dodecane, which is approximately 0.15 wt%[150].

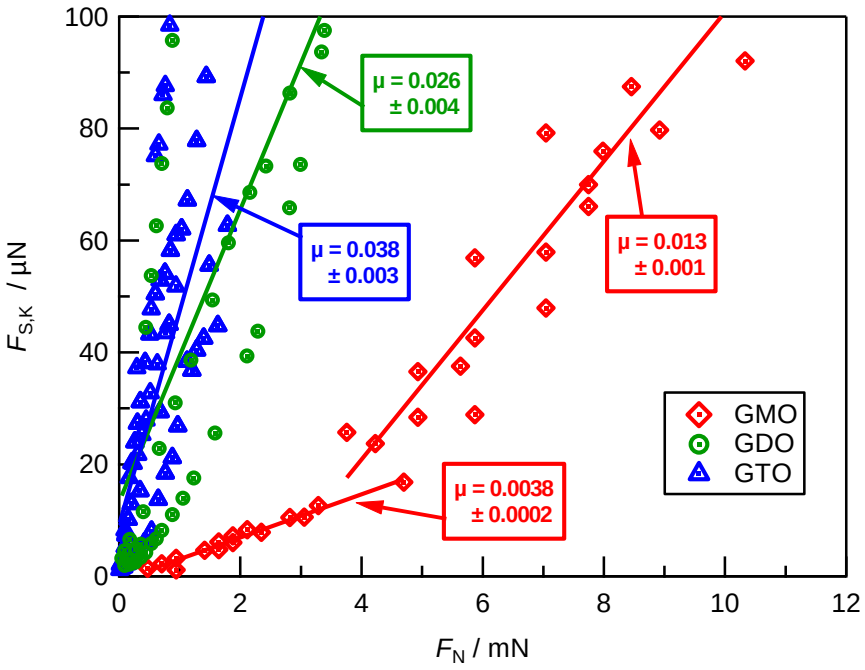


**Figure 29**

Normal and shear forces between mica sheets across 1 wt% solutions. Data shown from at least two independent experiments using different mica pieces for each solution.

Experiments with GMO solutions were found to be highly reproducible, with very little scatter in the measured $F_{S,k}$ as a function of $F_N$ when comparing between different experiments and different contact areas within an experiment. This seems to suggest a high and even monolayer coverage. Adsorption of analogous fatty acids onto steel from non-polar solutions has been shown to result in adsorbed amounts of only about one half of that for a close packed monolayer[151]. However this difference could be explained by the different chemistry of the glycerol headgroup resulting in very favourable hydrogen-bonding interactions between neighbouring headgroups of the molecules in the monolayer. On the other hand for both GDO and GTO there is increased scatter in the friction forces for different contact areas (although the normal forces are extremely

reproducible) which suggests a somewhat patchy adsorption of surfactant with likely co-adsorption of dodecane at the surfaces.

For GMO solutions there is a low friction regime (μ = 0.0038) and a higher friction regime (μ = 0.013). The transition occurs generally in the range of loads $F_N$ = 3-6 mN, depending on the particular contact area. Although this change in friction behavior is likely to be due to the change in tilt angle or slight interdigitation of the GMO monolayers as they are increasingly confined, there does not seem to be a reproducible particular film thickness at which this occurs. The presence of a lower friction regime can similarly be observed for GDO and GTO solutions, however it occurs at much lower loads ($F_N$ < 1 mN) and is not always present depending on the particular contact point.

## 4.4 Mixtures of Surfactant Solutions

Given the contrasting structural and frictional properties of the different surfactants, it becomes useful to examine the behaviour of mixtures, given that GDO and GTO are often present in trace amounts in commercially available GMO samples. Results for an equal mass mixture GMO/GTO (making up a total concentration of 1 wt% additive) are shown in Figure 30 (top graph). The forces and distances are extremely similar to those measured for pure GMO solutions shown in Figure 27 apart from a few subtle differences.

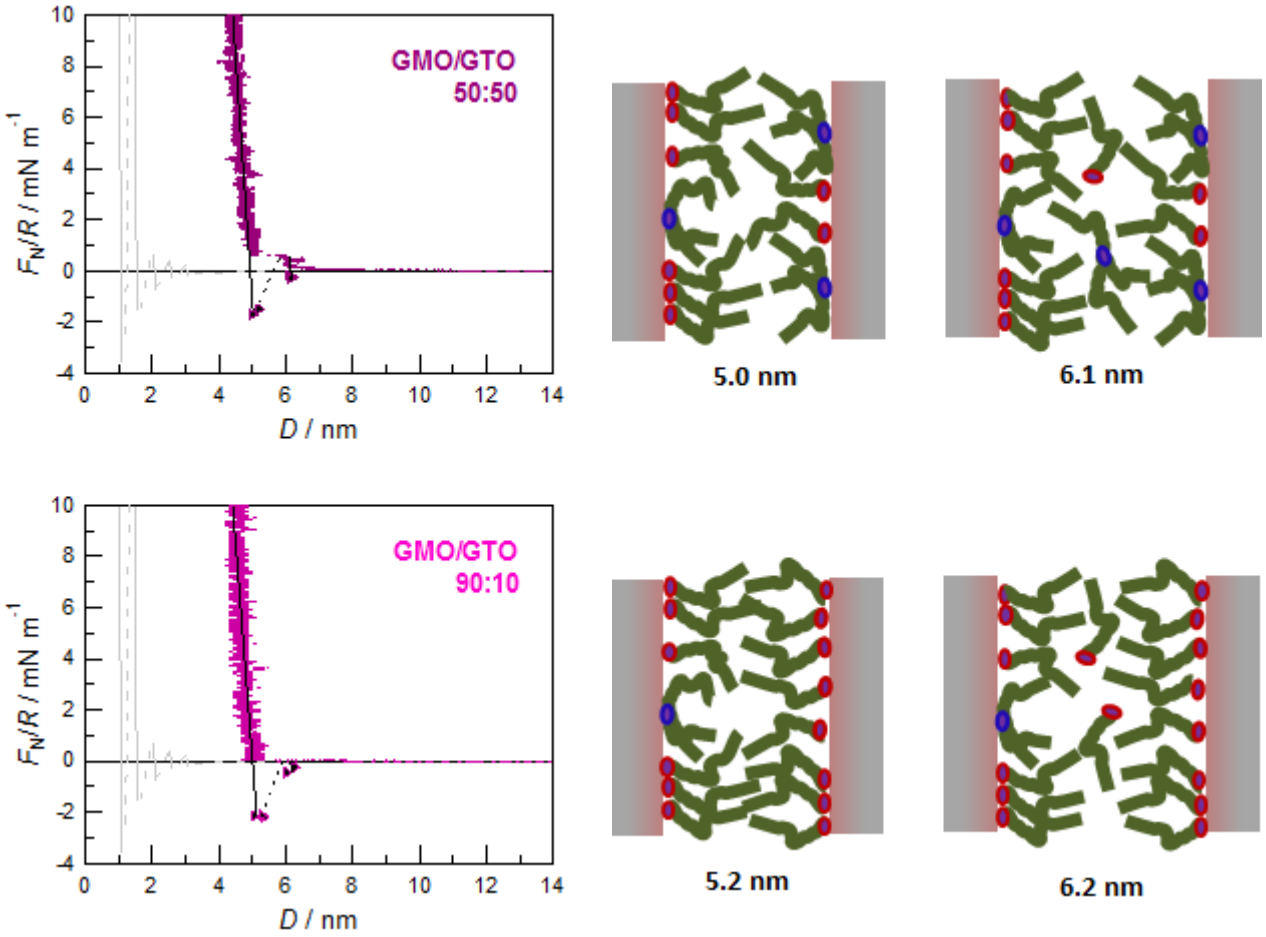


**Figure 30**

Experimental results for the force, $F_N/R$, between curved mica surfaces as a function of surface separation, $D$, across 1 wt% mixed solutions of GMO and GTO in dodecane: data is shown for 50:50 (top) and 90:10 (bottom) mass ratio of GMO:GTO. The measured forces are reproducible to within 0.3 nm over different experiments and over different contact areas within an experiment, but for clarity the repulsive walls are represented by one particular approach. Adhesive forces shown are averages for several different contact areas of the mica sheets. Also shown for comparison are the measured results for pure dodecane from Figure 23, represented by grey lines.

While the primary repulsive wall occurs at a very similar film thickness, the adhesion is slightly weaker. This distance likely corresponds to the upright GMO molecules contacting each other, but GTO molecules also adsorbed at the surfaces reduces this

contact adhesion. The distance difference between the primary and secondary adhesive minima is also a few Angstroms larger for the mixture, since the GTO molecules which are present are less likely to lie parallel to the surface with the other dodecane molecules, hence taking up slightly more space. Similar conclusions can be drawn from the 90:10 mixture also shown in Figure 30, but in this case the normal forces are even more similar to the pure GMO solution.

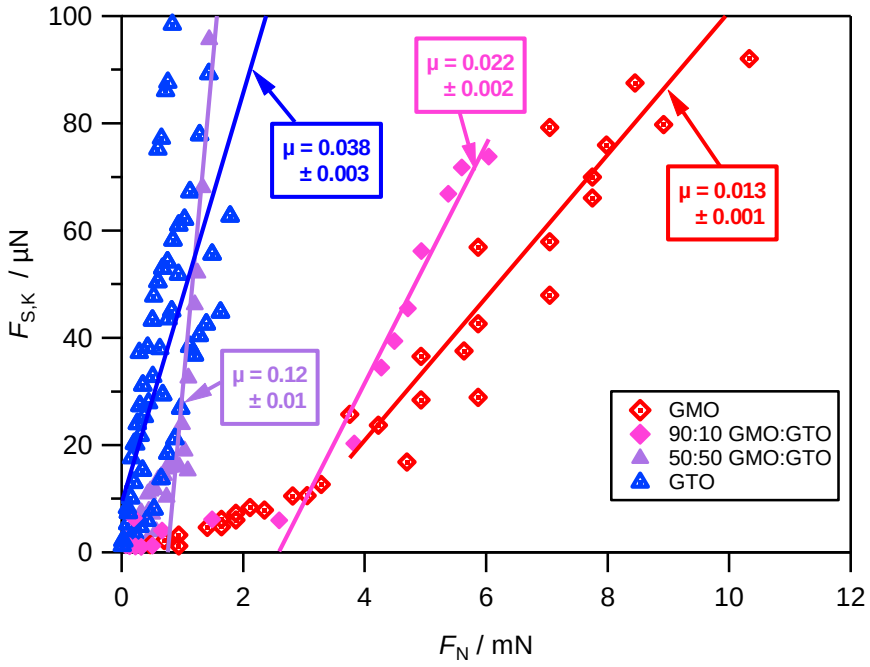


**Figure 31**

Normal and shear forces between mica sheets across 1 wt% mixed GMO/GTO solutions in dodecane: data is shown for 50:50 and 90:10 mass ratio of GMO:GTO. Also shown for comparison is the measured data for the pure GMO and GTO 1 wt% solutions.

Interestingly, it appears that mixing GMO and GTO more equally results in higher friction coefficients than for either of the pure surfactants (Figure 31). This is most likely due to significant interpenetration and interdigitation between the GMO and GTO domains of opposing surfaces, which could cause significant pinning of the film and consequently higher friction forces. For smaller amounts of added GTO the increase in

friction is small, suggesting the effect of trace impurities is not of great concern. However these results show that other surfactants often present in lubricant formulations in large amounts, can very much complicate the friction if they have varied shapes and sizes and are also surface active.

## 4.5 Comparison Between Mica-Mica and Mica-Metal Surfaces

Smooth metal surfaces for surface force measurements can be prepared by template stripping from mica either with glue[125] or by diffusion bonding[152], typically affording RMS roughnesses 0.2-0.4 nm. Rougher surfaces can be prepared by evaporation directly onto mica immediately before the experiment, with resulting RMS roughnesses in the range ~1-1.5 nm. In this section measurements were made between one mica surface and one metal surface, with the metal surface also acting as the mirror for FECO interferometry in a two-layer interferometer.

Normal force measurements for a 1 wt% solution of GTO in dodecane across mica and silver surfaces gave very similar distances compared to those for the liquid between two mica surfaces. However the exact film thickness is not meaningful at a molecular level since the asperities of the silver are elastically deformed in strong adhesive contact during the air calibration, and hence the measured liquid film thickness appears comparatively thicker when the asperities are undeformed. Relatedly, the adhesion of the contacting monolayers also decreases with increasing roughness as expected.

Although there is scatter between different experiments and contact areas within an experiment, friction across the film seems lowest when two mica surfaces are used (Figure 32). One immediate explanation is a greater surface affinity of the surfactant

molecules to the mica surface. However it appears that the friction is slightly higher for a rougher silver film compared to one template stripped from mica, and so the lower friction observed between mica surfaces may be due to its atomically smooth surface.

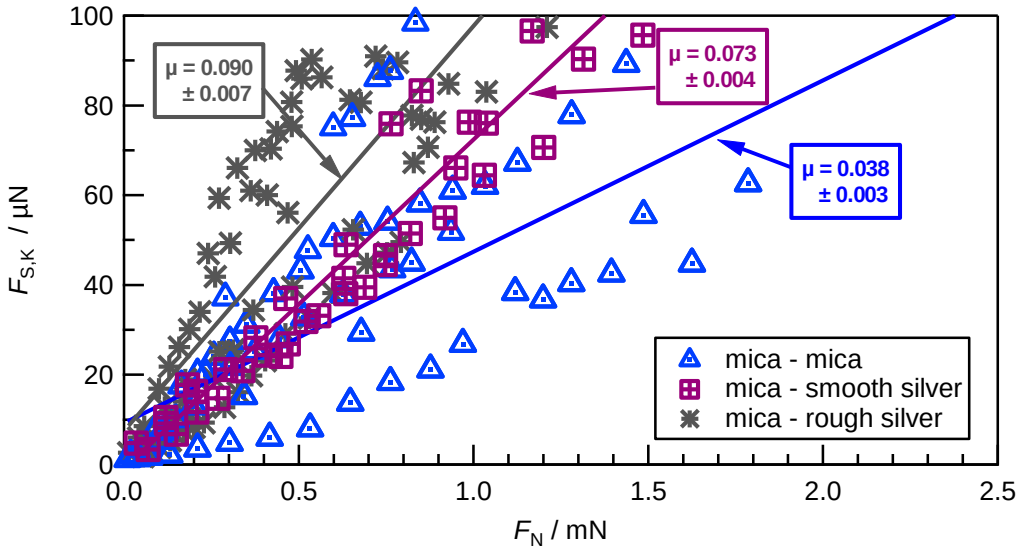


**Figure 32**

Normal and shear forces measured between mica sheets across 1 wt% solutions of GTO in dodecane between mica and silver surfaces.

## 4.6 Summary

Control experiments with the pure solvent, dodecane, revealed solid-like layers exhibiting high friction and with stick-slip behaviour. Variability in friction coefficients from experiment to experiment and between different research groups makes this a very interesting topic but beyond the scope of this chapter, which focuses on friction modification by various surfactants. Nevertheless it is useful to measure the structural and shear properties of the pure alkane base oil for comparison and to establish purity.

Each of the friction modifiers studied (GMO, GDO and GTO) significantly reduce friction compared to the dodecane base oil, although GMO provides the most efficient lubrication. GMO forms adsorbed, upright monolayer structure. Friction is smooth sliding with low friction coefficients ($\mu \leq 0.013$). GDO and GTO also preferentially adsorb to the surfaces and significantly reduce the friction across the base oil.

While the adsorbed GMO monolayer structure dictates the normal forces in mixed solutions, it is clear from the shear measurements that there are significant amounts of GTO also present in the films. Importantly, the results presented in this chapter demonstrate that whilst small fractions of GTO 'contamination' in GMO solutions will not cause hugely detrimental effects or the lubrication of sliding surfaces, a larger fraction of GTO (equal to GMO by mass) causes a substantial increase in the friction coefficient. Since the mechanism is likely to involve disruption of the uniform GMO layer, similar disruptive outcomes are likely to arise with other competing surface-active components and this should be an important direction for future study.

# 5 STRUCTURE OF PURE IONIC LIQUIDS CONFINED TO NANO-FILMS

## 5.1 Introduction

Ionic liquids have a wide variety of applications in confined films, ranging from nanoparticle stabilisation to lubrication and their use as novel electrolytes. Perhaps the most exciting applications involve their use as electrolytes for energy storage devices[153], which has driven recent research to further explore the properties of ionic liquids at electrochemical interfaces[118, 154]. Nanoporous electrodes have in particular attracted considerable attention owing to their enhanced capacitance properties when ion dimensions match pore sizes[155-159].

The behaviour of ionic liquids in narrow pores and in thin films is complex compared to that of the bulk liquid[160]. In recent years it has become generally well established that ionic liquids can form layered structures of alternating cation- and anion-enriched layered structures at surfaces, which arise due to surface charge or preferential adsorption of a particular ion. Such structures have been experimentally verified by x-ray reflectivity[105-106], atomic force microscopy[107, 111, 161-164], and surface force measurements[108, 120-121, 165]. However the double layer properties have been the subject of active discussion[166-170], with the results of this chapter contributing to this new understanding.

Pyrrolidinium-based ionic liquids have similar melting points and viscosities compared to the most commonly studied imidazolium-based analogues[171]. The major driving force

for their study at surfaces so far has been for electrochemical applications, due to their large electrochemical windows[172-173] as compared to other ionic liquids. In this chapter, surface force measurements were used to investigate the structuring of a series of dialkylpyrrolidinium and imidazolium-based ionic liquids of different alkyl chain lengths confined between negatively charged mica surfaces.

**Table 2** A summary of the ionic liquids investigated here

| Name | Chemical Structure | Abbreviation |
|---|---|---|
| 1-butyl-1-methylpyrrolidinium *bis*[(trifluoromethane)sulfonyl]imide | 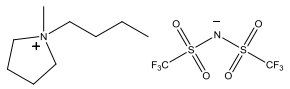 | $[C_4C_1Pyrr][NTf_2]$ |
| 1-hexyl-1-methylpyrrolidinium *bis*[(trifluoromethane)sulfonyl]imide | 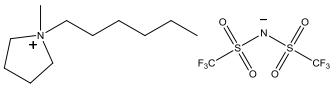 | $[C_6C_1Pyrr][NTf_2]$ |
| 1-octyl-1-methylpyrrolidinium *bis*[(trifluoromethane)sulfonyl]imide | 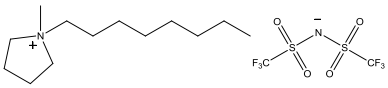 | $[C_8C_1Pyrr][NTf_2]$ |
| 1-decyl-1-methylpyrrolidinium *bis*[(trifluoromethane)sulfonyl]imide | 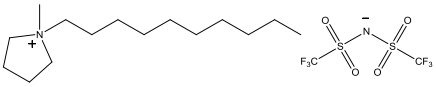 | $[C_{10}C_1Pyrr][NTf_2]$ |
| 1-butyl-3-methylimidazolium *bis*[(trifluoromethane)sulfonyl]imide | 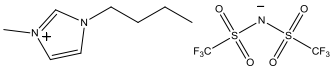 | $[C_4C_1Im][NTf_2]$ |
| 1-hexyl-3-methylimidazolium *bis*[(trifluoromethane)sulfonyl]imide | 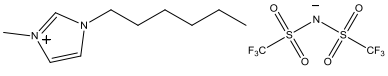 | $[C_6C_1Im][NTf_2]$ |

## 5.2 Structural Forces Across Confined Ionic Liquids

Force profiles for $[C_nC_1Pyrr][NTf_2]$, with $n$ = 4, 6, 8 and 10, are reported in Figure 34 and show results from 2-6 different experiments (each employing different mica pieces) for each ionic liquid. For $n$ = 4, 6 and 8, the force profiles show oscillations in $F_N$ with

respect to *D* as observed previously for other ionic liquids[108, 113, 120-121, 174] and non-polar liquids[10, 29] when the liquid is structured in ordered layers between the surfaces. The force profiles obtained are similar: each shows four distinct energy minima at similar *D* values for the three ionic liquids (*n* = 4, 6 and 8). The repeat distances are indicative of cation-anion layer structure in the films, based on electrostatic and geometric arguments, as follows.

i. In order to preserve electroneutrality of the confined ionic liquid, each maximum in the force law must represent squeeze-out of an equal number of cations and anions.

ii. The difference in separation between the repulsive walls is close to the thickness of an ion pair, or a cation layer adjacent to an anion layer, with the cation hydrocarbon tails in the plane of the surfaces.

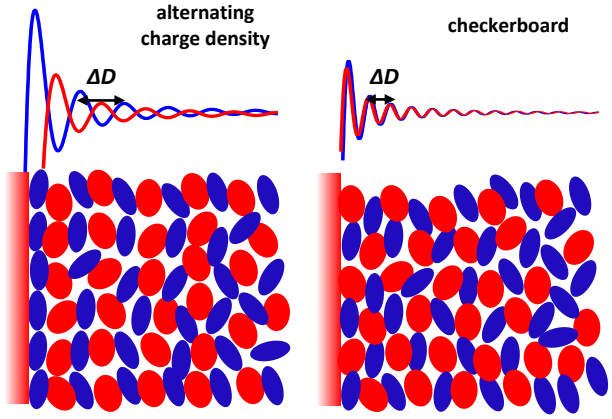


**Figure 33**

Possible layering arrangements of ionic liquid ions at a charged surface

Together, these arguments (as well as simulation studies[115, 117]) strongly imply that the layers are arranged as stacks of alternating cation-anion layers. This interpretation of the oscillatory forces is in line with previous studies of other ionic liquids at surfaces and in confined films[107-108, 120-121, 161]. If the structure was instead composed of a 'checkerboard' structure, with equally mixed cations and anions in each layer, the

oscillatory period in these experiments should be almost half of what is typically observed. The mismatch in size and shape of the ions would also not be expected to lead to such strong oscillatory forces.

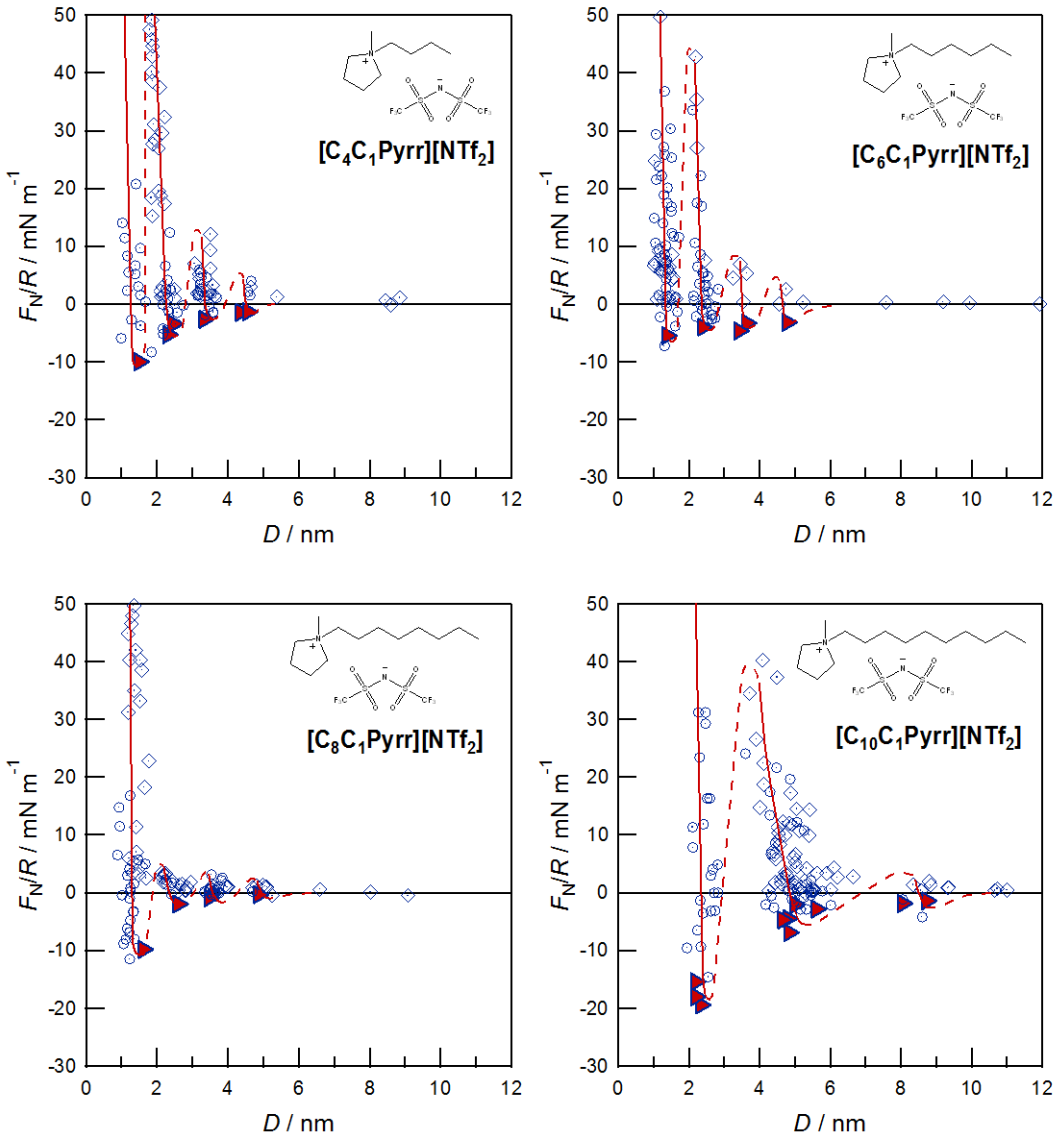


**Figure 34**

Experimental results for the force, $F_N/R$, measured between curved mica surfaces as a function of surface separation, $D$, across ionic liquids $[C_nC_1Pyrr][NTf_2]$, with $n$ = 4, 6, 8 and 10, confined between mica surfaces.

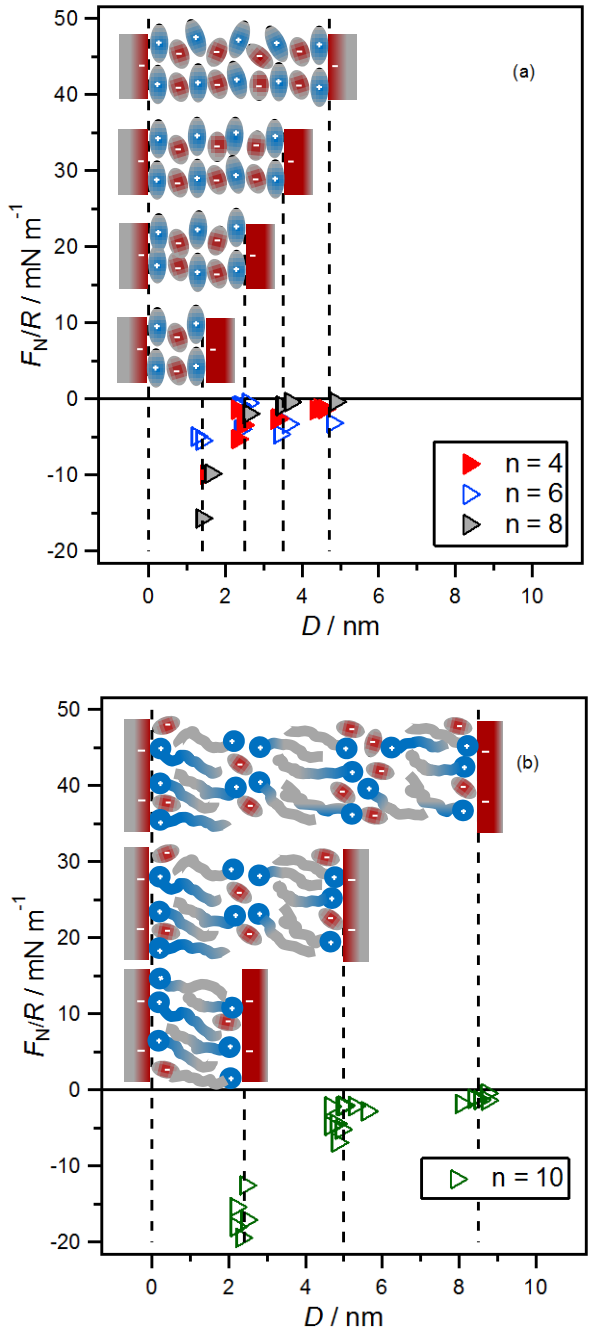


**Figure 35**

Measured force minima and suggested ion arrangements for the (a) monolayer- and (b) bilayer-forming pyrrolidinium-based ionic liquids studied here

For $[C_nC_1Pyrr][NTf_2]$, with $n$ = 4, 6 and 8, the closest minimum is at $D \approx 1.4$ nm. This thinnest film most likely corresponds to three ion layers ($i$ = 3) due to the requirement

for excess cations in the film to neutralise the negative mica charge[175]: next to each negatively charged mica surface lies an electrostatically bound layer of cations, with an intermediate 'sandwiched' layer consisting mostly of anions. Similarly, for larger *D* at 2.5 nm, 3.5 nm and 4.5 nm, there are stable configurations corresponding to 5, 7 and 9 ion layers (*i* = 5, 7 and 9) respectively, as depicted in Figure 35. The film could not be squeezed down to a single cation layer (*i* = 1) for these pyrroldinium-based ionic liquids under the forces applied here, but for other ionic liquids such as those with an imidazolium cation this usually occurs at sufficiently high enough loads[108].

The similar layer repeat distances for these three liquids of different cation alkyl chain lengths suggest that the cations tend to lie with their alkyl chains parallel to the surface (Figure 35a). However the significantly weaker force magnitudes exhibited by $[C_8C_1Pyrr][NTf_2]$ could indicate the alkyl chains starting to cause disorder in the interfacial structure and this could be a hint as to the structuring transition observed between *n* = 8 and *n* = 10.

As seen from Figure 34, the situation is more complex for $[C_{10}C_1Pyrr][NTf_2]$. This liquid exhibits strong oscillatory forces – indicating a layered structure in the film – but with repeat distances too large to be explained simply by squeeze-out of a single cation-anion layer. Repeating the experiment with samples from different synthesis batches gave identical results, strongly suggesting that the ionic liquids are highly pure and that this different interfacial structure is not an effect of contamination. To explain the observed larger *D* values it is important to note that ionic liquids with more amphiphilic cations (i.e. containing longer alkyl chains) can self-assemble into structures which collect together the polar and non-polar moieties[176-178].

These measurements suggest that such self-assembly occurs for $[C_{10}C_1Pyrr][NTf_2]$ confined to films between mica surfaces. The clear oscillations indicate an ordered and repeating structure, most feasibly consisting of bilayers confined between the surfaces.

The self-assembly is most likely driven by the unfavourable interface between hydrocarbon and charged groups relative to more favourable ion-ion interactions. However, when comparing the layer thickness with the ion dimensions it is clear that there must be significant, if not full, interdigitation of the decyl chains in its bilayer structure; the extended length of the cation including van der Waals radii is ~1.9 nm, while the observed thickness of the bilayers is 2.3-2.8 nm. Thus it is reasonable to assume that for this $[C_{10}C_1Pyrr][NTf_2]$ ionic liquid, three stable confinement-induced layer configurations are observed consisting of one, two, or three layers of interdigitated cation bilayers; shown schematically in Figure 35b. The bilayer thickness increases slightly for thicker and less confined films, indicating a reduced amount of interdigitation.

These observed layering structures in confined films differ from the sponge-like and percolating structures observed in bulk ionic liquids[176-178]. The difference is likely to be due to a combination of the ion-surface interactions, the symmetry breaking effect of the surface, and the entropy loss due to confinement. The bulk structure of pyrrolidinium-based ionic liquids also has increased ordering on the mesoscale as alkyl chain length increases[179], with the observation of a first sharp diffraction peak in X-ray scattering experiments indicating nanostructure when $n > 8$. This transition in bulk structure is likely to be due to similar inter-ionic forces as the structuring transition reported here, although in the bulk liquid structure the transition is gradual with the peak growing as $n$ increases, compared to the discontinuous change reported here for a confined liquid film. The suggested interdigitated chain structure for the bilayers fits well with the data observed here and bears notable resemblance with the bulk crystal structures however there are other possible conformations such as *crumpled* or *tilted* alkyl chains in the bilayers which cannot be excluded.

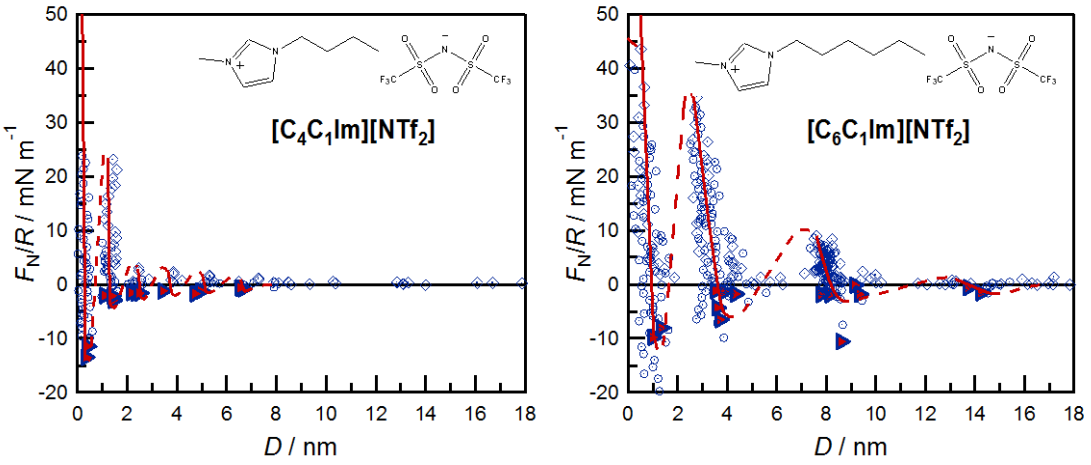


**Figure 36**

Experimental results for the force, $F_N/R$, measured between curved mica surfaces as a function of surface separation, $D$, across ionic liquids $[C_nC_1Im][NTf_2]$, with $n$ = 4 and 6, confined between mica surfaces.

Similar experiments with 1-alkyl-3-methylimidazolium-based analogues are shown in **Figure 36**, and also show pronounced oscillatory forces. While $[C_4C_1Im][NTf_2]$ shows very similar film thicknesses for stable structures to the monolayer-forming pyrrolidinium-based ionic liquids, increasing the chain length of the cation from butyl to hexyl results in a dramatically different interfacial structure for $[C_6C_1Im][NTf_2]$. This is attributed to a flip from monolayer to bilayer structure, as explained for $[C_{10}C_1Pyrr][NTf_2]$. However a closer inspection of the bilayer repeat-spacing compared to ion dimensions reveals differences in the bilayer structure of $[C_6C_1Im][NTf_2]$ compared to $[C_{10}C_1Pyrr][NTf_2]$: the $[C_6C_1Im]^+$ cations adopt an end-to-end orientation, with little or no interdigitation of the alkyl chains in the bilayers. The origin of this contrasting bilayer structure, and the differing chain length at which the monolayer-to-bilayer crossover occurs is discussed in detail in section 5.4.

## 5.3 Analysis of Monolayer Structures

Two general features of all of the force profiles here are worth noting: (a) for a given liquid, the *period* of oscillation is somewhat larger for thicker films, indicating ion packing that is less perfect (or layers which are more dynamic or disordered) with increasing distance from the surface. The electrostatic interactions result in ions nearest to the surface being held more tightly, with ions further away exhibiting more fluid-like behaviour within a layer. Interestingly, even neutral non-polar molecules behave in a similar manner when confined between mica,[180] suggesting that the liquid molecules simply pack more efficiently adjacent to a surface irrespective of charge. (b) The oscillatory profiles show greatest magnitude of force for the close mica-mica separation distances and decreasing *amplitude* as the mica-mica separation increases. Thus a greater force is required to disrupt the layering for thinner films, and this is likely to be related to decreasing ion-purity – either excess of anions or cations in a particular layer – which decays exponentially from the surface.

Is the structure observed in confined liquids induced by the confinement itself, or is the order present at each individual surface independently of the other? Although the results of these oscillatory force profiles seem qualitatively similar to those of spherical non-polar liquids[10, 29, 181] and even linear alkanes[58], the origin of structuring could be very different. For non-polar molecular liquids, layered structures upon confinement to thin films are only observed for molecules with a high degree of symmetry which are able to pack together efficiently at film thicknesses corresponding to integral numbers of molecular layers. Importantly, high pressures are not required, suggesting that this liquid to solid-like phase transition is due to geometric constraints alone.[49] Not unexpectedly, mixtures of liquids with differing molecular dimensions such as the addition of cyclohexane to OMCTS[47] leads to a reduction in both the range and magnitude of the structural force with increasing mole fraction of either of the liquids.

Ionic liquids, with their asymmetric ion shapes and frequent mismatch in size between cations and anions, would not be expected to form such rich, layered structures induced by confinement alone. Indeed, experiments using a similar apparatus with ionic liquids between ultrasmooth methyl-terminated surfaces (SAM-coated mica) exhibit no pronounced layering[121]. X-ray reflectivity data has drawn similar comparisons about ionic liquid structure at a single, charged surface such as mica and at uncharged graphene.[175]

Instead of simply being confinement-induced, the layering structure observed in ionic liquids is charge-templated and has been observed in many systems as long as the surfaces hold a net charge[117, 122]. In the case of the mica surfaces used here, the origin of the negative charge is dissolution of $K^+$ ions from the (001) plane leaving a negative charge shared between oxygen atoms on the underlying aluminosilicate layer. The solubility of $K^+$ in these pyrrolidinium ionic liquids is high[182], and the ion-exchange of $K^+$ for imidazolium on mica[183] appears to also be favourable, together providing the driving force for removal of the $K^+$ in the ionic liquids. The maximum possible density of negative charge on the mica surface, $1e$ / 0.48 $nm^2$ (which would arise if every $K^+$ ion is dissociated), is close to approximately *half* the positive charge density on a full monolayer of [$C_4C_1$Im] cations[108].

Indeed, it appears from the force profile for all the ionic liquids studied here the positive charge density of the first cation monolayer is greater than the negative charge density of the mica surface. Thus a full cation monolayer which is attracted to the negative surface *overscreens* the surface charge and kicks-off an oscillation between positive and negative overscreening, as has been well documented[117, 184]. Thus the force measured between two mica surfaces, each 'dressed in its own ion layers', is in fact the result of interference between the two ordered structures emanating from each surface.

## 5.4 Analysis of Bilayer Structures

The monolayer-to-bilayer transition and the resulting bilayer architecture for the pyrrolidinium-based ionic liquids differs in two ways to that of their imidazolium-based analogues, and in this section the molecular origins are qualitatively accounted for.

**(1) The crossover from monolayer to bilayer behaviour occurs at different chain lengths for imidazolium- and pyrrolidinium-based ionic liquids with the same anion.** For imidazolium cations the crossover in behaviour occurs between alkyl chain lengths of 4 and 6 carbons, whilst for pyrrolidinium cations the crossover is between 8 and 10 carbons. This is likely due to more favourable cation-cation interactions in the case of imidazolium cations: the planar delocalised rings can interact favourably through π-π stacking[185-186], allowing close approach of the alkyl chains and favourable dispersion interactions in the non-polar regions. Pyrrolidinium cations, on the other hand, cannot stack at such close spacing and so require longer alkyl chains to drive bilayer formation. Atomistic molecular dynamics simulations of the same imidazolium-based ionic liquids studied here have revealed an equivalent crossover in orientational ordering at a mica surface[187]: imidazolium cations with ethyl or butyl groups were found to lie with their alkyl tails parallel to the surface, while cations with hexyl or octyl tails were oriented perpendicular to it. Cation orientation at a silica surface seems to similarly depend on alkyl chain length, regardless of anion.[188] Bulk nanostructure appears at equivalently longer alkyl chain lengths for pyrrolidinium compared to imidazolium ionic liquids[104, 189]. The weaker force magnitudes measured for confined $[C_8C_1Pyrr][NTf_2]$ are another hint as to the origin of the structural transition: the longer alkyl chains mean that the ion occupies more area within a layer in monolayer structures. This anion-cation area mismatch eventually frustrates the monolayer structure and favours bilayers.

**(2) The layer thickness of the bilayers indicates qualitatively different architectures for imidazolium- and pyrrolidinium-based bilayers.** The layer thickness of the bilayer structures as shown in Figure 37 indicate qualitatively different bilayer architectures for the imidazolium and pyrrolidinium ionic liquids in two important ways.

***Firstly***: comparing the measured bilayer thickness dimensions of the extended ions suggests *toe-to-toe* bilayers for $[C_6C_1Im][NTf_2]$, but for $[C_{10}C_1Pyrr][NTf_2]$ the alkyl chains are significantly *interdigitated* (crumpled or tilted chains may also compatible with the measured thickness).

***Secondly***: from the measured film thicknesses, the $[NTf_2]$ anions are likely to be sitting separately on top of the cation headgroups in the case of $[C_6C_1Im][NTf_2]$ bilayers, whereas the $[NTf_2]$ anions are located between the cation headgroups – in the same plane – in the case of $[C_{10}C_1Pyrr][NTf_2]$ bilayers. These features are represented schematically in Figure 37.

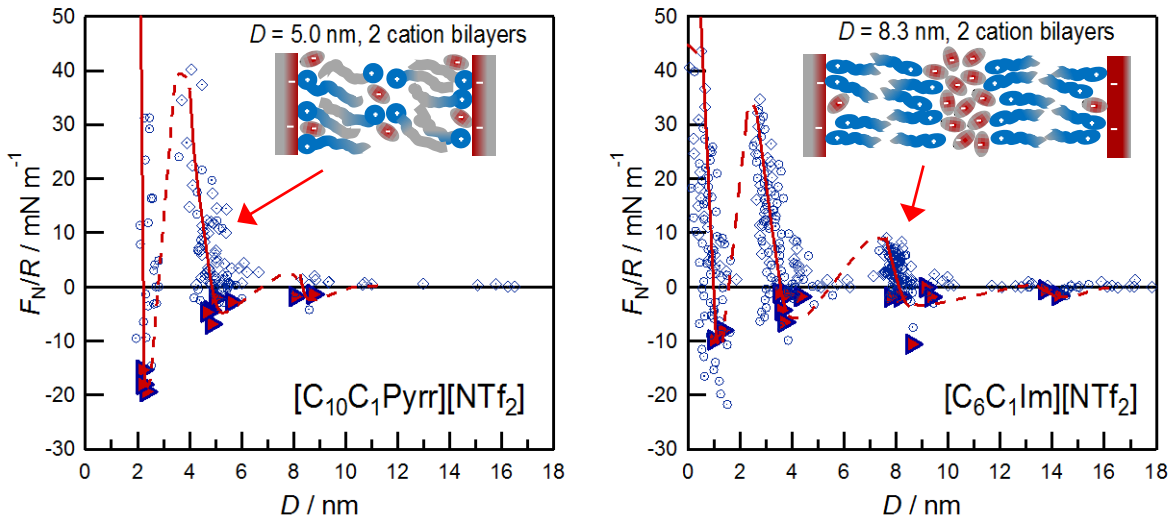


**Figure 37**

Comparison of force profiles and suggested bilayer structures for $[C_{10}C_1Pyrr][NTf_2]$ and $[C_6C_1Im][NTf_2]$.

What is the driving force for the different bilayer architectures? One might start to rationalise these differences by considering the possibility of π-π stacking for the imidazolium cations leading to close approach of the cations and exclusion of the [$NTf_2$] to a separate layer above and below. Despite their positive charge, favourable π-π stacking structures can be expected between imidazolium cations[185-186]. In contrast the pyrrolidinium ionic liquids have less favourable headgroup interactions (since no π-π stacking is possible) which also encourages the anions to intercalate between the cation headgroups and screen their repulsive electrostatic interactions. The inclusion of the anions within the bilayer for [$C_{10}C_1$Pyrr][$NTf_2$] leads to some contact between the [$NTf_2$] anion and the non-polar tails of the cation; in fact this is not unexpected since this polarisable anion can engage well in dispersion interactions. As a result of the inclusion of [$NTf_2$] anions between the cations of the pyrrolidinium bilayer, the cross-sectional area of each ion pair is very much larger than the cross-section of the hydrocarbon tail. This results in the significant interdigitation of the hydrocarbon chains in the bilayer in order to optimally fill the space in the film, and thus smaller measured bilayer thickness compared to imidazolium. This difference is in accordance with small and wide angle scattering experiments on bulk ionic liquids where the smaller non-polar domains detected for piperidinium ionic liquids (in comparison to imidazolium analogues) were attributed to the bulky and non-aromatic headgroup[190].

Having made such observations, the bilayer structures could be rationalised using a single geometrical factor or *packing parameter*, *P*, as is commonly employed to explain self-assembled architectures in water:

$$P = v_c / a.l_c$$

Where $v_c$ is the volume of the alkyl chain, $l_c$ is the length of the alkyl chain, and $a$ is the headgroup area including cation and anion. Although the data suggests that the anions

are between the headgroups for the $[C_{10}C_1Pyrr][NTf_2]$ and outside of the cation bilayer for $[C_6C_1Im][NTf_2]$ there remain several possibilities for their relative positions which lead to a range of possible values for the headgroup area, *a*.

| Bilayer-forming ionic liquids | $[C_6C_1Im][NTf_2]$ | | | $[C_{10}C_1Pyrr][NTf_2]$ | |
|---|---|---|---|---|---|
| Possible ion orientations | 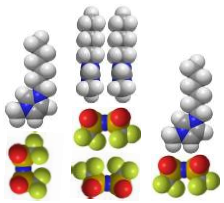 A B C | | | 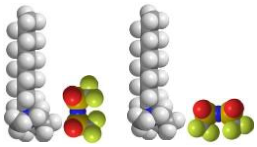 D E | |
| *V* / nm$^3$ | 0.162 | 0.324 | 0.162 | 0.27 | 0.27 |
| *A* / nm$^2$ | 0.189 | 0.490 | 0.490 | 0.427 | 0.728 |
| *L* / nm | 0.87 | 0.87 | 0.87 | 1.45 | 1.45 |
| Packing parameter | 0.99 | 0.76 | 0.38 | 0.44 | 0.26 |

**Figure 38**

Table showing possible cation-anion arrangements for the two bilayer-forming ionic liquids and the resulting estimated packing parameters for each

Nonetheless, by considering the possible positions which give rise to the maximum and minimum possible headgroup areas, limiting values of *P* for each ionic liquid can be obtained. These orientations and the resulting packing parameters are shown in Figure 38. For $[C_6C_1Im][NTf_2]$ three possible anion-cation positions are shown: A and B are most likely, and lead to $P \sim 0.8 - 1.0$ in line with the observed toe-to-toe bilayer structure. For $[C_{10}C_1Pyrr][NTf_2]$ the most likely of the two orientations shown is D which leads to $P \sim 0.4$; again in line with the observed interdigitation in the bilayer. Although this packing parameter analysis is merely demonstrated to be reasonable in this case – since knowledge of the structures from the measurements is used to predict the orientations – it may be usefully applied to other ionic liquid structures with varying

ion dimensions in rationalising or predicting self-assembled structures at charged surfaces.

## 5.5 Summary

In summary, surface force measurements were carried out to demonstrate oscillatory force behaviour between mica surfaces across a homologous series of pyrrolidinium-based and imidazolium-based ionic liquids, allowing determination of dimensions of layered structures in the ionic liquid films. A transition was discovered between two different interfacial structures upon increasing the alkyl chain length of the cation.

Ionic liquids containing cations with a short alkyl chain form alternating layers of cations and anions when confined to thin films. However a cation with a longer alkyl chain leads to bilayer formation. In the case of pyrrolidinium cations the bilayers are greatly interdigitated, most likely due to the chemistry and shape of the headgroup and the need for the ions to fill space most effectively. An interesting point is this common feature of a cross-over from monolayer to bilayer structure observed for both imidazolium-based and pyrrolidinium-based ionic liquids, yet with differing 'critical' (cross-over) chain length and different bilayer architecture for these two classes of ionic liquids.

# 6 STRUCTURE OF IONIC LIQUID MIXTURES CONFINED TO NANO-FILMS

## 6.1 Introduction

The 'designer solvent' concept of ionic liquids has led to intense study in recent decades in order to understand how altering ionic liquid ions affects the physical and chemical properties of the ionic liquid. More recently, there has been much interest in using mixtures of ionic liquids as a route to further tune the liquid properties and achieve greater flexibility with a smaller range of components[191-192]. To this end, several systems involving ionic liquid mixtures in confinement are studied in this chapter.

It was shown in the previous chapter that the interfacial structure can depend critically on the amphiphilicity of the ions, where ions containing short alkyl chains form alternating cation-anion monolayers and with more amphiphilic ions self-assembling to form bilayers in confinement. This chapter begins with the study of an equimolar mixture of monolayer and bilayer-preferring ionic liquids to provide more insight into the driving forces for meso-structuring.

Ionic liquids have generated increasing interest in recent years as potential electrolytes for lithium-ion batteries[193] due to their non-volatility, non-flammability and wide electrochemical window. In the next section of this chapter, some experiments are presented with confined mixtures of an ionic liquid with a lithium solute. A better understanding of the double layer structure would aid in the development of these electrolytes for use in lithium ion batteries.

Despite their outstanding electrochemical properties, the low conductivity of ionic liquids when compared to conventional electrolytes is of concern. The high viscosity of ionic liquids – due to their large molecular mass, strong electrostatic forces and ion aggregation – can be lowered by mixing with commonly used molecular solvents[194-196], drastically boosting their ionic conductivity. Such mixtures of ionic liquids with solvents are widely used, particularly for double-layer capacitors. There are currently many uncertainties about the charge storage mechanisms, and experiments directly probing the structure at the solid-liquid interface are scarce, and so in the final section of this chapter are presented a study of mixtures of an ionic liquid with propylene carbonate, a non-aqueous polar solvent. The liquids are fully miscible and allow investigation from 0-100% ionic liquid in propylene carbonate solvent.

## 6.2 An Equimolar Mixture of Monolayer and Bilayer-Preferring Ionic Liquids Confined to Nano-Films

Given the dramatically different structures for short and long chain ionic liquids presented in the previous chapter, it is particularly interesting to investigate ionic liquid mixtures in thin films. Figure 39 presents the interaction force between mica surfaces across the equimolar binary mixture $[C_4C_1Pyrr]_{0.5}[C_{10}C_1Pyrr]_{0.5}[NTf_2]$. An oscillatory structural force is clearly evident, yet it is different to either of the pure ionic liquids $[C_4C_1Pyrr][NTf_2]$ or $[C_{10}C_1Pyrr][NTf_2]$. The layer thickness of the mixture differs appreciably from those of alternating ion layers (monolayers) but are much more similar to those of the bilayers as seen for pure $[C_{10}C_1Pyrr][NTf_2]$ (data is also plotted in Figure 39 for comparison).

The similarity in the *D*-values suggests alkyl chain segregation and bilayer-like structures in the $[C_4C_1Pyrr]_{0.5}[C_{10}C_1Pyrr]_{0.5}[NTf_2]$ mixture. However the layers are slightly thinner than for pure $[C_{10}C_1Pyrr][NTf_2]$ and the force required to disrupt the bilayer-like structure is substantially lower. The shallow slope of the $F_N/R$ vs $D$ for the 2-bilayer film (at around 4 nm) indicates that the bilayers are highly compressible, although the extent to which they can be compressed (difference in the layer thickness between its force minimum and maximum) is similar to pure $[C_{10}C_1Pyrr][NTf_2]$.

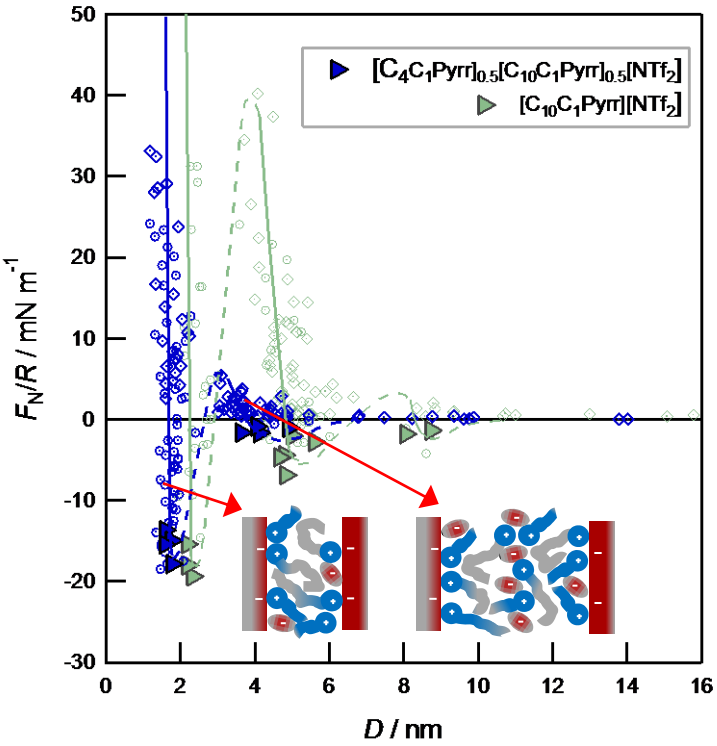


**Figure 39**

Measured normal force, $F_N$, normalised by radius of curvature, $R$, between mica surfaces across a binary equimolar mixture of $[C_4C_1Pyrr][NTf_2]$ and $[C_{10}C_1Pyrr][NTf_2]$. Also shown for comparison are results for pure $[C_{10}C_1Pyrr][NTf_2]$. Schematics below indicate possible layering structures for one and two mixed cation bilayers.

It is immediately clear that the structural forces for the binary mixture are different to either of the pure liquids: this implies that both [$C_4C_1$Pyrr] and [$C_{10}C_1$Pyrr] cations are present in the confined film, rather than one component being substantially more surface active than the other and thus segregating from the bulk mixture in the thin film. This is in agreement with angle-resolved x-ray photoelectron spectroscopy of an ionic liquid mixture at the liquid-vacuum interface, showing homogeneous distribution and no specific enrichment of longer chain cations[197].

The oscillatory structural forces show repulsive walls with layer thicknesses too great to be explained by monolayer arrangements and similar to those observed for the pure [$C_{10}C_1$Pyrr][$NTf_2$] interdigitated bilayers; thus suggesting a bilayer-type structure is present in the confined mixture. Although the bilayers have similar thickness to the pure [$C_{10}C_1$Pyrr][$NTf_2$] bilayers (in fact slightly thinner), they are substantially more compressible and have lower force required to rupture or squeeze-out the bilayers due to the increased disorder.

Why does an equimolar mixture of monolayer and bilayer preferring ionic liquids take on the structure of the longer-chain cation rather than the shorter-chain cation? One would have expected that the ‘average’ chain length would determine the structure, since this gives the fraction of the liquid taken up by non-polar groups. However the mean alkyl chain length for this mixture is 7 carbons per ion pair, whereas it is shown in this chapter that pure [$C_8C_1$Pyrr][$NTf_2$] still forms monolayers. So it appears that the longer of the chains dictates the structure in this case.

## 6.3 Ionic Liquid Mixtures with Lithium Solutes for Battery Electrolytes

Due to their non-volatility and wide electrochemical window, ionic liquids have generated increasing interest in recent years as potential electrolytes for lithium-ion batteries[193]. Conventional electrolytes are composed of lithium salts such as $LiPF_6$ in an organic solvent such as ethylene carbonate. Organic solvents decompose on electrodes during initial charging, generating a solid electrolyte interphase (SEI) at the surface. This layer is electrically insulating but an ionic conductor for lithium ions[198], and prevents further electrolyte decomposition upon subsequent charges. However short circuits can lead to overheating and ignition of the organic solvent, which is problematic. Lithium electrolytes based on ionic liquids are a promising approach to limit flammability and volatility for safer electrolytes. Lithium salts are solid at room temperature, and while it is not possible to directly use an ionic liquid as a battery electrolyte, dissolving a lithium salt $[Li^+][X^-]$ in an ionic liquid $[A^+][X^-]$ affords the ionic liquid mixture $[Li^+]_m[A^+]_n[X^-]_{m+n}$. Here some initial experiments are presented which examine the double layer structure of such a mixture, $Li_{0.2}[C_2C_1Im]_{0.8}[NTf_2]$.

The measured force profile for $[C_2C_1Im][NTf_2]$ shown in Figure 40 is similar to those of the monolayer-forming ionic liquids shown in the previous chapter. Neat $[C_2C_1Im][NTf_2]$ confined between mica surfaces shows seven oscillations, corresponding to film thicknesses ranging from $i$ = 1 to $i$ = 13. Adding a small amount of $LiNTf_2$ salt to $[C_2C_1Im][NTf_2]$ to make the mixture: $Li_{0.2}[C_2C_1Im]_{0.8}[NTf_2]$, considerably reduces the structuring to only two measurable oscillations. The first of these oscillations is at a distance corresponding to one monolayer of cations ($i$ = 1) and has an adhesive pull-off force extremely similar to neat $[C_2C_1Im][NTf_2]$. This suggests that $[C_2C_1Im]^+$ cations preferentially adsorb to the surface in the mixture, since significant coadsorption of the much smaller $Li^+$ ions would be expected to alter the electrostatic component of adhesion (this inference is further supported by friction

measurements across this cation monolayer for both the neat ionic liquid and the mixture shown in the next chapter).

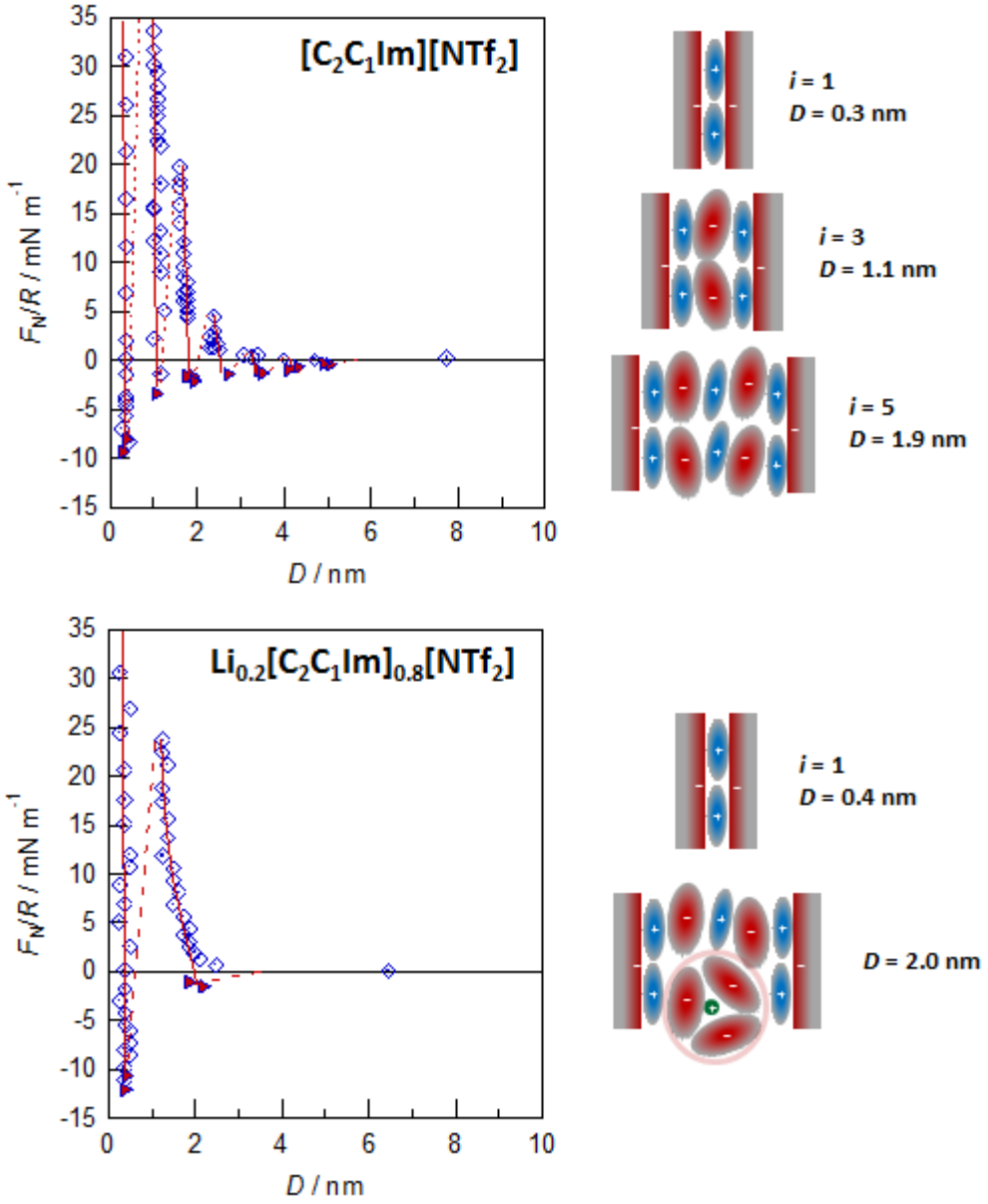


**Figure 40**

Measured normal force, $F_N$, normalised by radius of curvature, $R$, between mica surfaces across neat $[C_2C_1Im][NTf_2]$, and a mixture of $LiNTf_2$ with $[C_2C_1Im][NTf_2]$ in a 1:4 molar ratio. Schematics indicate the likely layering structures for the measured distances.

It is tempting to compare this result to molecular dynamics simulations of mixtures of $[C_4C_1Im][BF_4]$ with $LiBF_4$ and $KBF_4$, which also showed preferential adsorption of imidazolium cations and much weaker ion layering than for neat $[C_4C_1Im][BF_4]$, although at charged graphene surfaces[199]. In fact, the extreme similarity in range and magnitude of the measured forces in the literature using an AFM tip at mica surfaces and at both single crystal Au(111) and HOPG surfaces with applied potential suggests the ionic liquid structuring is dominated by electrostatics and not altered significantly by different surface chemistry.

The second oscillation in the confined mixture $Li_{0.2}[C_2C_1Im]_{0.8}[NTf_2]$ occurs at a distance of 2.0 nm (although it is compressible to 1.3 nm with sufficient force). This compressibility suggests a greater extent of mixing of ions, with adjustments in orientation and positioning occurring with increasing force. The thickness of this layer is much larger than the thickness for three confined ion layers for neat $[C_2C_1Im][NTf_2]$, which is the next expected stable configuration of ions after that of a confined cation monolayer. To explain this thicker layer, it is important to note that stable anionic clusters have been documented between $Li^+$ cations and $NTf_2^-$ anions[200-201]. From simulations, $[Li[NTf_2]_3]^{2-}$ are the most likely clusters at the concentration used here[201], and in fact the measured film dimensions agree better with these than other possible anionic clusters such as $[Li[NTf_2]_2]^-$ or $[Li[NTf_2]_4]^{3-}$, although the presence of these other clusters is also possible.

These anionic clusters have been proposed to account for differences in cathodic stability for lithium solutes in different ionic liquids[202]. AFM measurements with LiCl dissolved in $[C_6C_1Im][FAP]$ on Au(111) at different potentials show only a weakening of the ionic liquid layering at negative potentials, indicating that the anion of the lithium solute has a strong effect on the surface structure of the ionic liquid mixture.

## 6.4 Double Layer Structure in Ionic Liquid/Solvent Mixtures

Ionic liquid organic electrolytes - commonly using acetonitrile or propylene carbonate as the solvent - are widely used for double-layer capacitors, although there are still uncertainties about how the ions and solvent details relate to the charging mechanisms in devices. It has been shown that increased capacitance can be achieved by using pore sizes smaller than the size of an ion with an associated solvent molecule[155, 159] indicating that at least partial desolvation of the ions must occur. This closer proximity of ions to the electrode pore walls might be responsible for the excess charge density on the electrode, given that the solvent is not able to screen the charge. Much work has since focused on this anomalous increase in capacitance by studying structure and dynamics of ion adsorption and desolvation in confinement[203-210].

Although simulations have offered many useful molecular insights on the structural and capacitive properties of ionic liquids between planar electrodes, experiments directly probing the structure at the solid-liquid interface are scarce, and so here experiments are presented of solutions of an ionic liquid in propylene carbonate, a non-aqueous polar solvent. Interaction forces between mica sheets were measured at incremental steps in concentration ranging from the pure solvent to the pure ionic liquid. Results are shown in Figures 41-44 and summarised in Figure 45.

The force profile between mica surfaces across pure propylene carbonate is shown in Figure 41. The measured force is oscillatory in nature for small separations, corresponding to sequential squeeze-out of molecular solvent layers from the gap between the surfaces. These results are in agreement with previous surface force measurements of non-aqueous polar solvents confined between mica surfaces[74-76]. The oscillations have a periodicity equal to the molecule size, and are

qualitatively similar to the structural forces first observed for non-polar liquids[9-10]. However with polar liquids, electrolytes are soluble and the mica sheets are negatively charged due to some potassium ions dissociating from the surface. This results in a weak, long range repulsive force measured between the similarly charge surfaces accurately described by DLVO theory down (see the inset to Figure 41) to the small separations where effects of molecular packing become most dominant. The very low ionic concentration, $c$ = 6 × $10^{-6}$ M, in the fit is likely due to dissociated potassium ions from the mica and possibly includes $H^+$ leached from glassware, or dissolved $HCO_3^-$.

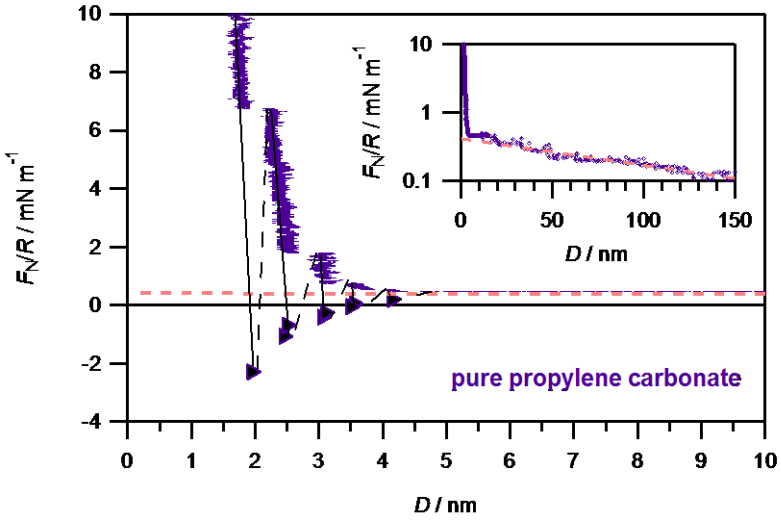


**Figure 41**

Measured normal force, $F_N$, normalised by radius of curvature, $R$, between mica surfaces across pure propylene carbonate. The dashed (pink) line is the best fit of the linear part of the force profile to DLVO theory, corresponding to $c$ = 6 × $10^{-6}$ M and $\psi_0$ = 94 mV. The inset shows the same data on a logarithmic force scale and expanded distance scale.

When the ionic liquid $[C_4C_1Pyrr][NTf_2]$ is added to make a dilute electrolyte solution at a concentration of 0.01 M (Figure 42), the measured repulsive force is again in very good agreement with double-layer theory, with deviations at

small separations due to molecular layering of solvent molecules. At long range the measured repulsive force agrees well with DLVO theory, giving $c$ = $0.8 \times 10^{-2}$ M, and at short range the oscillatory forces seem to be additive to the long range double layer force.

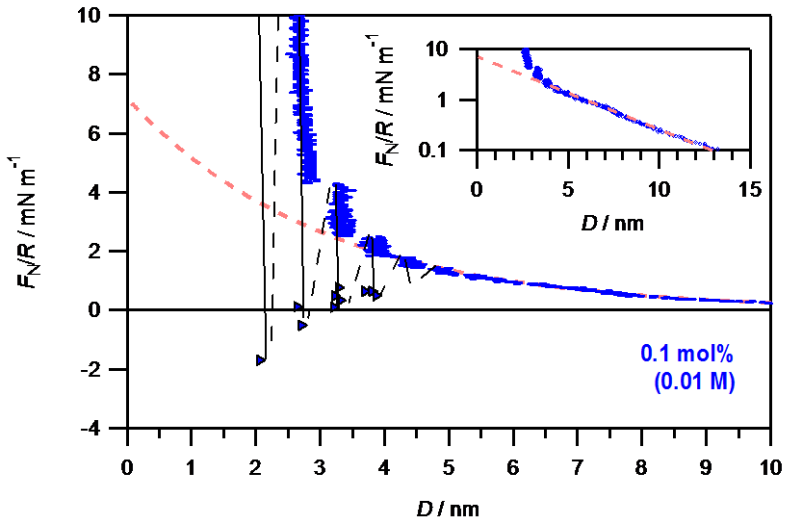


**Figure 42**

Measured normal force, $F_N$, normalised by radius of curvature, $R$, between mica surfaces across a 0.01 M solution of $[C_4C_1Pyrr][NTf_2]$ in propylene carbonate. The dashed (pink) line is the best fit of the linear part of the force profile to DLVO theory, corresponding to $c = 0.8 \times 10^{-2}$ M and $\psi_0$ = 32 mV. The inset shows the same data on a logarithmic force scale and expanded distance scale.

A more concentrated solution of 1 M (Figure 43a) shows molecular layering at small separations again indicative of propylene carbonate layering. Ions, which must be present in the confined films, are packed within the solvent layers, and their size and shape is such that they only interfere with packing to a little extent. Five molecular layers can be measured at this 1 M concentration, compared to eight for the pure solvent. This behaviour continues up to a concentration of 2 M (Figure 43b), but with weaker force

magnitudes for equivalent numbers of confined layers.

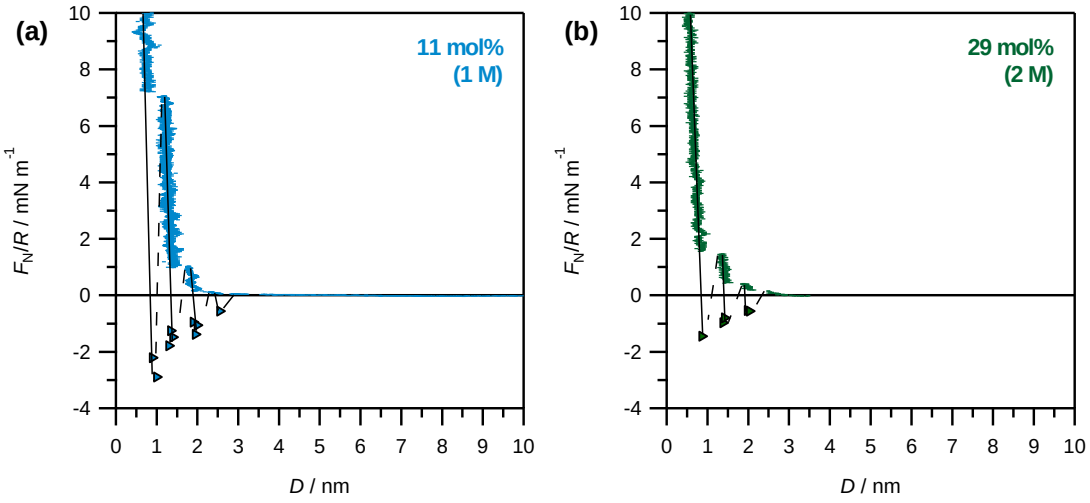


**Figure 43**

Measured normal force, $F_N$, normalised by radius of curvature, $R$, between mica surfaces across 1 M and 2 M solutions of $[C_4C_1Pyrr][NTf_2]$ in propylene carbonate.

For concentrations of 2.5 M and above, a distinct switch in the film structure becomes apparent, as follows. For a 2.5 M solution (Figure 44a), the periodicity of the oscillations changes compared to lower concentrations, and the forces also become larger in magnitude compared to similar $D$ values for the 2 M solution. Increasing the ionic concentration further to 3M (Figure 44b), results in similar layering behaviour with this larger periodicity, and with more pronounced oscillations. This increases in strength and range right up to the pure $[C_4C_1Pyrr][NTf_2]$ ionic liquid (Figure 44c), which corresponds to a 3.3 M concentration. The force profile for the pure ionic liquid $[C_4C_1Pyrr][NTf_2]$ shown in Figure 44 is similar to that for the same ionic liquid shown earlier in this chapter (Figure 34), but here the distance changes are resolved with greater resolution and more oscillations are detected using a camera to photograph the interference fringes. The distance between the measured stable film thicknesses in the pure ionic liquid is determined as 0.8 ± 0.04 nm, which is in good agreement with the work of Hayes *et al.*, who

resolved layer spacings at approximately 0.79 nm intervals for the same ionic liquid confined between a $Si_3N_4$ AFM tip and mica surface[112].

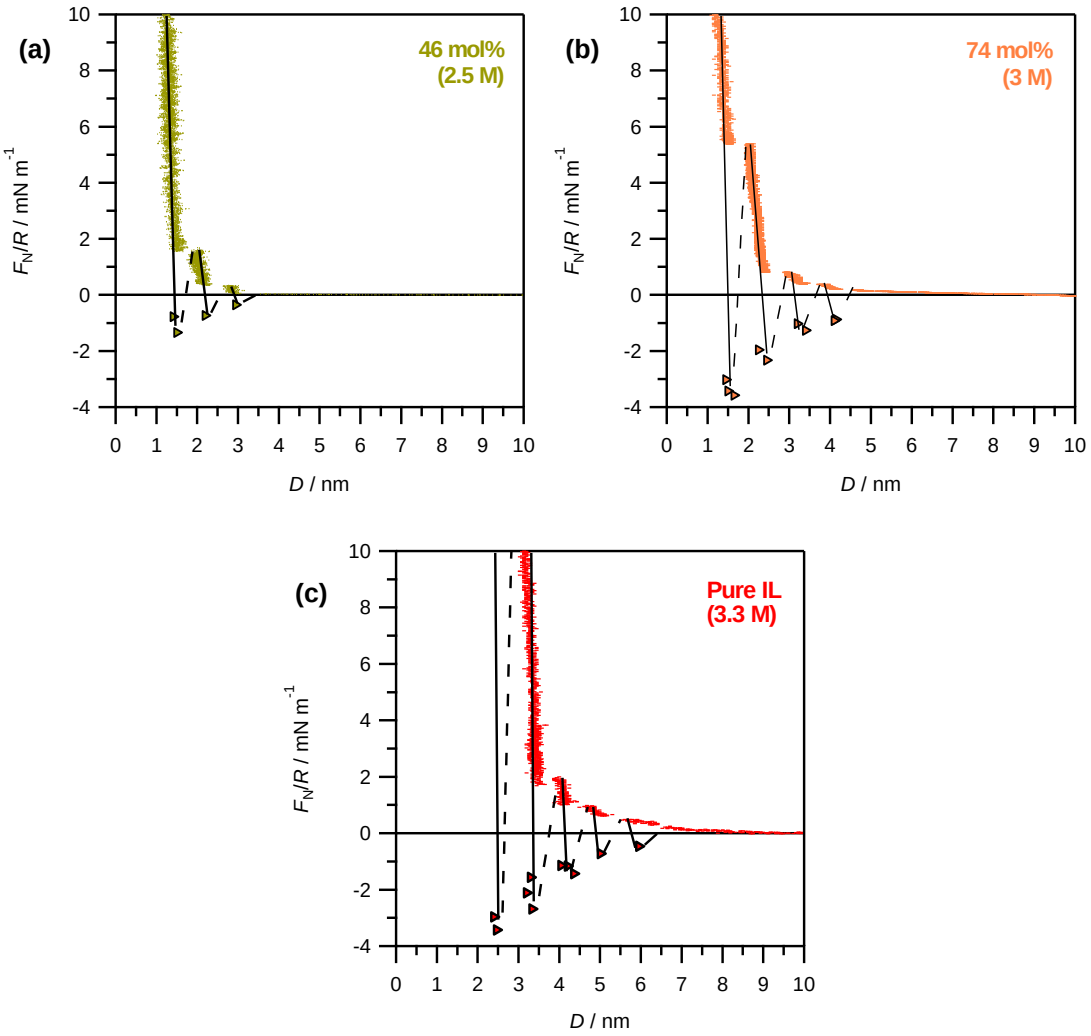


**Figure 44**

Measured normal force, $F_N$, normalised by radius of curvature, $R$, between mica surfaces across (a) 2.5 M, (b) 3 M and (c) 3.3 M (pure ionic liquid) solutions of $[C_4C_1Pyrr][NTf_2]$ in propylene carbonate.

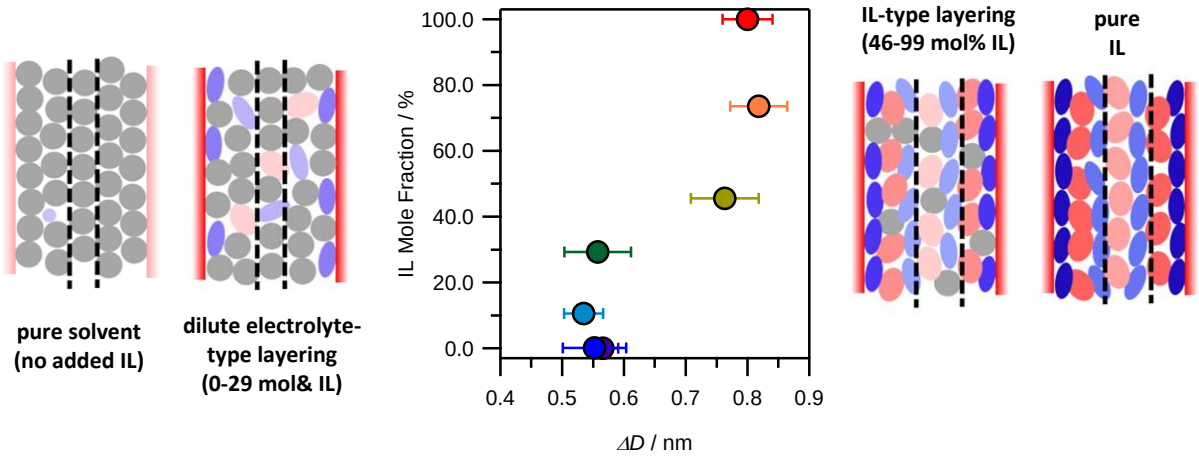


**Figure 45**

Summary showing force profiles for all concentrations studied, from the pure propylene carbonate (PC) solvent with no added electrolyte to the pure ionic liquid, $[C_4C_1Pyrr][NTf_2]$. Also shown is the average layer thickness for each concentration.

What is apparent from the force measurements is that at a critical concentration there appears to be a crossover from *density oscillations* (driven by solvent) to *charge density oscillations* (driven by ionic liquid), which have different periodicities. The propylene carbonate solvent is polar with a large molecular dipole moment (4.9 D) and so competes well with cations at the mica surface. However once the ionic concentration of the solution is high enough, the layer adjacent to the mica surface develops an excess positive charge high enough to *overscreen* the negative surface charge. This overscreening behaviour[117, 211] results in alternating positive and negative excess charge density decaying away from the surface for several layers into the bulk liquid, with this interplay between charge correlations and geometric confinement determining the measured forces as a function of film thickness[212].

For this ionic liquid and solvent the concentration range at which this

crossover occurs seems to be in the range 2.0-2.5 M, and is measurable for the first few near surface layers. One can envisage a certain concentration immediately prior to this crossover, where the cations and solvent molecules present in the first molecular layer have an excess positive charge such that they perfectly screen the mica surface charge, which would be detected in these measurements as the highest concentration at which purely density oscillations are measured (or no oscillations at all, but just a repulsive hard wall with an adhesive minimum at 0-1 nm). However there may be possible complications related to charge regulation since the mica surface charge is not controlled. An analogous behavioural transition has recently been predicted by simulations for pure ionic liquids by modifying the surface potential of the electrode and/or varying ion dimensions to *tune* this overscreening structure in a similar way[213-214].

These results of concentration dependent structure in ionic liquid-based electrolytes at charged surfaces are of interest to current researchers in the field of electrical double layer capacitors, where ionic liquids are typically dissolved in solvents such as acetonitrile or propylene carbonate. Concentrations of 1-2 M seem to be an optimal concentration in many recent experiments, and conventional thinking is that higher concentrations lead to higher electrolyte viscosities with sluggish ion dynamics in pores reducing performance. While the electrolyte concentration should most certainly be sufficiently high to ensure good ionic conductivity, these measurements suggest that the concentrations should also not be so high that there is overscreening at the electrode surfaces, which is known to be detrimental to capacitance.

The effect of a non-aqueous polar solvent such as propylene carbonate appears to be different to that of water in two ways:

i) Firstly, although layered structures have previously been observed with aqueous solutions of a protic ionic liquid above a certain

concentration[113], at lower concentrations the van der Waals attraction between the surfaces made any structure (if present) inaccessible to measurement. This is most likely related to water's tendency to remain liquid-like in confinement[77] due to suppression of its highly directional hydrogen-bonded networks.

ii) Secondly, while the effect of incorporated water on confined ionic liquids is to swell the layer thickness by several angstroms[165] (and also shown in the next chapter for a bilayer-forming ionic liquid), it is interesting that the observed layer thickness of the confined ionic liquid remains unchanged upon addition of a small amount of propylene carbonate. This could be related to the different solvation properties or possibility of hydrogen-bonding occurring between water and the ions. Alternatively it could largely be a size effect, given that water is half the size of propylene carbonate it might perhaps pack into the ion layers in a different way to a solvent molecule of comparable dimensions to the ions. Instead the propylene carbonate molecules appear to intercalate into the ion layers, leaving their thickness unchanged but lowering the force magnitudes due to a decreasing extent of overscreening.

## 6.5 Summary

An equimolar mixture of monolayer and bilayer preferring ionic liquids takes on the structure of the longer-chain cation rather than the shorter-chain cation. This is perhaps surprising, given that the 'average' chain length is 7 carbons per ion pair and it is shown that pure $[C_8C_1Pyrr][NTf_2]$ still forms monolayers. So it appears that the longer of the chains dictates the structure in this case. It would be interesting to see how the concentration of $[C_{10}C_1Pyrr][NTf_2]$ in $[C_4C_1Pyrr][NTf_2]$ alters the structure: how little

$[C_{10}C_1Pyrr][NTf_2]$ need one to add to $[C_4C_1Pyrr][NTf_2]$ in order to induce it to switch from monolayer to bilayer structure?

The addition of lithium solute to an ionic liquid can have a marked effect on its double layer structure, and it is to be expected that the effect depends on the particular solute, ionic liquid and concentration. The results shown here are useful for the development of Li-ion cells based on ionic liquid electrolytes, since the approach of ions to electrode surfaces for electrochemical reactions hinges on the double layer structure at the electrode.

Measurements using mixtures of ionic liquid with propylene carbonate, a polar non-aqueous solvent, reveal a crossover from solvent layering (with incorporated ions) to ionic overscreening above a certain ionic concentration. These results directly demonstrate the use of solvent to tune overscreening structures of ionic liquids at charged surfaces, in addition to varying the surface charge or ion dimensions. This behaviour is to be expected for any polar liquid in the absence of hydrogen bonding, however the exact concentrations at which the effects are observed most certainly depend on the particular ionic liquid and solvent polarity[215]. This interplay and competition between the solvent dipole moment and ionic concentration determines the near-surface structure.

Together these results provide important insights for their use as electrolytes confined to narrow pores and thin films in electrochemical devices. Pyrrolidinium-based ionic liquids in particular are particularly attractive for these electrochemical applications due to their wide electrochemical window and chemical stability compared to other ionic liquids and conventional solvents. These results also have direct implications for ionic liquids stabilizing nanoparticles with their layered structures, and in solvating polar or non-polar solutes. They are also critical in determining molecular mechanisms of boundary lubrication with ionic liquids, as shown in the next chapter.

# 7 MOLECULAR MECHANISMS OF SHEAR ACROSS IONIC LIQUID NANO-FILMS

## 7.1 Introduction

Their remarkable properties, including high thermal stability, negligible vapour pressure, and propensity to form robust layers at surfaces make ionic liquids extremely interesting as potential lubricants. While they are expensive to manufacture in large quantities, of particular interest is their use as specialist lubricants in high vacuum or extreme temperature conditions. Two industrial applications of ionic liquids have been recently realised, inspired by the friction measurements presented in this thesis.

Ionic liquids are also prospective lubricants for nanoscale devices, where lubrication must be achieved with ultra-thin films, typically only a few molecular layers in thickness. At such small length scales, surface forces dominate and it becomes critical to understand molecular friction, adhesion and wear mechanisms at the nanoscale. Understanding these lubrication mechanisms becomes even more important considering the plethora of 'tailor-made' ionic liquids which could be synthesised.

Despite the burgeoning interest in ionic liquids and their intricate nano-structure in recent years, very little is currently known about their mechanism of lubrication[108, 216-217]. This chapter describes friction measurements between mica surfaces across films ionic liquid. Key features are established distinct from earlier studies[108, 216-218]: friction is measured across ionic liquid films of precisely controlled thickness (number of ion layers), at both positive and negative applied loads, and the adhesion and real contact area are measured concurrently.

In Chapter 5 it was established that pure ionic liquids can form either monolayer or bilayer structures in films between mica sheets. In this chapter, measurements of friction forces are presented for each of these structural arrangements. In section 7.2 the friction mechanisms across $[C_4C_1Pyrr][NTf_2]$, a monolayer-forming ionic liquid, are presented. The key features of interest are how the friction is dissipated in the confined ionic film and how the friction behaviour varies for different numbers of confined layers.

Then in section 7.3 the friction mechanisms across $[C_{10}C_1Pyrr][NTf_2]$, a bilayer-forming ionic liquid, are described. The results allow elucidation of several mechanistic insights into boundary lubrication. When considering friction across bilayers, the question arises, how would ionic liquid bilayers slide across each other? Alkyl chains are commonly thought to reduce friction and wear: the canonical perception involves amphiphilic boundary lubricant molecules adhered to the shearing surfaces and sliding at the interface where the tails meet. Whereas for confined ionic liquid bilayers, one could postulate that shear could occur at three distinct planes: (i) at the ion/mica interface, (ii) between the alkyl chains of the bilayers, or (iii) within the ionic region between bilayers. Measurement of friction forces for one and two bilayers of $[C_{10}C_1Pyrr][NTf_2]$ with or without the addition of small amounts of water enable elucidation of the likely shear planes and sliding mechanisms in the confined films.

## 7.2 Stiction, Stick-Slip and Quantized Friction Across Monolayer Forming Ionic Liquids

To obtain insight into the molecular reorganization of the ionic liquid films taking place during shear, high resolution traces were recorded of the lateral force, $F_L$ as a function of lateral displacement of the top surface for a range of $F_N$ and $v_S$. Figure 46 shows an example raw data friction trace for a film of $[C_4C_1Pyrr][NTf_2]$ confined to seven ion layers. The traces reveal stiction spikes at the onset of sliding (Figure 46B), with shearing of the film then progressing by way of a series of regular stick-slip cycles characterized by saw-tooth motion.

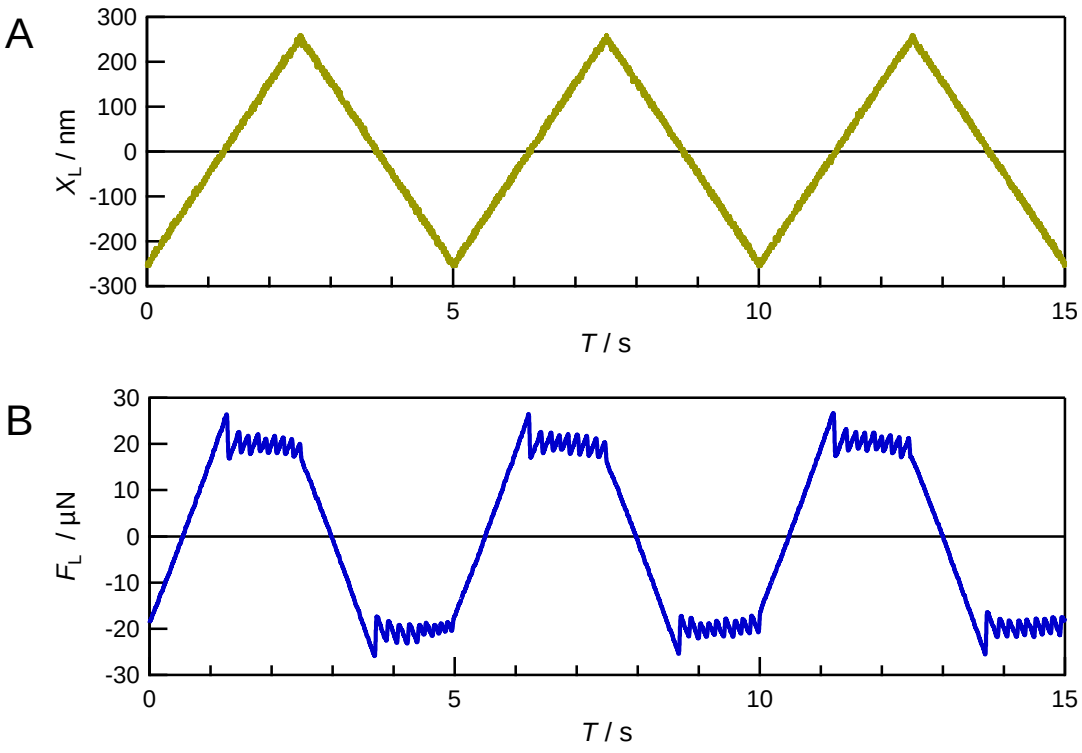


**Figure 46**

(A) Back-and-forth lateral displacement of one of the surfaces relative to the other at constant velocity ($v_S$ = 205 $nms^{-1}$) (B) Friction traces showing $F_L$ transmitted across a film of $[C_4C_1Pyrr][NTf_2]$ at constant thickness ($i$ = 7) to the opposite surface at fixed load ($F_N$ = 52.6 µN).

Once the direction of applied lateral motion is reversed, similar behavior is observed in the opposite direction. One back-and-forth cycle of this shear behavior can be plotted as a function of lateral displacement, resulting in a friction loop. Figure 47 shows example overlaid friction loops for different values of $F_N$. If the confined film supports a finite stress then during initial translation, $F_L$ will increase up to a stiction yield force, $F_{S,y}$. Shearing then proceeds by stick-slip, with $F_L$ ranging between a minimum of the *kinetic* friction force, $F_{S,k}$ at the stick-point, and a maximum of the *static friction* force, $F_{S,st}$, at the slip-point. At this $v_S$, $F_{S,y} > F_{S.st}$, giving rise to an observed stiction spike, of height $F_{S,y} - F_{S.k}$. These features are labelled clearly for the $F_N$ = 160.4 μN friction loop in Figure 47.

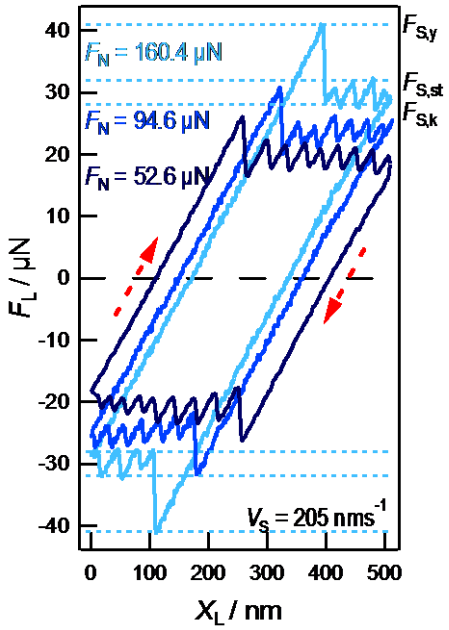


**Figure 47**

Friction loops showing $F_L$ as a function of $X_L$ for one representative sliding cycle for different values of $F_{N,}$ across a $[C_4C_1Pyrr][NTf_2]$ film at constant $v_S$. The film thickness is the same as for the raw data trace shown in Figure 46.

Qualitatively similar results were observed for $i$ = 9, 7, 5, and 3 films. Over the range of $F_N$ and $v_S$ studied all of these films exhibit a well defined yield point, with $F_{S,y}$ increasing in magnitude as $F_N$ increases, and stiction spikes at the onset of sliding. At a

critical shear velocity, $v_{S,}$ (Figure 48B), the stick-slip disappears and above this velocity the film then shears with a smooth sliding motion (Figure 48C). It is notable that $F_{S,k}$ is independent of $v_S$, whilst $F_{S,y}$ is weakly dependent on $v_S$.

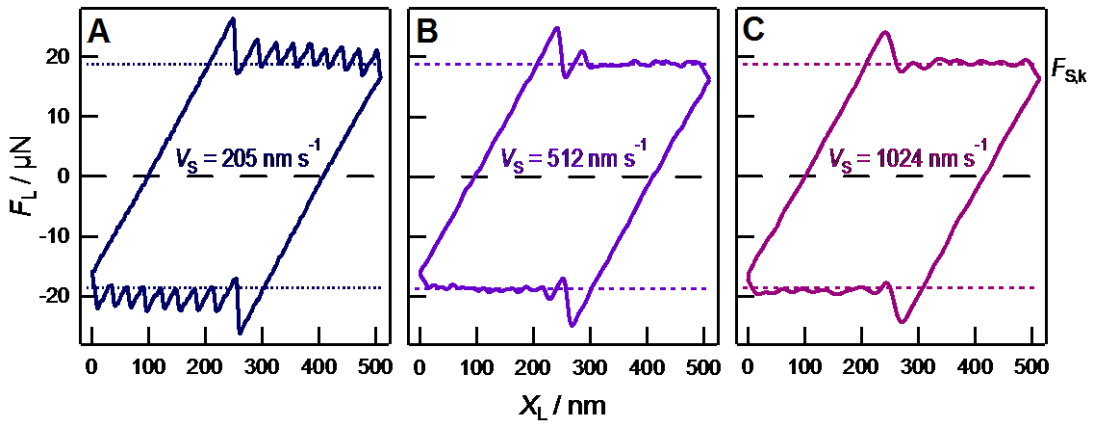


**Figure 48**

Friction loops showing $F_L$ as a function of $X_L$ for one representative sliding cycle, for different $V_S$ at the same [$C_4C_1$Pyrr][$NTf_2$] film thickness and fixed load ($F_N$ = 52.6 μN) as for the raw data traces shown in Figure 46.

As a result of the oscillatory force-law between the surfaces across this liquid it is possible to vary $F_N$ – over a certain range including positive and negative values – while the number of ion layers, $i$, in the film remains constant. By performing this compression/de-compression for different values of $i$, and at the same time applying lateral displacement to the top surface and detecting the resulting $F_L$, it is possible to measure $F_{S,k}$ as a function of $F_N$ for each number of ion layers between the surfaces. The combined results for several different experiments is shown in Figure 49, and reveals quantized friction regimes for different film thicknesses. Thus there exists a friction-load relationship for each value of $i$, and the friction is multi-valued for each single value of load.

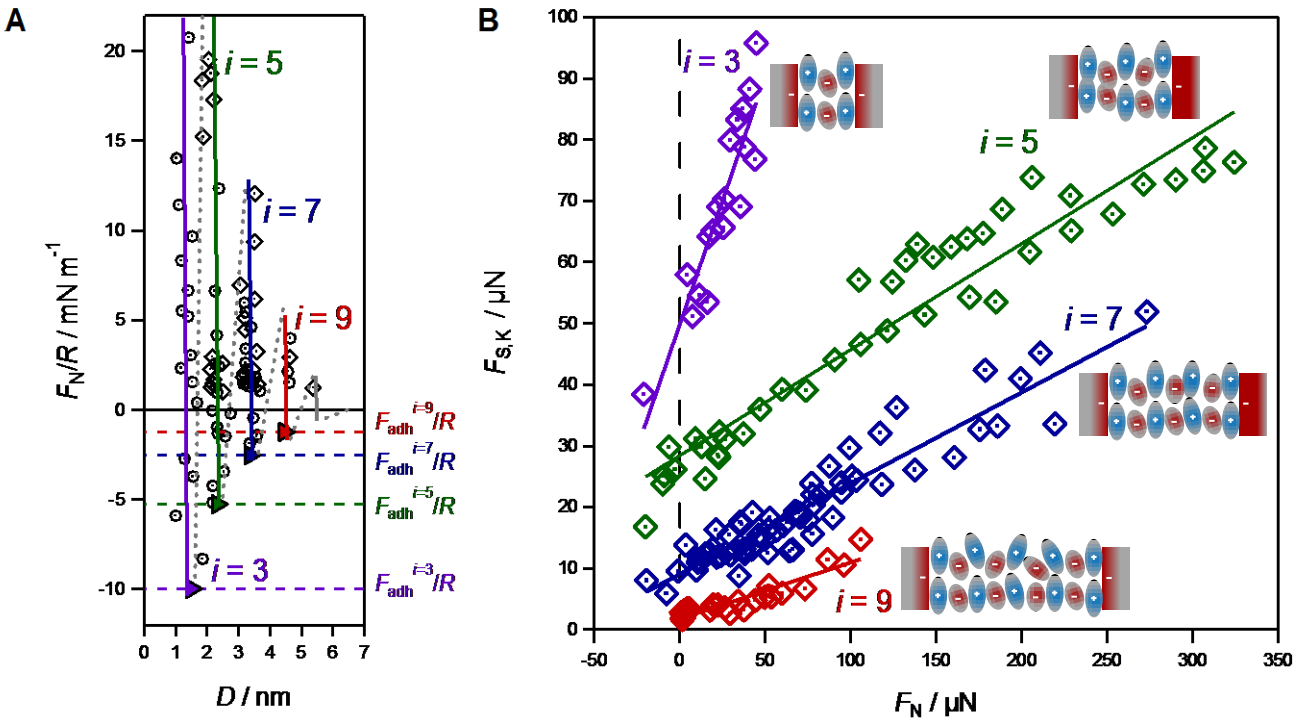


**Figure 49**

(A) Oscillatory forces measured between mica surfaces across $[C_4C_1Pyrr][NTf_2]$ reproduced from Chapter 5 (B) Normal and shear forces between mica surface measured across different numbers of confined ion layers for $[C_4C_1Pyrr][NTf_2]$. The lines are linear fits to the data.

Each of the quantized friction regimes follows an approximately linear $F_{S,k}$ *vs.* $F_N$ relationship with non-zero $F_{S,k}$ measured at zero (and negative) values of $F_N$. The friction at zero applied load originates in the contribution from the adhesion force between the surfaces, $F_{adh}$, which is different for each number of layers, $i$, as seen from the measured $F_N$ minima in Figure 49A. $F_{S,k}$ can be expressed as a linear combination of load-dependent and adhesion-dependent contributions[219]:

$$F_{S,k}{}^{i} = \mu^{i} F_N + \alpha^{i} \left( \frac{A^{i}.F_{adh}{}^{i}}{\pi d^{i} R} \right)$$

where $\mu$ is the load-controlled friction coefficient, $\alpha$ is the adhesion-controlled friction coefficient, $A^i$ is the flat contact area, $d^i$ is the distance between the shearing liquid layers, and superscripts $i$ denote values for a film containing $i$ layers.

In these experiments, $F_{adh}{}^i$ , $F_{S,k}{}^i$ , $R$, and $d^i$ are directly measured whilst controlling $F_N$. The resolution in the contact diameter is only ~1 µm and not accurately measurable at these relatively low values of $F_N$, but can be determined using the JKR equation after *in-situ* calibration of the elastic modulus[220] of the lens-glue-mica system. This involves the application of much larger normal forces and measurements of the flattened contact area directly from the interference fringes was fitted using the JKR equation. Thus it was possible to determine values of the coefficients $\mu^i$ and $\alpha^i$ for each discrete film thickness. For the films consisting of 9, 7 and 5 ion layers $\mu^i$ increases gradually in the range 0.082 – 0.172 (±0.008), as shown in Table 2. For $i$ = 3, the gradient is much steeper giving $\mu^{i=3} = 0.812 \pm 0.090$.

**Table 2** Load and adhesion friction coefficients with their propagated errors

| $i$ | $\mu^i$ | error | $F_{adh}$ (µN) | error | $F_S$ at $F_N$=0 | error | $d^i$(nm) | error | $A_0$(µm$^2$) | $\alpha^i$ | error |
|---|---|---|---|---|---|---|---|---|---|---|---|
| 9 | **0.082** | 0.008 | 12.28 | 3.07 | 1.22 | 0.37 | 0.50 | 0.05 | 12.76 | **0.18** | 0.13 |
| 7 | **0.125** | 0.006 | 25.32 | 6.33 | 7.96 | 0.57 | 0.45 | 0.05 | 20.67 | **0.22** | 0.09 |
| 5 | **0.172** | 0.008 | 52.71 | 13.18 | 28.67 | 1.35 | 0.45 | 0.05 | 33.71 | **0.23** | 0.08 |
| 3 | **0.812** | 0.090 | 99.67 | 24.92 | 49.79 | 2.59 | 0.50 | 0.05 | 51.54 | **0.15** | 0.09 |

The adhesion contribution to the friction gives coefficients with closely similar values for all $i$; $\alpha^i = 0.19 \pm 0.04$. The increase in $\mu^i$ as $i$ decreases is likely due to the greater degree of interlocking of the layers for small $i$: the layers closer to the mica surfaces are more ordered, and have greater anion/cation excess concentration, and therefore have greater inter-layer attractions for the same value of contact area and a greater activation barrier for 'unlocking' the surfaces to allow shear.

The clear yield points in the stick-slip traces indicate solid-like behavior of the ionic liquid confined to films of $i \leq 9$ ion layers. Subsequent stick-slip behavior observed at lower $v_S$ is most often attributed to a series of freeze-melt transitions[221-222]. However in the case of ionic liquids a full-film melt is unlikely due to the high Coulombic energy barrier of ions swapping between layers, so the stick-slip is likely to involve either interlayer slips[223] or intra-layer (two dimensional) melting. Furthermore, the particularly high values of $F_{S,k}^{i=3}$ compared to $F_{S,k}^{i>3}$ indicates that mid-film cation layers – the structural feature present in films of greater thickness but not in the $i = 3$ film – may shear-melt or slip at lower stress than the other layers and thus be responsible for the lower yield force of the thicker films.

In general, pyrrolidinium-based ionic liquids confined to molecularly thin films require greater force to squeeze-out successive layers compared to their imidazolium-based analogues, allowing distinct friction regimes to be measured for even up to film thicknesses of $i = 9$. The *quantized friction* presented here is a direct result of the multiple discrete values of the adhesion-controlled contribution to the total friction, and is expected to be general for liquids which form layered structures in thin films. Indeed, experiments with a range of other ionic liquids reveal quantized friction regimes corresponding to the layer structure in every case, although the friction is often below the resolution of the instrument for the thicker films.

One other example of quantized friction across ionic liquids is shown for $[C_2C_1Im][NTf_2]$ in Figure 50. For this liquid there are three measurable friction regimes, corresponding to one, three and five confined ion layers. Overall the behaviour of $[C_2C_1Im][NTf_2]$ is very similar to that of $[C_4C_1Pyrr][NTf_2]$, with different friction coefficients for each of the stable film thicknesses.

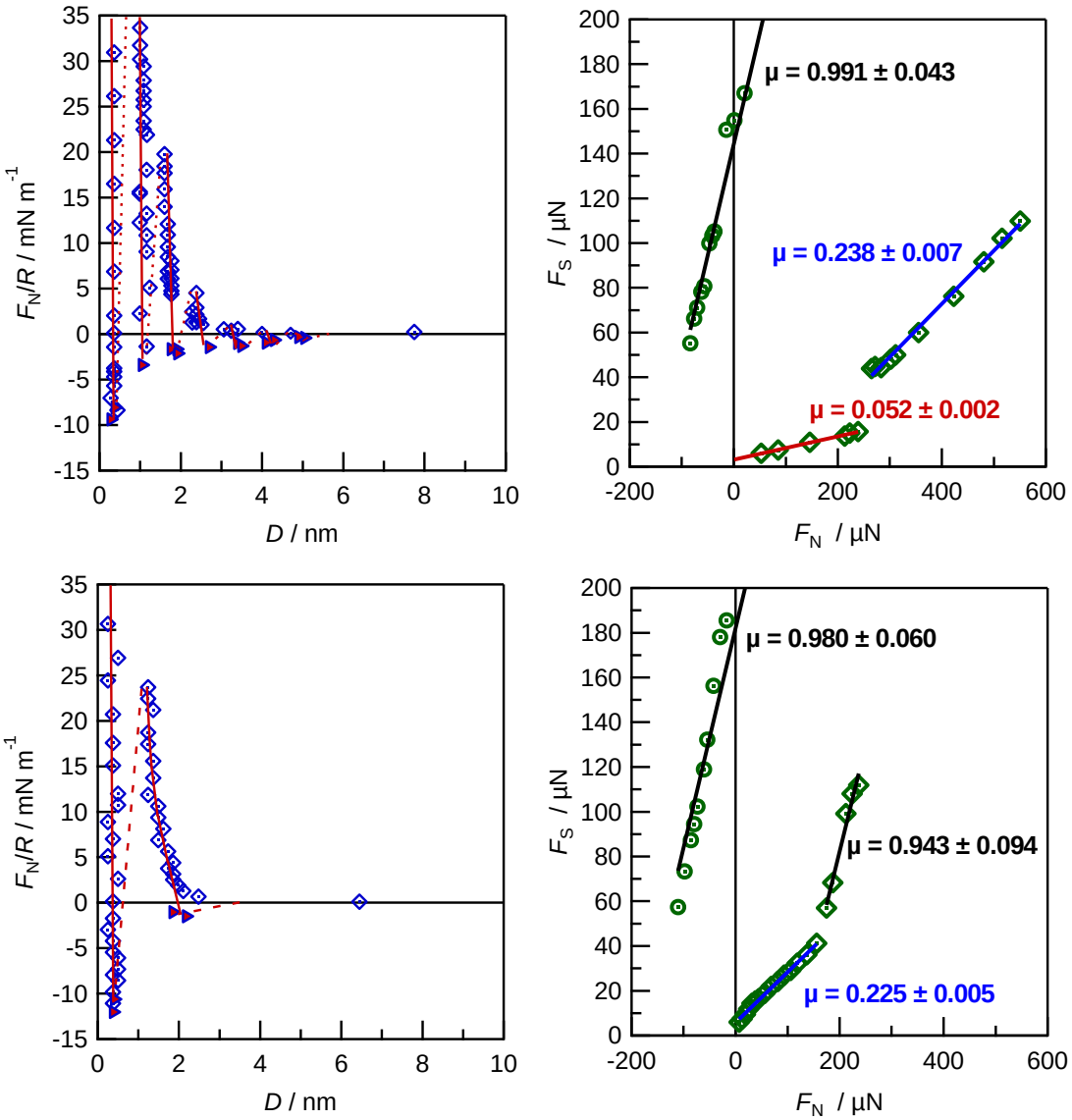


**Figure 50**

Normal and shear forces between mica surface across $[C_2C_1Im][NTf_2]$ and the mixture $Li_{0.2}[C_2C_1Im]_{0.8}[NTf_2]$. The lines are linear fits to the data. Schematics indicate the likely layering structures, with dashed lines showing the likely shear planes.

Interestingly, $[C_2C_1Im][NTf_2]$ exhibits smooth sliding over the range of velocities investigated, likely to a different (or lack of) lateral order of ions within the layers. In fact, similar experiments with $[C_4C_1Im][NTf_2]$, which differs only in the alkyl chain length of the cation, exhibits irregular stick-slip (not shown here), demonstrating the complex friction behaviour depending on the ion structure.

Comparing the friction across a single confined cation monolayer for $[C_2C_1Im][NTf_2]$, with the mixture $Li_{0.2}[C_2C_1Im]_{0.8}[NTf_2]$, gives an extremely similar friction coefficient. This indicates $Li^+$ ions are not present immediately adjacent to the mica surface as discussed in the previous chapter. The second oscillation for the confined mixture $Li_{0.2}[C_2C_1Im]_{0.8}[NTf_2]$ exhibits a different non-linear friction with two regimes; at a film thickness of ~2 nm, the friction coefficient stays constant ($\mu$ = 0.225 ± 0.005) despite gradual compression of the film to ~1.3 nm. Up to this point the behavior is more similar to $i$ = 3 for the neat $[C_2C_1Im][NTf_2]$ liquid, despite the film thickness being closer to that for $i$ = 5. This is most likely due to the anionic lithium clusters preventing sliding between the ions in the middle of the film, as shown by the likely shear planes shown as dashed lines in Figure 50.

At a distance of 1.2-1.4 nm for the mixture, the friction coefficient abruptly increases to a much higher value ($\mu$ = 0.943 ± 0.094), remarkably similar to that of the confined cation monolayer in the same liquid mixture ($\mu$ = 0.980 ± 0.060). One explanation is a shift in the shear plane to the mica surface; this could possibly be due to different $[NTf_2]^-$ orientations at a certain normal force which cause pinning and interlocking with the $[C_2C_1Im]^+$ ions at the mica surface, which act to increase the friction above that of the $[C_2C_1Im]^+$ ions at the mica interface. This behaviour is reversible, such that the surfaces always separate from the same adhesive minimum at ~2 nm regardless of the extent of confinement beforehand (as long as squeeze-out to a single cation monolayer did not occur).

These results rationalize previous reports of discontinuities in the friction across molecular liquids when the number of layers changes[219-220], here demonstrating multiple quantized friction regimes with varying friction coefficients and quantifying the effects of adhesion on the overall friction force. This result helps explain the boundary lubrication of rough surfaces where the liquid film is of varying thicknesses across the

contact zone: the total friction is made up of differently weighted contributions from each film thickness despite uniform applied load. Thus the quantized friction regimes resolved using atomically-smooth surfaces will provide a link between single-asperity and rough-contact friction.

## 7.3 Sliding Mechanisms Across a Bilayer Forming Ionic Liquid

Given that the $F_N$ vs. $D$ behaviour is also oscillatory for $[C_{10}C_1Pyrr][NTf_2]$, the friction force ($F_S$) can be measured across each of three, two, and one $[C_{10}C_1Pyrr][NTf_2]$ bilayers between the mica sheets in a similar way to that shown for $[C_4C_1Pyrr][NTf_2]$ monolayers in the previous section. By measuring $F_S$ whilst varying $F_N$, including negative values of $F_N$ in the case of adhesive regimes, distinct friction versus load laws for each number of bilayers were recorded.

Figure 51 shows that for a film ~8.5 nm thick consisting of three bilayers, the friction force is below the resolution of the instrument. For a film of 5.0 nm, consisting of two bilayers, a small but measurable friction force is detected that varies linearly with applied load; $F_S$, vs. $F_N$, gives a low friction coefficient $\mu = 0.0072 \pm 0.0064$ for two bilayers. Squeezing out another bilayer results in a film ~2.4 nm thick, corresponding to one bilayer between the surfaces, with a concomitant abrupt increase in friction. The friction across one bilayer can also be fitted as a linear function of load (a JKR-type fit is also possible within the experimental scatter), giving rise to a much higher coefficient of $\mu = 0.45 \pm 0.04$. In this case of one ionic liquid bilayer, there is also a large adhesion contribution to the measured friction; this manifests itself in the 130 μN friction force measure at zero applied load.

Comparing these values for $[C_{10}C_1Pyrr][NTf_2]$ to those obtained for $[C_4C_1Pyrr][NTf_2]$ which forms monolayers (not bilayers) in thin films, it is noteworthy that the friction for two bilayers is lower than for any of the measured monolayer regimes (9, 7, 5 and 3 ion monolayers), where the friction for one bilayer is higher than for any of the monolayer regimes. While two (or more) bilayers are extremely lubricating, once the film is squeezed down to one bilayer, it becomes very sticky.

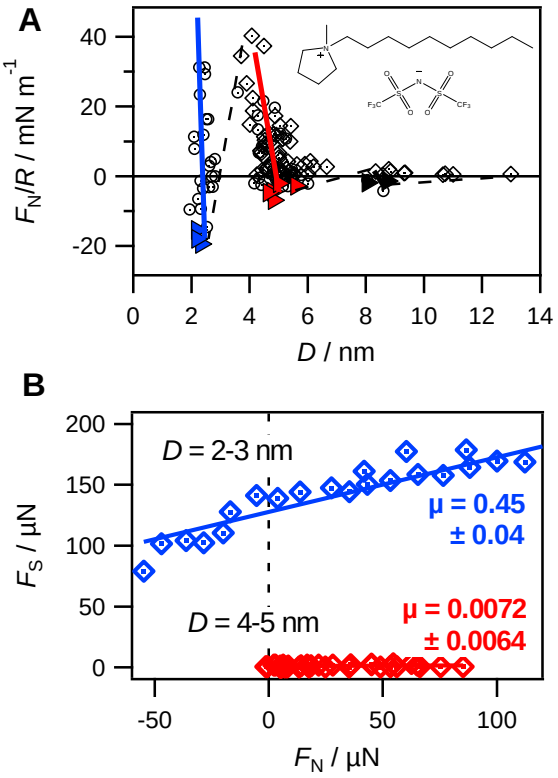


**Figure 51**

Normal and shear forces between mica sheets across $[C_{10}C_1Pyrr][NTf_2]$ thin films. (A) $F_N/R$ vs. $D$, showing the sequential squeeze-out of bilayers as described in the previous chapter. (B) $F_S$ vs. $F_N$ measured for one and two bilayers; the friction across one bilayer is shown in blue and corresponds to the blue region in (A). Similarly, the friction across two bilayers is shown in red and corresponds to the red region in (A). Lines are linear fits to data from four separate experiments using different pairs of mica sheets.

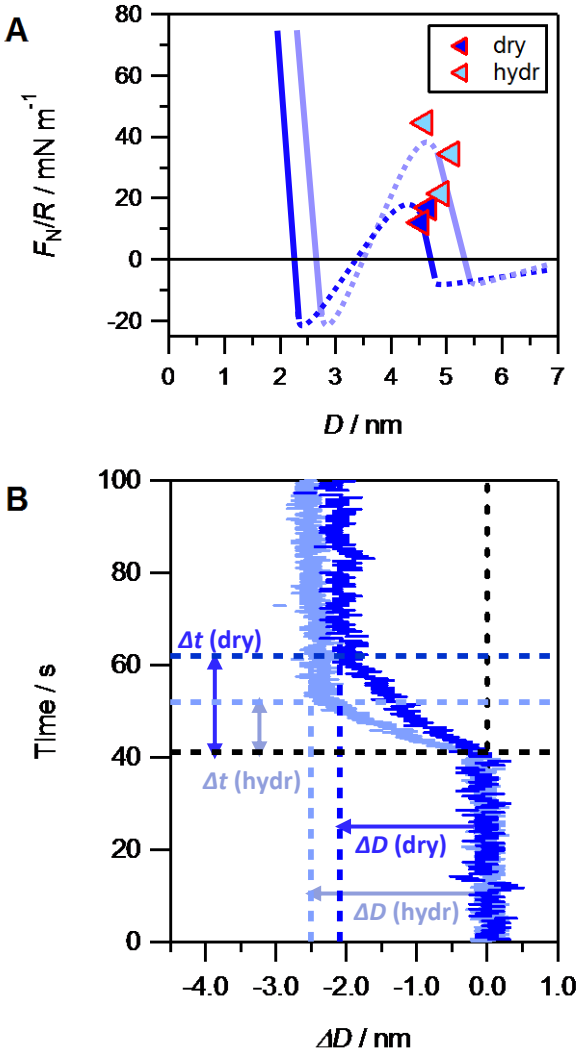


**Figure 52**

(A) $F_N/R$ vs. $D$ with points marking the maxima for wet and dry $[C_{10}C_1Pyrr][NTf_2]$. Lines are sketched to show the force laws (as in Figure 51A) for wet and dry $[C_{10}C_1Pyrr][NTf_2]$ with data points removed for clarity. Only the maximum points are shown to demonstrate the higher load required to squeeze out hydrated bilayers. (B) Traces showing the squeeze-out: film thicknesses as a function of time recorded during the transition from two bilayers to one bilayer for wet (light blue) and dry (dark blue) $[C_{10}C_1Pyrr][NTf_2]$, with dashed lines indicating $\Delta D$ and $\Delta t$ for the transition in each case. $R$ was very closely similar in the two cases.

The effect of small quantities of water incorporated into the ionic liquid on the $F_N$ vs. $D$ profiles is presented in Figure 52A. The arrangement of ions in the confined film remains similar when the ionic liquid is wet, as revealed by the oscillatory profiles with peaks in force corresponding to one, two, and three bilayers as for the dry system, although the force required to rupture each bilayer is higher than for the respective dry bilayers. The presence of water within the bilayer structure causes a small but clearly measurable dilation of the bilayers.

Figure 52B shows the film thickness transition between one and two bilayers is 2.1 nm for the dry ionic liquid and 2.5 nm for the wet ionic liquid. The hydration of the ionic liquid thus causes a dilation of 0.4 nm due to the presence of water in the mid-plane ion region. Looking more closely at the kinetics of the 'squeeze-out' process for wet and dry bilayers it can be seen that once sufficient load is applied for two bilayers to rupture and give way to a single bilayer, the squeeze-out process occurs more quickly when water is present than for the dry bilayers, i.e., $\Delta t(\text{dry}) > \Delta t(\text{hydr})$.

Having established structural properties of the hydrated bilayer structure, the effect of hydration (incorporated water) on the shear stress at each film thickness was examined (Figure 53). As for the dry ionic liquid, distinct 'quantized' friction regimes are observed for one bilayer and for two bilayers of the hydrated ionic liquid between the surfaces. Friction measurements across one bilayer of humidified ionic liquid show little difference compared to one bilayer of the dry ionic liquid; there is a small difference in intercept due to the adhesion contribution to friction, but the friction coefficient (gradient) remains closely similar – as shown in Figure 53A. In dramatic contrast, the friction across a film of two bilayers is increased by more than an order of magnitude by the presence of hydration water (Figure 53B). Furthermore, it is evident that added water is causing an incease in the adhesion contribution to friction, manifested as the larger $F_S$ at $F_N = 0$ for the wet ionic liquid.

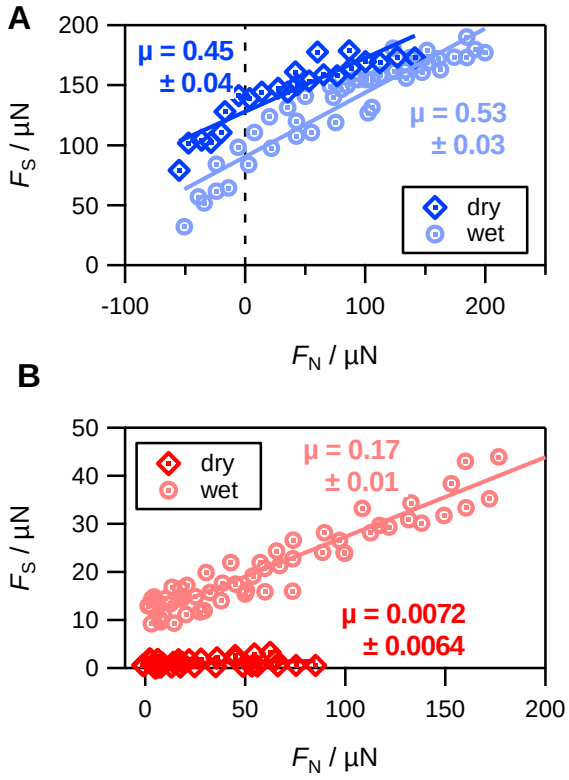


**Figure 53**

Effect of hydration on friction across one and two bilayers. (A) $F_S$ vs. $F_N$ measured across one confined bilayer for the dry liquid (diamonds) and for the liquid exposed to ambient humidity (circles). (B) $F_S$ vs. $F_N$ measured across two confined bilayers for the dry liquid (diamonds) and for the liquid exposed to ambient humidity (circles). Lines shown are linear fits to data from seven experiments each using different pairs of mica sheets.

For clarity of reference in the following discussion, key points from the results described above are now summarised:

**Observations**.

(i) The force required to shear a film of 2 bilayers is much less than that for 1 bilayer, at the same value of normal load. This is irrespective of whether the bilayers are dry or hydrated.

(ii) The force required to shear one bilayer is similar for dry and for hydrated bilayers.

(iii) The force required to shear two bilayers is much reduced, by 1-2 orders of magnitude, for dry compared to hydrated bilayers.

(iv) Hydration of the bilayers causes a swelling of 0.4 nm per bilayer.

(v) The load (or normal force, $F_N$) required to reduce the film thickness from two bilayers to one bilayer is greater for hydrated than for dry bilayers.

(vi) The adhesion force associated with pull-apart from two bilayers is similar (the same within experimental scatter) for wet and dry bilayers.

(vii) The rate of squeeze-out from two bilayers to one bilayer is faster for wet than for dry bilayers.

**Assumptions**.

(i') Incorporated water goes to the charged interface(s) rather than the alkyl region(s), as indicated in Figure 54.

(ii') Shearing occurs solely at the plane(s) of lowest shear stress

From these observations and assumptions the following mechanistic implications can be deduced, which include the likely planes of shear for bilayer films:

Implications.

(I) **A film consisting of 1 bilayer shears at the alkyl region**. (From observation ii and assumption i'). The negligible effect of water on the shear of one bilayer implies that the shear plane is not significantly affected by incorporation of water into the liquid. Since water is likely to reside in the ion-rich regions, and not in the hydrophobic alkyl regions, this implies that the shear of one bilayer takes place at the alkyl plane. Small differences in the friction between one dry bilayer and one hydrated bilayer might have been expected due to changes of density and interdigitation in the alkyl

region when the ionic headgroups are hydrated, but interestingly the coefficient of friction remains closely similar; therefore it can be deduced that the interdigitation and fluidity of the alkyl regions remain largely unchanged by hydration of the head groups up to these amounts of water.

(II) **A film consisting of two (dry) bilayers shears at the mid-plane ion region** (from observation i and assumption ii'). This follows from the observation that friction is much lower for two bilayers than for one bilayer so the active shear plane must be not present in a one bilayer film, otherwise it would also allow the same lower stress shearing for 1 bilayer. The only such feature, present in a two bilayer film but not in a one bilayer film, is the mid-plane ion region.

(III) **Hydration of the bilayers involves incorporation of approximately one or two hydration shells of water, or molecular layers of water, into the mid-plane ion region; and this acts to increase order in the ion region** (from observations iii, iv, and v, and assumption i'). The difference in liquid film thickness between two bilayers and one bilayer was observed to be 0.4 nm for hydrated compared to dry bilayers; i.e. $\Delta D_{hydr} = \Delta D_{dry} + 0.4$ nm , where $\Delta D = D$(2 bilayers) – $D$(1 bilayer). This increase in thickness caused by hydration corresponds roughly to the diameter of one water molecule per bilayer, so we suggest a picture of roughly one molecular monolayer of water incorporated into the headgroup region of each bilayer. The precise arrangement or structure of the hydrated film cannot be determined in the present experiments. The outcome of this hydration appears to be a *solidification* of the bilayers, possibly due to an increase in order of the ions within the layers: this is seen in both the normal force profiles, where hydrated bilayers require a greater load to be ruptured than dry bilayers, and in the shear forces where two hydrated bilayers required a greater lateral force to be sheared past one another.

(IV) **A film consisting of two hydrated bilayers shears at the mid-plane ion region; however the friction at this plane is much increased by hydration of the ions** (from observations i and iii, and assumptions i'. and ii'.) Although $F_S$ (at any given value of $F_N$) is greater by 1-2 orders of magnitude for two hydrated compared to two dry bilayers, it remains enormously less than the friction across one bilayer: $F_S$ at $F_N$ = 0 is an order of magnitude less and $\mu$ is a factor of 2-3 less, than for 1 bilayer. Thus the shearing remains at the mid-plane ionic interface for two hydrated bilayers (the feature not available to a one bilayer system), with the incorporated hydration at this plane leading to an increase in the friction (both gradient and intercept). This *increase* in friction in the presence of hydration water is perhaps surprising (although it does reinforce work of Espinosa-Marzal which also reported increase in friction with wetter ionic liquids[165, 224]), since water might be expected to 'lubricate' the ion-ion relative motion, either (a) by increasing ion-ion separation and so reducing the interaction potential between shearing layers, or (b) by the 'hydration lubrication' mechanism involving dissipation by rapid interchange of neighbouring water molecules[225-226]. This apparent 'stiffening' of the layers with respect to shear suggests the mid-plane ion region is more ordered in the presence of a monolayer of water, with water perhaps facilitating a more ordered packing of the cation headgroups.

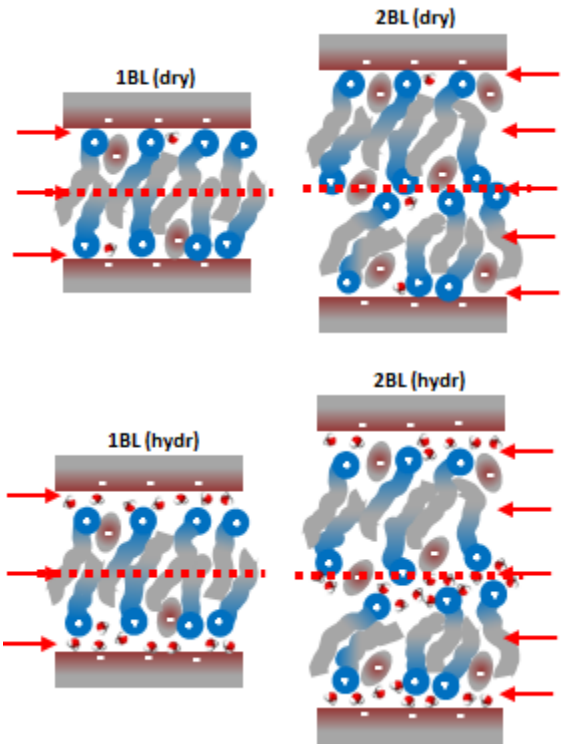


**Figure 54**

Schematic representations of the systems studied: one dry bilayer '1BL (dry)', two dry bilayers '2BL (dry)', one hydrated bilayer '1BL (hydr', and two hydrated bilayers '2BL (hydr)'. The diagrams indicate the active planes of shear (labelled with red dashed lines) as indicated in the text.

(V) **The plane of shear is not necessarily equivalent to the plane of (de)adhesion** (from observations iii, iv and vi, and assumption i'). Despite the large effect of water on shear of two bilayers (including the adhesion contribution to friction), water has no effect on their measured pull-off force. This implies that the plane of shear, which has a certain adhesion associated with it that contributed to the measured friction force, is not equivalent to the plane of de-adhesion[85]. In fact, the process of pulling the surfaces apart may not involve de-adhesion at a single plane and is likely to involve more complex molecular rearrangements as bulk liquid enters the film. Importantly, this implies that the measured adhesion is not always equivalent to the adhesion force contributing to adhesion controlled friction.

(VI) **Squeeze-out can occur by a mechanism quite distinct from shear** (from observations iii, v and viii, and assumption i'). Comparison between the effect of water on shear of two bilayers (i.e., to increase the friction) and its effect on the rate of squeeze-out (more rapid) appears surprising; if water causes a solidification and shear stiffening (implication iii), then why should the squeeze-out process from two bilayers to one bilayer happen more quickly? It appears that the mechanism of squeeze-out is different for dry and hydrated bilayers. One possible description is the following. The more fluid dry bilayers squeeze out via a viscous mechanism related to shearing of the layers, 'shearing off' a layer. The wet bilayers are much more solid-like at the plane of shear, and therefore, this mechanism is not favoured. Instead, once a higher normal load is reached, a more catastrophic event involving melting (i.e., molecular reorganisations breaking up the bilayers) occurs, allowing molecules to squeeze-out more rapidly.

## 7.4 Summary

These high resolution measurements reveal the following notable features for the first time in ionic liquid: (i) discrete friction regimes for each number of ion layers in the film, leading to multi-valued friction as a function of load; (ii) stick-slip friction observed below a critical velocity for certain ionic liquids; and (iii) different friction coefficients measured for each film thickness. This latter point implies that the mechanism of friction across ionic liquids is qualitatively different to non-polar liquids, where the friction coefficients are essentially independent of film thickness except for the last confined molecular layer[140, 220].

In combination these implications constitute a picture of the subtle friction mechanisms at play in systems of one and two bilayers. Most significantly, a film of lubricant thick

enough to contain two (or more) bilayers will shear along the ionic planes rather than at the alkyl planes, and the friction coefficient of these planes can be orders of magnitude lower than for a single confined bilayer. These conclusions are pertinent to the understanding of lubrication in ionic liquids, and one imagines the same molecular mechanisms are likely to hold in other multi-lamellar phases such as liquid crystals or surfactant solutions at high concentration. Put together, these findings point at new ways to control friction in microscopic systems and to develop ionic liquid lubricants for specialized applications.

# 8 SUMMARY AND OUTLOOK

This thesis explores the nanostructure of a variety of non-aqueous liquids and solutions confined to thin films, and the effect of their film structure on molecular mechanisms of friction and lubrication. The results are exclusively surface force measurements with extreme sensitivity and resolution in shear stress and surface separation. The systems investigated include organic friction modifiers commonly used in engine oil additives, and ionic liquids, whose properties makes them promising both as electrolytes at nanoporous electrodes and as specialist lubricants.

Chapter 4 compares and contrasts film structures and lubricating behavior for various surfactants dissolved in dodecane, a model base oil. Pure dodecane forms solid-like films when confined to molecular dimensions, generally with high friction and with stick-slip behaviour. All surfactants studied significantly reduce friction of the base oil when added in small amounts by adsorbing as monolayers to the surfaces, with their orientation with respect to the surface determined by molecular structure. Friction across these confined films exhibits smooth sliding with low friction coefficients.

Experiments with mixtures of added GMO and GTO surfactant suggest that there is no preferential adsorption of a particular molecule. While the adsorbed GMO monolayer structure dictates the measured normal forces in mixed solutions, it is clear from the shear measurements that there are significant amounts of GTO also present at the surfaces. For up to small amounts of GTO added to a predominantly GMO solution (10:90 mass ratio), the reduction in lubrication is small. However when present in larger amounts (50:50 mass ratio), the friction coefficient can increase by an order or

magnitude compared to GTO solutions and two orders of magnitude compared to GMO solutions.

It would be very interesting to examine the adsorption behaviour using QCM, spectroscopy[227] or AFM under liquid to determine adsorbed amounts and morphology of the monolayers adsorbed from solution. This would be particularly interesting for the surfactant mixtures, where competition at the surfaces with other additives in formulations such as detergents and dispersants can affect the adsorbed film. At the macroscopic scale, changing one component in a lubricant formulation can have marked and unexplained effects on its lubricating behaviour. As such, what may appear to be only a moderately performing friction modifier in a base oil may actually be excellent in a fully formulated engine oil. Thus it is incredibly important to understand molecular mechanisms of how the additive molecules interact both with each other and at the surfaces, and these surface force measurements provide valuable information on film structure and friction reduction to compare with recent molecular dynamics simulations of similar model systems[94, 228].

Chapter 5 presents measurements with nano-confined ionic liquids, directly revealing with molecular resolution the pronounced layered structures. Varying the alkyl chain length of the ionic liquids revealed a dramatic cross-over in the interfacial layering structure, from alternating cation- and anion-enriched monolayers for ionic liquids with short alkyl chains, to bilayer formation for more amphiphilic ions. The ‘monolayers’ consist of anions sandwiched between monolayers of cations with the alkyl chains generally lying parallel to the surface. The ‘bilayers’ consist of cations lying more perpendicular to the surface, allowing segregation of the non-polar moieties away from ionic regions. The extent of alkyl chain interdigitation was found to depend on both the chemistry and geometry of the ions. The preference for bilayer structures when the alkyl chains exceed a critical value is reminiscent of amphiphile self-assembly in water, albeit

with the additional constraint that with no solvent all of the space must be filled by the ions.

The results presented in this thesis have contributed substantially towards current understanding of ionic liquid structure at interfaces and in confined geometries. Among the most promising applications is their use as electrolytes for energy storage devices such as supercapacitors - particularly when confined in nanoporous electrode structures - which show enhanced capacitance properties when ion dimensions match pore sizes. Much recent work in the literature has focused on the structure and dynamics of ion adsorption at electrodes, with simulations offering many useful molecular insights. However experiments directly probing the structure at the solid-liquid interface are scarce and thus these surface force measurements contribute to the development of electrochemical devices based on ionic liquid electrolytes.

There is currently also great interest in the nano-scale mechanisms of friction and lubrication with ionic liquids, which combine many useful physical properties, and the dynamics of ionic liquids in confinement are unusual compared to either aqueous or non-aqueous liquids. While ionic liquids are expensive to manufacture in large quantities, of particular interest is their use as specialist lubricants in high vacuum or extreme temperature conditions. With the ongoing miniaturisation of devices they are also prospective lubricants for nano/microelectromechanical systems (NEMS/MEMS), where lubrication must be achieved with ultra-thin films, typically only a few molecular layers. At such small length scales, surface forces dominate and it becomes critical to understand molecular friction, adhesion and wear mechanisms at the nanoscale.

Chapter 6 shows measurements of the friction force transmitted between the surfaces across ionic liquid films, showing clear evidence for ‘quantized’ friction. Multiple friction-load regimes with different friction coefficients are measured for different numbers of layers for the same ionic liquid. Thus there is no single-valued friction-load

relationship for a particular liquid. Adhesive contributions to friction, which depend on the number of confined layers, result in significant friction at zero and even negative applied loads. Importantly, the results not only provide information on friction dissipation mechanisms of ionic liquids, but also help to explain the difference in friction measured between rough contacts and that measured between extremely smooth surfaces or single asperities. This is a long-standing problem in the field of tribology since even highly polished surfaces have roughness at the nanoscale resulting in different film thicknesses at the same sliding interface.

Ionic liquids display different friction coefficients depending on the number of confined layers. In contrast, non-polar liquids generally exhibit a higher friction coefficient, similar for each layer (although the oscillatory nature of the structural forces also leads to quantized friction in these cases, due to the varying adhesion contribution to friction for each layer). One puzzling feature is that sliding between ion layers in ionic liquids can result in much lower friction coefficients compared to molecular liquids, which might be unexpected due to strong electrostatic interactions between ion layers of opposite charge in the films. This hints at the importance of disorder in-plane, reducing the activation barrier to molecular hopping taking place at the shearing interface.

One strong argument to explain the higher friction coefficients for molecular liquids (which form layered structures) compared to ionic liquids could be that slip may in fact be occurring at the liquid/wall interface for molecular liquids, given that the friction coefficients are so similar for different numbers of confined non-polar molecules. Shear melting phase transitions are a popular mechanism to explain stick-slip friction in confined liquids[229]. However, shear melting is unfavourable for ionic liquid films due to the high coulombic penalty of ions swapping between layers. The extreme similarity in stick-slip behavior for pyrrolidinium-based ionic liquids and for non-polar molecular liquids suggests a different mechanism to shear-melting may be taking place. Other possible mechanisms include - but are not limited to – molecules melting only in a

particular layer during the ‘slip’ phase, or something more akin to solid-on-solid sliding, where the surfaces periodically ‘stick’ and ‘slip’ due to elastic deformations within the solid-like film.

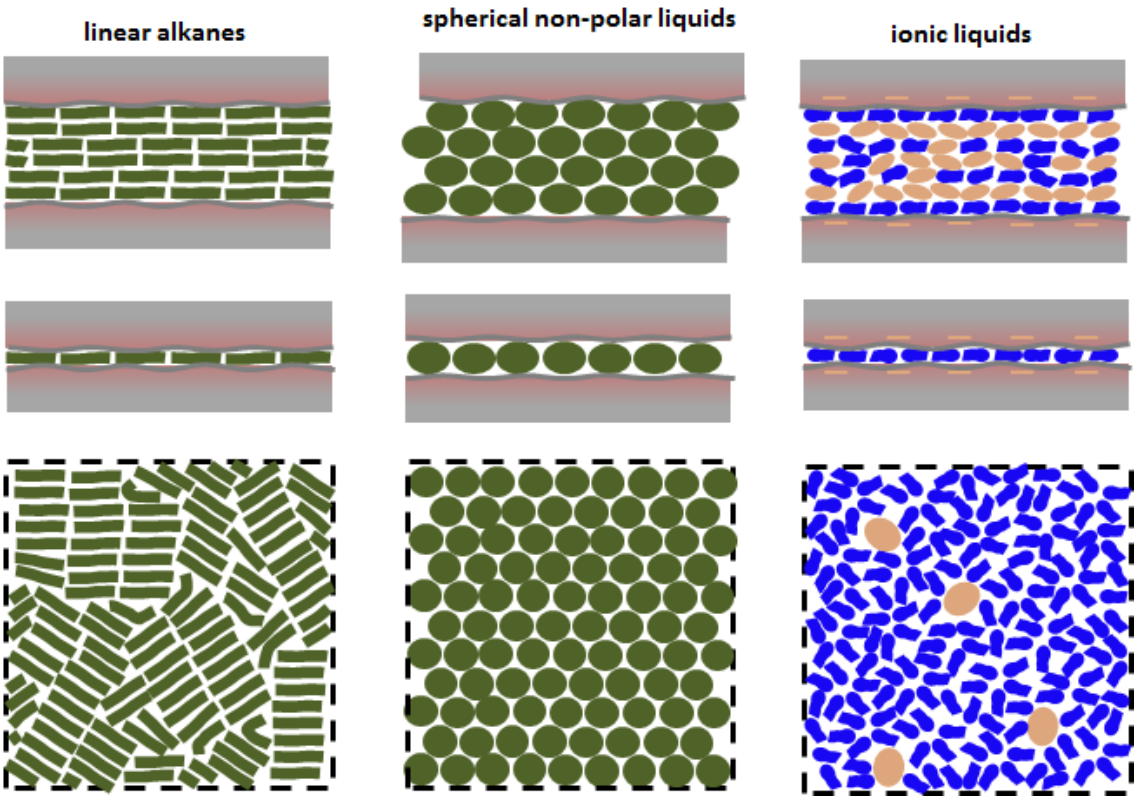


**Figure 55**

Schematics of confined liquids showing layered structures in the direction normal to the surface and lateral order within a particular liquid layer.

For ionic liquids, the measured oscillatory structural forces reveal order in the direction normal to the surface, but the lateral structure is much more disordered[230-231]. Conversely, molecular liquids which solidify in confinement order themselves in close packed structures with molecules in layers commensurate with respect to each other[232]. In such cases the friction between layers may be very high, and so slip may instead be occurring at the mica interface, which is most certainly not commensurate with the liquid. That cyclohexane has greater friction than for OMCTS with the same number of

layers[139] has been attributed to the smaller size of cyclohexane molecules and greater 'apparent roughness' of the mica surfaces (at the atomic level), suggesting further that the slip plane for these liquids may be at the mica interface. For linear alkanes this is further complicated by mosaic-like structures which can form 'crystalline bridges' across the film[146].

Comparing friction forces measured for different numbers of ionic liquid bilayers with or without the addition of small amounts of water enables elucidation of shear planes and sliding mechanisms in the confined films. Most significantly, a film of lubricant thick enough to contain two (or more) bilayers will shear along the ionic planes of the bilayers rather than at the alkyl planes, and the friction coefficient of these planes can be orders of magnitude lower than for a single confined bilayer, where sliding must take place between the alkyl chains. These conclusions are pertinent to the understanding of lubrication in ionic liquids, and one imagines similar molecular mechanisms are likely to hold in other multi-lamellar phases such as liquid crystals or surfactant solutions at high concentration. These molecular mechanisms of ion lubrication differ markedly from the results described in Chapter 4, and from the prevailing paradigm in non-aqueous lubrication in general, which asserts in essence that surfaces coated in amphiphiles slide past each other by way of the 'slippery' exposed alkyl chains while the polar headgroups remain anchored at the surface.

One exciting future direction is the use of electrochemical methods to control structure and friction in electrolyte films[233], and particularly of interest is to investigate charging dynamics of ions in confinement[209-210, 234]. Mixing large ions with neutral solvent molecules and monitoring the confined film thickness could help distinguish between possible expulsion of ions from the film, adsorption of counterions into the film, or exchange between ions and counterions upon changing the applied surface potential. Diffusion bonded metal surfaces[152], which may be smoother than those prepared by conventional template stripping with glue[125] could be a useful route to explore. Another

method of preparing atomically smooth conducting surfaces is to use graphene, recently demonstrated to control double layer forces across aqueous electrolytes[126]. Molecular dynamics simulations have shown recently that charging dynamics can be considerably accelerated with the use of ionophobic pores[235]. Indeed, different flow properties of ionic liquids have been observed experimentally at methyl-terminated surfaces compared to mica[121]. However carbon-based materials are widely studied as electrodes and are already 'ionophobic', so perhaps a more careful selection of electrolyte systems with high cohesive energy density may improve performance.

More generally, techniques to examine the properties of the confined films *in situ* during shear, such as sum frequency generation spectroscopy[236], x-ray diffraction[237], fluorescence spectroscopy[238] could uncover fundamental phenomena of energy dissipation in friction for different systems. There are many parameters to investigate, and the elucidation of intermolecular and surface interactions both at a fundamental level and when applied to a wide variety of practical systems remains an exciting challenge for the future.

# 9 REFERENCES


1. Tabor, D.; Winterton, Direct measuement of normal and retarded van der Waals forces. *Proceedings of the Royal Society of London Series a-Mathematical and Physical Sciences* **1969,** *312* (1511), 435-&.

2. Israelachvili, J. N.; Tabor, D., Measurement of van der Waals dispersion forces in range 1.5 to 130 nm. *Proceedings of the Royal Society of London Series a-Mathematical and Physical Sciences* **1972,** *331* (1584), 19-&.

3. Derjaguin, B. V.; Landau, L., *Acta Physicochim* **1941,** *14*, 633.

4. Verwey, E. J.; Overbeek, J. T. G., *Theory of the Stability of Lyophobic Colloids* **1948**.

5. Israelachvili, J. N., Adhesion Forces Between Surfaces in Liquids and Condensable Vapors. *Surface Science Reports* **1992,** *14* (3), 109-159.

6. Dzyaloshinskii, I. E.; Lifshitz, E. M.; Pitaevskii, L. P., *Adv. Phys.* **1961,** *10*, 165.

7. Israelachvili, J., *Intermolecular & Surface Forces (Second Edition)* **1991**.

8. Chan, D. Y. C.; Pashley, R. M.; White, L. R., A simple algorithm for the calculation of the electrostatic repulsion between identical charged surfaces in electrolyte. *Journal of Colloid and Interface Science* **1980,** *77* (1), 283-285.

9. Horn, R. G.; Israelachvili, J. N., Direct Measurement of Forces due to Solvent Structure. *Chemical Physics Letters* **1980,** *71* (2), 192-194.

10. Horn, R. G.; Israelachvili, J. N., Direct measurement of structural forces between 2 surfaces in a non-polar liquid. *Journal of Chemical Physics* **1981,** *75* (3), 1400-1411.

11. Mitchell, D. J.; Ninham, B. W.; Pailthorpe, B. A., Solvent structure in particle interactions. Part 2.-Forces at short range. *Journal of the Chemical Society, Faraday Transactions 2: Molecular and Chemical Physics* **1978,** *74* (0), 1116-1125.

12. van Megen, W.; Snook, I., Solvent structure and solvation forces between solid bodies. *Journal of the Chemical Society, Faraday Transactions 2: Molecular and Chemical Physics* **1979,** *75* (0), 1095-1102.

13. Israelachvili, J. N.; Adams, G. E., Measurement of Forces Between 2 Mica Surfaces in Aqueous-Electrolyte Solutions in Range 0-100 nm. *Journal of the Chemical Society-Faraday Transactions I* **1978,** *74*, 975-&.

14. Pashley, R. M., DLVO and hydration forces between mica surfaces in LI+,Na+,K+, and Cs+ electrolyte solutions: - a correlation of double-layer and hydration forces with surface cation-exchange properties. *Journal of Colloid and Interface Science* **1981,** *83* (2), 531-546.

15. Pashley, R. M., Hydration forces between mica surfaces in aqueous electrolyte solutions. *Journal of Colloid and Interface Science* **1981,** *80* (1), 153-162.

16. Israelachvili, J. N.; Pashley, R. M., Molecular layering of water at surfaces and origin of repulsive hydration forces. *Nature* **1983,** *306* (5940), 249-250.

17. Pashley, R. M.; Israelachvili, J. N., Molecular layering of water in thin films between mica surfaces and its relation to hydration forces. *Journal of Colloid and Interface Science* **1984,** *101* (2), 511-523.

18. Espinosa-Marzal, R. M.; Drobek, T.; Balmer, T.; Heuberger, M. P., Hydrated-ion ordering in electrical double layers. *Physical Chemistry Chemical Physics* **2012,** *14* (17), 6085-6093.

19. Baimpos, T.; Shrestha, B. R.; Raman, S.; Valtiner, M., Effect of Interfacial Ion Structuring on Range and Magnitude of Electric Double Layer, Hydration, and Adhesive Interactions between Mica Surfaces in 0.05–3 M Li+ and Cs+ Electrolyte Solutions. *Langmuir* **2014,** *30* (15), 4322-4332.

20. Evans, D. F.; Wennerström, H., *The Colloidal Domain: Where Physics, Chemistry, Biology, and Technology Meet*. Wiley: 1999.

21. Chandler, D., Interfaces and the driving force of hydrophobic assembly. *Nature* **2005,** *437* (7059), 640-647.

22. Christenson, H. K.; Claesson, P. M., Direct measurements of the force between hydrophobic surfaces in water. *Advances in Colloid and Interface Science* **2001,** *91* (3), 391-436.

23. Tabor, R. F.; Grieser, F.; Dagastine, R. R.; Chan, D. Y. C., The hydrophobic force: measurements and methods. *Physical Chemistry Chemical Physics* **2014,** *16* (34), 18065-18075.

24. Silbert, G.; Ben-Yaakov, D.; Dror, Y.; Perkin, S.; Kampf, N.; Klein, J., Long-Ranged Attraction between Disordered Heterogeneous Surfaces. *Physical Review Letters* **2012,** *109* (16), 168305.

25. Attard, P., Thermodynamic Analysis of Bridging Bubbles and a Quantitative Comparison with the Measured Hydrophobic Attraction. *Langmuir* **2000,** *16* (10), 4455-4466.

26. Tyrrell, J. W. G.; Attard, P., Atomic Force Microscope Images of Nanobubbles on a Hydrophobic Surface and Corresponding Force−Separation Data. *Langmuir* **2002,** *18* (1), 160-167.

27. Attard, P., Nanobubbles and the hydrophobic attraction. *Advances in Colloid and Interface Science* **2003,** *104* (1–3), 75-91.

28. Tabor, R. F.; Wu, C.; Grieser, F.; Dagastine, R. R.; Chan, D. Y. C., Measurement of the Hydrophobic Force in a Soft Matter System. *The Journal of Physical Chemistry Letters* **2013,** *4* (22), 3872-3877.

29. Klein, J.; Kumacheva, E., Simple liquids confined to molecularly thin layers. I. Confinement-induced liquid-to-solid phase transitions. *Journal of Chemical Physics* **1998,** *108* (16), 6996-7009.

30. Binnig, G.; Quate, C. F.; Gerber, C., Atomic Force Microscope. *Physical Review Letters* **1986,** *56* (9), 930-933.

31. Binnig, G.; Rohrer, H.; Gerber, C.; Weibel, E., Tunneling through a controllable vacuum gap. *Applied Physics Letters* **1982,** *40* (2), 178-180.

32. Abraham, F. F., The interfacial density profile of a Lennard-Jones fluid in contact with a (100) Lennard-Jones wall and its relationship to idealized fluid/wall systems: A Monte Carlo simulation. *The Journal of Chemical Physics* **1978,** *68* (8), 3713-3716.

33. Magda, J. J.; Tirrell, M.; Davis, H. T., Molecular dynamics of narrow, liquid-filled pores. *The Journal of Chemical Physics* **1985,** *83* (4), 1888-1901.

34. Evans, R.; Marini Bettolo Marconi, U., Phase equilibria and solvation forces for fluids confined between parallel walls. *The Journal of Chemical Physics* **1987,** *86* (12), 7138-7148.

35. Evans, R.; Parry, A. O., Liquids at interfaces: what can a theorist contribute? *Journal of Physics: Condensed Matter* **1990,** *2* (S), SA15.

36. Tarazona, P.; Marconi, U. M. B.; Evans, R., Phase equilibria of fluid interfaces and confined fluids. *Molecular Physics* **1987,** *60* (3), 573-595.

37. Vanderlick, T. K.; Scriven, L. E.; Davis, H. T., Molecular theories of confined fluids. *The Journal of Chemical Physics* **1989,** *90* (4), 2422-2436.

38. Kjellander, R.; Marčelja, S., Inhomogeneous Coulomb fluids with image interactions between planar surfaces. I. *The Journal of Chemical Physics* **1985,** *82* (4), 2122-2135.

39. Mitchell, D. J.; Ninham, B. W.; Pailthorpe, B. A., Solvent structure in particle interactions. Part 2. - Forces at short range. *Journal of the Chemical Society, Faraday Transactions 2: Molecular and Chemical Physics* **1978,** *74*, 1116-1125.

40. Gao, J.; Luedtke, W. D.; Landman, U., Structure and solvation forces in confined films: Linear and branched alkanes. *The Journal of Chemical Physics* **1997,** *106* (10), 4309-4318.

41. Porcheron, F.; Schoen, M.; Fuchs, A. H., Monte Carlo simulation of a complex fluid confined to a pore with nanoscopically rough walls. *The Journal of Chemical Physics* **2002,** *116* (13), 5816-5824.

42. Ghatak, C.; Ayappa, K. G., Solvation force, structure and thermodynamics of fluids confined in geometrically rough pores. *The Journal of Chemical Physics* **2004,** *120* (20), 9703-9714.

43. Hertz, H.; Reine, J., On the contact of elastic solids. *Angew. Math.* (92), 156.

44. Johnson, K. L.; Kendall, K.; Roberts, A. D., Surface Energy and the Contact of Elastic Solids. *Proceedings of the Royal Society of London. A. Mathematical and Physical Sciences* **1971,** *324* (1558), 301-313.

45. Derjaguin, B. V.; Muller, V. M.; Toporov, Y. P., Effect of contact deformations on the adhesion of particles. *Journal of Colloid and Interface Science* **1975,** *53* (2), 314-326.

46. Christenson, H. K.; Blom, C. E., Solvation Forces and Phase-Separation of water in a Thin-Film of Nonpolar Liquid between Mica Surfaces. *Journal of Chemical Physics* **1987,** *86* (1), 419-424.

47. Christenson, H. K., Forces Between Solid-Surfaces in a Binary Mixture of Non-Polar Liquids. *Chemical Physics Letters* **1985,** *118* (5), 455-458.

48. Christenson, H. K.; Horn, R. G.; Israelachvili, J. N., Measurement of Forces due to Structure in Hydrocarbon Liquids. *Journal of Colloid and Interface Science* **1982,** *88* (1), 79-88.

49. Klein, J.; Kumacheva, E., Confinement-induced phase transitions in simple liquids. *Science* **1995,** *269* (5225), 816-819.

50. Kumacheva, E.; Klein, J., Simple liquids confined to molecularly thin layers. II. Shear and frictional behavior of solidified films. *Journal of Chemical Physics* **1998,** *108* (16), 7010-7022.

51. Vanalsten, J.; Granick, S., Molecular tribometry of ultrathin liquid-films. *Physical Review Letters* **1988,** *61* (22), 2570-2573.

52. Granick, S., Motions and Relaxations of Confined Liquids. *Science* **1991,** *253* (5026), 1374-1379.

53. Yoshizawa, H.; Israelachvili, J., Fundamental mechanisms of interfacial friction .2. Stick-slip friction of spherical and chain molecules. *Journal of Physical Chemistry* **1993,** *97* (43), 11300-11313.

54. Gee, M. L.; McGuiggan, P. M.; Israelachvili, J. N.; Homola, A. M., Liquid to Solid-Like Transitions of Molecularly Thin-Films Under Shear. *Journal of Chemical Physics* **1990,** *93* (3), 1895-1906.

55. Granick, S., Soft matter in a tight spot. *Physics Today* **1999,** *52* (7), 26-31.

56. Harrowell, P., On the Microscopic Nature of Stick?Slip Behavior in Lubricating Films. In *Supramolecular Structure in Confined Geometries*, American Chemical Society: 1999; Vol. 736, pp 104-126.

57. Israelachvili, J.; McGuiggan, P.; Gee, M.; Homola, A.; Robbins, M.; Thompson, P., Liquid Dynamics in Molecularly Thin-Films. *Journal of Physics-Condensed Matter* **1990,** *2*, SA89-SA98.

58. Christenson, H. K.; Gruen, D. W. R.; Horn, R. G.; Israelachvili, J. N., Structuring in Liquid Alkanes Between Solid-Surfaces - Force Measurements and Mean-Field Theory. *Journal of Chemical Physics* **1987,** *87* (3), 1834-1841.

59. Groszek, A. J., Selective adsorption at Graphite/Hydrocarbon Interfaces. *Proceedings of the Royal Society of London Series a-Mathematical and Physical Sciences* **1970,** *314* (1519), 473-&.

60. Grosserhode, M.; Findenegg, G. H., Formation of Ordered Monolayers of Non-Alkanes at Cleavage Face of Nickel Chloride. *Journal of Colloid and Interface Science* **1978,** *64* (2), 374-376.

61. Qian, L. M.; Luengo, G.; Perez, E., How linear molecules resist to shear: the origin of nanoscale friction. *Science in China Series G-Physics Mechanics & Astronomy* **2004,** *47*, 15-20.

62. Zhu, Y.; Granick, S., Reassessment of Solidification in Fluids Confined between Mica Sheets. *Langmuir* **2003,** *19* (20), 8148-8151.

63. Israelachvili, J.; Maeda, N.; Akbulut, M., Comment on Reassessment of Solidification in Fluids Confined between Mica Sheets. *Langmuir* **2006,** *22* (5), 2397-2398.

64. Granick, S.; Zhu, Y.; Lin, Z.; Bae, S. C.; Wong, J. S.; Turner, J., Reply to Comment on Reassessment of Solidification in Fluids Confined between Mica Sheets. *Langmuir* **2006,** *22* (5), 2399-2401.

65. Zhu, Y.; Granick, S., Superlubricity: A Paradox about Confined Fluids Resolved. *Physical Review Letters* **2004,** *93* (9), 096101.

66. Gourdon, D.; Israelachvili, J., Comment on "Superlubricity: A Paradox about Confined Fluids Resolved". *Physical Review Letters* **2006,** *96* (9), 099601.

67. Wong, J. S.; Bae, S. C.; Anthony, S.; Zhu, Y.; Granick, S., Wong et al. Reply. *Physical Review Letters* **2006,** *96* (9), 099602.

68. Perkin, S.; Chai, L.; Kampf, N.; Raviv, U.; Briscoe, W.; Dunlop, I.; Titmuss, S.; Seo, M.; Kumacheva, E.; Klein, J., Forces between mica surfaces, prepared in different ways, across aqueous and nonaqueous liquids confined to molecularly thin films. *Langmuir* **2006,** *22* (14), 6142-6152.

69. Cummings, P. T.; Docherty, H.; Iacovella, C. R.; Singh, J. K., Phase transitions in nanoconfined fluids: The evidence from simulation and theory. *AIChE Journal* **2010,** *56* (4), 842-848.

70. Helmholtz, H., *Wiss. Abhandl. Physik. Tech. Reichsanstalt* **1879,** (1), 925.

71. Gouy, G., *J. Phys. Radium* **1910,** (9), 457.

72. Chapman, D. L., *Philos. Mag.* **1913,** (6), 475.

73. Zhang, L. L.; Zhao, X. S., Carbon-based materials as supercapacitor electrodes. *Chemical Society Reviews* **2009,** *38* (9), 2520-2531.

74. Christenson, H. K.; Horn, R. G., Direct measurement of the force between solid surfaces in a polar liquid. *Chemical Physics Letters* **1983,** *98* (1), 45-48.

75. Christenson, H. K., DLVO (Derjaguin-Landau-Verwey-Overbeek) theory and solvation forces between mica surfaces in polar and hydrogen-bonding liquids. *Journal of the Chemical Society, Faraday Transactions 1: Physical Chemistry in Condensed Phases* **1984,** *80* (7), 1933-1946.

76. Christenson, H. K.; Horn, R. G., Forces between mica surfaces in ethylene glycol. *Journal of Colloid and Interface Science* **1985,** *103* (1), 50-55.

77. Raviv, U.; Laurat, P.; Klein, J., Fluidity of water confined to subnanometre films. *Nature* **2001,** *413* (6851), 51-54.

78. Raviv, U.; Perkin, S.; Laurat, P.; Klein, J., Fluidity of Water Confined Down to Subnanometer Films. *Langmuir* **2004,** *20* (13), 5322-5332.

79. Klein, J.; Raviv, U.; Perkin, S.; Kampf, N.; Chai, L.; Giasson, S., Fluidity of water and of hydrated ions confined between solid surfaces to molecularly thin films. *Journal of Physics-Condensed Matter* **2004,** *16* (45), S5437-S5448.

80. Jagla, E. A., Boundary lubrication properties of materials with expansive freezing. *Physical Review Letters* **2002,** *88* (24), 2455041-2455044.

81. Leng, Y.; Cummings, P. T., Hydration structure of water confined between mica surfaces. *The Journal of Chemical Physics* **2006,** *124* (7), -.

82. Gaisinskaya, A.; Ma, L.; Silbert, G.; Sorkin, R.; Tairy, O.; Goldberg, R.; Kampf, N.; Klein, J., Hydration lubrication: exploring a new paradigm. *Faraday Discussions* **2012,** *156* (0), 217-233.

83. Klein, J., Hydration lubrication. *Friction* **2013,** *1* (1), 1-23.

84. Briscoe, W. H.; Titmuss, S.; Tiberg, F.; Thomas, R. K.; McGillivray, D. J.; Klein, J., Boundary lubrication under water. *Nature* **2006,** *444* (7116), 191-194.

85. Briscoe, W. H.; Klein, J., Friction and adhesion hysteresis between surfactant monolayers in water. *Journal of Adhesion* **2007,** *83* (7), 705-722.

86. Raviv, U.; Giasson, S.; Kampf, N.; Gohy, J.-F.; Jerome, R.; Klein, J., Lubrication by charged polymers. *Nature* **2003,** *425* (6954), 163-165.

87. Raviv, U.; Giasson, S.; Kampf, N.; Gohy, J.-F.; Jérôme, R.; Klein, J., Normal and Frictional Forces between Surfaces Bearing Polyelectrolyte Brushes. *Langmuir* **2008,** *24* (16), 8678-8687.

88. Chen, M.; Briscoe, W. H.; Armes, S. P.; Klein, J., Lubrication at Physiological Pressures by Polyzwitterionic Brushes. *Science* **2009,** *323* (5922), 1698-1701.

89. Tang, Z.; Li, S., A review of recent developments of friction modifiers for liquid lubricants (2007–present). *Current Opinion in Solid State and Materials Science* **2014,** *18* (3), 119-139.

90. Abraham, M. A.; W.D., D.; R., B., *An investigation into the effect of zinc dithiophosphate on ASTM sequence VIA fuel economy*. Society of Automobile Engineers: New York, N.Y., ETATS-UNIS, 1996; p 10.

91. Ruths, M.; Ohtani, H.; Greenfield, M.; Granick, S., Exploring the "friction modifier" phenomenon: nanorheology of n-alkane chains with polar terminus dissolved in n-alkane solvent. *Tribology Letters* **1999,** *6* (3-4), 207-214.

92. Zhu, Y.; Ohtani, H.; Greenfield, M.; Ruths, M.; Granick, S., Modification of Boundary Lubrication by Oil-Soluble Friction Modifier Additives. *Tribology Letters* **2003,** *15* (2), 127-134.

93. Greenfield, M. L.; Ohtani, H., Packing of Simulated Friction Modifier Additives under Confinement. *Langmuir* **2005,** *21* (16), 7568-7578.

94. Doig, M.; Warrens, C. P.; Camp, P. J., Structure and Friction of Stearic Acid and Oleic Acid Films Adsorbed on Iron Oxide Surfaces in Squalane. *Langmuir* **2013,** *30* (1), 186-195.

95. Lundgren, S. M.; Ruths, M.; Danerlov, K.; Persson, K., Effects of unsaturation on film structure and friction of fatty acids in a model base oil. *Journal of Colloid and Interface Science* **2008,** *326* (2), 530-536.

96. Campen, S.; Green, J.; Lamb, G.; Atkinson, D.; Spikes, H., On the Increase in Boundary Friction with Sliding Speed. *Tribology Letters* **2012,** *48* (2), 237-248.

97. Beltzer, M.; Jahanmir, S., Effect of additive molecular structure on friction. *Lubrication Science* **1988,** *1* (1), 3-26.

98. Wang, Y.; Voth, G. A., Unique Spatial Heterogeneity in Ionic Liquids. *Journal of the American Chemical Society* **2005,** *127* (35), 12192-12193.

99. Triolo, A.; Russina, O.; Bleif, H.-J.; Di Cola, E., Nanoscale Segregation in Room Temperature Ionic Liquids. *The Journal of Physical Chemistry B* **2007,** *111* (18), 4641-4644.

100. Canongia Lopes, J. N. A.; Pádua, A. A. H., Nanostructural Organization in Ionic Liquids. *The Journal of Physical Chemistry B* **2006,** *110* (7), 3330-3335.

101. Bhargava, B. L.; Devane, R.; Klein, M. L.; Balasubramanian, S., Nanoscale orgainsation in room temperature ionic liquids: a course grained molecular dynamics simulation study. *Soft Matter* **2007,** *3*, 1395-1400.

102. Hayes, R.; El Abedin, S. Z.; Atkin, R., Pronounced Structure in Confined Aprotic Room-Temperature Ionic Liquids. *The Journal of Physical Chemistry B* **2009,** *113* (20), 7049-7052.

103. Perkin, S., Ionic liquids in confined geometries. *Physical Chemistry Chemical Physics* **2012,** *14*, 5052-62.

104. Li, S.; Bañuelos, J. L.; Guo, J.; Anovitz, L.; Rother, G.; Shaw, R. W.; Hillesheim, P. C.; Dai, S.; Baker, G. A.; Cummings, P. T., Alkyl Chain Length and Temperature Effects on Structural Properties of Pyrrolidinium-Based Ionic Liquids: A Combined Atomistic Simulation and Small-Angle X-ray Scattering Study. *The Journal of Physical Chemistry Letters* **2011,** *3* (1), 125-130.

105. Mezger, M.; Schroder, H.; Reichert, H.; Schramm, S.; Okasinski, J. S.; Schoder, S.; Honkimaki, V.; Deutsch, M.; Ocko, B. M.; Ralston, J.; Rohwerder, M.; Stratmann,

M.; Dosch, H., Molecular layering of fluorinated ionic liquids at a charged sapphire (0001) surface. *Science* **2008,** *322* (5900), 424-428.

106. Zhou, H.; Rouha, M.; Feng, G.; Lee, S. S.; Docherty, H.; Fenter, P.; Cummings, P. T.; Fulvio, P. F.; Dai, S.; McDonough, J.; Presser, V.; Gogotsi, Y., Nanoscale Perturbations of Room Temperature Ionic Liquid Structure at Charged and Uncharged Interfaces. *ACS Nano* **2012,** *6* (11), 9818-9827.

107. Atkin, R.; Warr, G. G., Structure in confined room-temperature ionic liquids. *Journal of Physical Chemistry C* **2007,** *111* (13), 5162-5168.

108. Perkin, S.; Albrecht, T.; Klein, J., Layering and shear properties of an ionic liquid, 1-ethyl-3-methylimidazolium ethylsulfate, confined to nano-films between mica surfaces. *Physical Chemistry Chemical Physics* **2010,** *12* (6), 1243-1247.

109. Wakeham, D.; Hayes, R.; Warr, G. G.; Atkin, R., Influence of Temperature and Molecular Structure on Ionic Liquid Solvation Layers. *Journal of Physical Chemistry B* **2009,** *113* (17), 5961-5966.

110. Atkin, R.; El Abedin, S. Z.; Hayes, R.; Gasparotto, L. H. S.; Borisenko, N.; Endres, F., AFM and STM Studies on the Surface Interaction of [BMP]TFSA and [EMIm]TFSA Ionic Liquids with Au(111). *Journal of Physical Chemistry C* **2009,** *113* (30), 13266-13272.

111. Hayes, R.; Borisenko, N.; Tam, M. K.; Howlett, P. C.; Endres, F.; Atkin, R., Double Layer Structure of Ionic Liquids at the Au(111) Electrode Interface: An Atomic Force Microscopy Investigation. *Journal of Physical Chemistry C* **2011,** *115* (14), 6855-6863.

112. Hayes, R.; El Abedin, S. Z.; Atkin, R., Pronounced Structure in Confined Aprotic Room-Temperature Ionic Liquids. *Journal of Physical Chemistry B* **2009,** *113* (20), 7049-7052.

113. Horn, R. G.; Evans, D. F.; Ninham, B. W., Double-layer and solvation forces measured in a molten-salt and its mixtures with water. *Journal of Physical Chemistry* **1988,** *92* (12), 3531-3537.

114. Reed, S. K.; Lanning, O. J.; Madden, P. A., Electrochemical interface between an ionic liquid and a model metallic electrode. *The Journal of Chemical Physics* **2007,** *126* (8), -.

115. Kornyshev, A. A., Double-layer in ionic liquids: Paradigm change? *Journal of Physical Chemistry B* **2007,** *111* (20), 5545-5557.

116. Bazant, M. Z.; Storey, B. D.; Kornyshev, A. A., Double Layer in Ionic Liquids: Overscreening versus Crowding. *Physical Review Letters* **2011,** *106* (4), 046102.

117. Lynden-Bell, R. M.; Frolov, A. I.; Fedorov, M. V., Electrode screening by ionic liquids. *Physical Chemistry Chemical Physics* **2012,** *14* (8), 2693-2701.

118. Fedorov, M. V.; Kornyshev, A. A., Ionic Liquids at Electrified Interfaces. *Chemical Reviews* **2014,** *114* (5), 2978-3036.

119. Ivaništšev, V.; Fedorov, M. V., Interfaces between charged surfaces and ionic liquids: Insights from molecular simulations. *Electrochemical Society Interface* **2013,** *23* (1), 65-69.

120. Ueno, K.; Kasuya, M.; Watanabe, M.; Mizukami, M.; Kurihara, K., Resonance shear measurement of nanoconfined ionic liquids. *Physical Chemistry Chemical Physics* **2010,** *12* (16), 4066-4071.

121. Bou-Malham, I.; Bureau, L., Nanoconfined ionic liquids: effect of surface charges on flow and molecular layering. *Soft Matter* **2010,** *6* (17), 4062-4065.

122. Hayes, R.; Warr, G. G.; Atkin, R., At the interface: solvation and designing ionic liquids. *Physical Chemistry Chemical Physics* **2010,** *12* (8), 1709-1723.

123. Horn, R. G.; Clarke, D. R.; Clarkson, M. T., Direct Measurement of Surface Forces Between Sapphire Crystals in Aqueous-Solutions. *Journal of Materials Research* **1988,** *3* (3), 413-416.

124. Horn, R. G.; Smith, D. T.; Haller, W., Surface Forces and Viscosity of water Measured Between Silica Sheets. *Chemical Physics Letters* **1989,** *162* (4-5), 404-408.

125. Chai, L.; Klein, J., Large Area, Molecularly Smooth (0.2 nm rms) Gold Films for Surface Forces and Other Studies. *Langmuir* **2007,** *23* (14), 7777-7783.

126. Britton, J.; Cousens, N. E. A.; Coles, S. W.; van Engers, C. D.; Babenko, V.; Murdock, A. T.; Koós, A.; Perkin, S.; Grobert, N., A Graphene Surface Force Balance. *Langmuir* **2014,** *30* (38), 11485-11492.

127. Horn, R. G.; Bachmann, D. J.; Connor, J. N.; Miklavcic, S. J., The effect of surface and hydrodynamic forces on the shape of a fluid drop approaching a solid surface. *Journal of Physics-Condensed Matter* **1996,** *8* (47), 9483-9490.

128. Israelachvili, J. N.; Alcantar, N. A.; Maeda, N.; Mates, T. E.; Ruths, M., Preparing contamination-free mica substrates for surface characterization, force measurements, and imaging. *Langmuir* **2004,** *20* (9), 3616-3622.

129. Lin, Z. Q.; Granick, S., Platinum nanoparticles at mica surfaces. *Langmuir* **2003,** *19* (17), 7061-7070.

130. Ohnishi, S.; Hato, M.; Tamada, K.; Christenson, H. K., Presence of particles on melt-cut mica sheets. *Langmuir* **1999,** *15* (9), 3312-3316.

131. Pincet, F.; Perez, E.; Wolfe, J., Does glue contaminate the surface forces apparatus. *Langmuir* **1995,** *11* (1), 373-374.

132. Froberg, J. C.; Ederth, T., On the possibility of glue contaminations in the surface force apparatus. *Journal of Colloid and Interface Science* **1999,** *210* (1), 215-217.

133. Williams, D. B. G.; Lawton, M., Drying of Organic Solvents: Quantitative Evaluation of the Efficiency of Several Desiccants. *The Journal of Organic Chemistry* **2010,** *75* (24), 8351-8354.

134. Ab Rani, M. A.; Brant, A.; Crowhurst, L.; Dolan, A.; Lui, M.; Hassan, N. H.; Hallett, J. P.; Hunt, P. A.; Niedermeyer, H.; Perez-Arlandis, J. M.; Schrems, M.; Welton, T.; Wilding, R., Understanding the polarity of ionic liquids. *Physical Chemistry Chemical Physics* **2011,** *13* (37), 16831-16840.

135. Men, S.; Lovelock, K. R. J.; Licence, P., X-ray photoelectron spectroscopy of pyrrolidinium-based ionic liquids: cation-anion interactions and a comparison to imidazolium-based analogues. *Physical Chemistry Chemical Physics* **2011,** *13* (33), 15244-15255.

136. Israelachvili, J., Thin-film studies using multiple-beam interferometry. *Journal of Colloid and Interface Science* **1973,** *44* (2), 259-272.

137. Israelachvili, J., Solvation Forces and liquid Structure, as Probed by Direct Force Measurements. *Accounts of Chemical Research* **1987,** *20* (11), 415-421.

138. Yoshizawa, H.; McGuiggan, P.; Israelachvili, J., Identification of a Second Dynamic State During Stick-Slip Motion. *Science* **1993,** *259* (5099), 1305-1308.

139. Israelachvili, J. N.; McGuiggan, P. M.; Homola, A. M., Dynamic Properties of Molecularly Thin Liquid Films. *Science* **1988,** *240* (4849), 189-191.

140. Israelachvili, J. N.; Chen, Y. L.; Yoshizawa, H., Relationship Between Adhesion and Friction Forces. *Journal of Adhesion Science and Technology* **1994,** *8* (11), 1231-1249.

141. Qian, L. M.; Luengo, G.; Perez, E., Thermally activated lubrication with alkanes: The effect of chain length. *Europhysics Letters* **2003,** *61* (2), 268-274.

142. Qian, L.; Luengo, G.; Douillet, D.; Charlot, M.; Dollat, X.; Perez, E., New two-dimensional friction force apparatus design for measuring shear forces at the nanometer scale. *Review of Scientific Instruments* **2001,** *72* (11), 4171-4177.

143. Bureau, L., Rate Effects on Layering of a Confined Linear Alkane. *Physical Review Letters* **2007,** *99* (22), 225503.

144. Charrault, E.; Banquy, X.; Kristiansen, K.; Israelachvili, J.; Giasson, S., Investigation on the Molecular Shear-Induced Organization in a Molecularly Thin Film of N-hexadecane. *Tribology Letters* **2013,** *50* (3), 421-430.

145. Jabbarzadeh, A.; Harrowell, P.; Tanner, R. I., Very Low Friction State of a Dodecane Film Confined between Mica Surfaces. *Physical Review Letters* **2005,** *94* (12), 126103.

146. Jabbarzadeh, A.; Harrowell, P.; Tanner, R. I., The structural origin of the complex rheology in thin dodecane films: Three routes to low friction. *Tribology International* **2007,** *40* (10–12), 1574-1586.

147. Gee, M. L.; Israelachvili, J. N., Interactions of surfactant monolayers across hydrocarbon liquids. *Journal of the Chemical Society, Faraday Transactions* **1990,** *86* (24), 4049-4058.

148. Chen, Y. L.; Helm, C. A.; Israelachvili, J. N., Measurements of the elastic properties of surfactant and lipid monolayers. *Langmuir* **1991,** *7* (11), 2694-2699.

149. Israelachvili, J. N.; Kott, S. J.; Gee, M. L.; Witten, T. A., Forces between mica surfaces across hydrocarbon liquids: effects of branching and polydispersity. *Macromolecules* **1989,** *22* (11), 4247-4253.

150. P.J. Dowding, personal communication.

151. Lundgren, S. M.; Persson, K.; Mueller, G.; Kronberg, B.; Clarke, J.; Chtaib, M.; Claesson, P. M., Unsaturated Fatty Acids in Alkane Solution: Adsorption to Steel Surfaces. *Langmuir* **2007,** *23* (21), 10598-10602.

152. Parker, J. L.; Christenson, H. K., Measurements of the forces between a metal-surface and mica across liquids. *Journal of Chemical Physics* **1988,** *88* (12), 8013-8014.

153. Simon, P.; Gogotsi, Y., Materials for electrochemical capacitors. *Nature Materials* **2008,** *7* (11), 845-854.

154. Merlet, C.; Rotenberg, B.; Madden, P. A.; Salanne, M., Computer simulations of ionic liquids at electrochemical interfaces. *Physical Chemistry Chemical Physics* **2013,** *15* (38), 15781-15792.

155. Chmiola, J.; Yushin, G.; Gogotsi, Y.; Portet, C.; Simon, P.; Taberna, P. L., Anomalous increase in carbon capacitance at pore sizes less than 1 nanometer. *Science* **2006,** *313* (5794), 1760-1763.

156. Merlet, C.; Rotenberg, B.; Madden, P. A.; Taberna, P.-L.; Simon, P.; Gogotsi, Y.; Salanne, M., On the molecular origin of supercapacitance in nanoporous carbon electrodes. *Nature Materials* **2012,** *11* (4), 306-310.

157. Jiang, D.-e.; Wu, J., Microscopic Insights into the Electrochemical Behavior of Nonaqueous Electrolytes in Electric Double-Layer Capacitors. *The Journal of Physical Chemistry Letters* **2013,** *4* (8), 1260-1267.

158. Feng, G.; Li, S.; Presser, V.; Cummings, P. T., Molecular Insights into Carbon Supercapacitors Based on Room-Temperature Ionic Liquids. *The Journal of Physical Chemistry Letters* **2013,** *4* (19), 3367-3376.

159. Chmiola, J.; Largeot, C.; Taberna, P.-L.; Simon, P.; Gogotsi, Y., Desolvation of Ions in Subnanometer Pores and Its Effect on Capacitance and Double-Layer Theory. *Angewandte Chemie International Edition* **2008,** *47* (18), 3392-3395.

160. Perkin, S., Ionic liquids in confined geometries. *Physical Chemistry Chemical Physics* **2012,** *14* (15), 5052-5062.

161. Zhang, X.; Zhong, Y.-X.; Yan, J.-W.; Su, Y.-Z.; Zhang, M.; Mao, B.-W., Probing double layer structures of Au (111)-BMIPF6 ionic liquid interfaces from potential-dependent AFM force curves. *Chemical Communications* **2012,** *48* (4), 582-584.

162. Black, J. M.; Walters, D.; Labuda, A.; Feng, G.; Hillesheim, P. C.; Dai, S.; Cummings, P. T.; Kalinin, S. V.; Proksch, R.; Balke, N., Bias-Dependent Molecular-Level Structure of Electrical Double Layer in Ionic Liquid on Graphite. *Nano Letters* **2013,** *13* (12), 5954-5960.

163. Hoth, J.; Hausen, F.; Mueser, M. H.; Bennewitz, R., Force microscopy of layering and friction in an ionic liquid. *Journal of Physics-Condensed Matter* **2014,** *26* (28).

164. Seddon, J. R. T., Conservative and Dissipative Interactions of Ionic Liquids in Nanoconfinement. *The Journal of Physical Chemistry C* **2014**.

165. Espinosa-Marzal, R. M.; Arcifa, A.; Rossi, A.; Spencer, N. D., Microslips to "Avalanches" in Confined, Molecular Layers of Ionic Liquids. *The Journal of Physical Chemistry Letters* **2013,** *5* (1), 179-184.

166. Gebbie, M. A.; Valtiner, M.; Banquy, X.; Fox, E. T.; Henderson, W. A.; Israelachvili, J. N., Ionic liquids behave as dilute electrolyte solutions. *Proceedings of the National Academy of Sciences of the United States of America* **2013,** *110* (24), 9674-9679.

167. Perkin, S.; Salanne, M.; Madden, P.; Lynden-Bell, R., Is a Stern and diffuse layer model appropriate to ionic liquids at surfaces? *Proceedings of the National Academy of Sciences of the United States of America* **2013,** *110* (44), E4121-E4121.

168. Yochelis, A., Transition from non-monotonic to monotonic electrical diffuse layers: impact of confinement on ionic liquids. *Physical Chemistry Chemical Physics* **2014,** *16* (7), 2836-2841.

169. Yochelis, A., Spatial Structure of Electrical Diffuse Layers in Highly Concentrated Electrolytes: A Modified Poisson–Nernst–Planck Approach. *The Journal of Physical Chemistry C* **2014,** *118* (11), 5716-5724.

170. Lee, A. A.; Vella, D.; Perkin, S.; Goriely, A., Are Room-Temperature Ionic Liquids Dilute Electrolytes? *The Journal of Physical Chemistry Letters* **2014,** *6* (1), 159-163.

171. Forsyth, S. A.; Batten, S. R.; Dai, Q.; MacFarlane, D. R., Ionic liquids based on imidazolium and pyrrolidinium salts of the tricyanomethanide anion. *Australian Journal of Chemistry* **2004,** *57* (2), 121-124.

172. Ong, S. P.; Andreussi, O.; Wu, Y. B.; Marzari, N.; Ceder, G., Electrochemical Windows of Room-Temperature Ionic Liquids from Molecular Dynamics and Density Functional Theory Calculations. *Chemistry of Materials* **2011,** *23* (11), 2979-2986.

173. Wibowo, R.; Jones, S. E. W.; Compton, R. G., Investigating the Electrode Kinetics of the Li/Li+ Couple in a Wide Range of Room Temperature Ionic Liquids at 298 K. *Journal of Chemical and Engineering Data* **2010,** *55* (3), 1374-1376.

174. Perkin, S.; Crowhurst, L.; Niedermeyer, H.; Welton, T.; Smith, A. M.; Gosvami, N. N., Self-assembly in the electrical double layer of ionic liquids. *Chemical Communications* **2011,** *47* (23), 6572-6574.

175. Zhou, H.; Rouha, M.; Feng, G.; Lee, S. S.; Docherty, H.; Fenter, P.; Cummings, P. T.; Fulvio, P. F.; Dai, S.; McDonough, J.; Presser, V.; Gogotsi, Y., Nanoscale Perturbations of Room Temperature Ionic Liquid Structure at Charged and Uncharged Interfaces. *ACS Nano* **2012**.

176. Wang, Y. T.; Voth, G. A., Unique spatial heterogeneity in ionic liquids. *J. Am. Chem. Soc* **2005,** *127* (35), 12192-12193.

177. Canongia Lopes, J. N. A.; Pádua, A. A. H., Nanostructural organization in ionic liquids. *Journal of Physical Chemistry B* **2006,** *110* (7), 3330-3335.

178. Triolo, A.; Russina, O.; Bleif, H.-J.; Di Cola, E., Nanoscale segregation in room temperature ionic liquids. *Journal of Physical Chemistry B* **2007,** *111* (18), 4641-4644.

179. Santos, C. S.; Murthy, N. S.; Baker, G. A.; Castner, E. W., Communication: X-ray scattering from ionic liquids with pyrrolidinium cations. *Journal of Chemical Physics* **2011,** *134* (12), 121101.

180. Horn, R.; Israelachvili, J., Direct measurements of structural forces between two surfaces in a nonpolar liquid. *Journal of Chemical Physics* **1981,** *75* (3), 1400-1411.

181. Christenson, H. K., Experimental Measurements of Solvation Forces in Non-Polar Liquids. *Journal of Chemical Physics* **1983,** *78* (11), 6906-6913.

182. Wibowo, R.; Aldous, L.; Jones, S. E. W.; Compton, R. G., The electrode potentials of the Group I alkali metals in the ionic liquid N-butyl-N-methylpyrrolidinium bis(trifluoromethylsulfonyl)imide. *Chemical Physics Letters* **2010,** *492* (4-6), 276-280.

183. Cipriano, B. H.; Raghavan, S. R.; McGuiggan, P. M., Surface tension and contact angle measurements of a hexadecyl imidazolium surfactant adsorbed on a clay surface. *Colloids and Surfaces A: Physicochemical and Engineering Aspects* **2005,** *262* (1-3), 8-13.

184. Fedorov, M. V.; Kornyshev, A. A., Ionic liquid near a charged wall: structure and capacitance of electrical double layer. *The Journal of Physical Chemistry B* **2008,** *112* (38), 11868-11872.

185. Matthews, R. P.; Welton, T.; Hunt, P. A., Competitive pi interactions and hydrogen bonding within imidazolium ionic liquids. *Physical Chemistry Chemical Physics* **2014,** *16* (7), 3238-3253.

186. Matthews, R., P.; Ashworth, C.; Welton, T.; Patricia, A., The impact of anion electronic structure: similarities and differences in imidazolium based ionic liquids. *Journal of Physics: Condensed Matter* **2014,** *26* (28), 284112.

187. Payal, R. S.; Balasubramanian, S., Orientational Ordering of Ionic Liquids near a Charged Mica Surface. *Chemphyschem* **2012,** *13* (7), 1764-1771.

188. Rollins, J. B.; Fitchett, B. D.; Conboy, J. C., Structure and orientation of the imidazolium cation at the room-temperature ionic liquid/SiO2 interface measured by sum-frequency vibrational spectroscopy. *Journal of Physical Chemistry B* **2007,** *111* (18), 4990-4999.

189. Santos, C. S.; Murthy, N. S.; Baker, G. A.; Castner, E. W., Communication: X-ray scattering from ionic liquids with pyrrolidinium cations. *Journal of Chemical Physics* **2011,** *134* (12), 4.

190. Triolo, A.; Russina, O.; Fazio, B.; Appetecchi, G. B.; Carewska, M.; Passerini, S., Nanoscale organization in piperidinium-based room temperature ionic liquids. *The Journal of Chemical Physics* **2009,** *130* (16), 164521-6.

191. Niedermeyer, H.; Hallett, J. P.; Villar-Garcia, I. J.; Hunt, P. A.; Welton, T., Mixtures of ionic liquids. *Chemical Society Reviews* **2012,** *41* (23), 7780-7802.

192. Fox, E. T.; Weaver, J. E. F.; Henderson, W. A., Tuning Binary Ionic Liquid Mixtures: Linking Alkyl Chain Length to Phase Behavior and Ionic Conductivity. *Journal of Physical Chemistry C* **2012,** *116* (8), 5271-5275.

193. Lewandowski, A.; Świderska-Mocek, A., Ionic liquids as electrolytes for Li-ion batteries—An overview of electrochemical studies. *Journal of Power Sources* **2009,** *194* (2), 601-609.

194. Chaban, V. V.; Prezhdo, O. V., Ionic and Molecular Liquids: Working Together for Robust Engineering. *The Journal of Physical Chemistry Letters* **2013,** *4* (9), 1423-1431.

195. Chaban, V. V.; Voroshyloya, I. V.; Kalugin, O. N.; Prezhdo, O. V., Acetonitrile Boosts Conductivity of Imidazolium Ionic Liquids. *Journal of Physical Chemistry B* **2012,** *116* (26), 7719-7727.

196. Borodin, O.; Henderson, W. A.; Fox, E. T.; Berman, M.; Gobet, M.; Greenbaum, S., Influence of Solvent on Ion Aggregation and Transport in PY15TFSI Ionic Liquid–Aprotic Solvent Mixtures. *The Journal of Physical Chemistry B* **2013,** *117* (36), 10581-10588.

197. Maier, F.; Cremer, T.; Kolbeck, C.; Lovelock, K. R. J.; Paape, N.; Schulz, P. S.; Wasserscheid, P.; Steinruck, H. P., Insights into the surface composition and enrichment effects of ionic liquids and ionic liquid mixtures. *Physical Chemistry Chemical Physics* **2010,** *12* (8), 1905-1915.

198. Fong, R.; von Sacken, U.; Dahn, J. R., Studies of Lithium Intercalation into Carbons Using Nonaqueous Electrochemical Cells. *Journal of the Electrochemical Society* **1990,** *137* (7), 2009-2013.

199. Mendez-Morales, T.; Carrete, J.; Perez-Rodriguez, M.; Cabeza, O.; Gallego, L. J.; Lynden-Bell, R. M.; Varela, L. M., Molecular dynamics simulations of the structure of the graphene-ionic liquid/alkali salt mixtures interface. *Physical Chemistry Chemical Physics* **2014,** *16* (26), 13271-13278.

200. Lassegues, J.-C.; Grondin, J.; Talaga, D., Lithium solvation in bis(trifluoromethanesulfonyl)imide-based ionic liquids. *Physical Chemistry Chemical Physics* **2006,** *8* (48), 5629-5632.

201. Monteiro, M. J.; Bazito, F. F. C.; Siqueira, L. J. A.; Ribeiro, M. C. C.; Torresi, R. M., Transport Coefficients, Raman Spectroscopy, and Computer Simulation of Lithium Salt Solutions in an Ionic Liquid. *The Journal of Physical Chemistry B* **2008,** *112* (7), 2102-2109.

202. Yamagata, M.; Nishigaki, N.; Nishishita, S.; Matsui, Y.; Sugimoto, T.; Kikuta, M.; Higashizaki, T.; Kono, M.; Ishikawa, M., Charge–discharge behavior of graphite negative electrodes in bis(fluorosulfonyl)imide-based ionic liquid and structural aspects of their electrode/electrolyte interfaces. *Electrochimica Acta* **2013,** *110* (0), 181-190.

203. Huang, J.; Sumpter, B. G.; Meunier, V., A Universal Model for Nanoporous Carbon Supercapacitors Applicable to Diverse Pore Regimes, Carbon Materials, and Electrolytes. *Chemistry – A European Journal* **2008,** *14* (22), 6614-6626.

204. Shim, Y.; Kim, H. J., Nanoporous Carbon Supercapacitors in an Ionic Liquid: A Computer Simulation Study. *ACS Nano* **2010,** *4* (4), 2345-2355.

205. Merlet, C.; Péan, C.; Rotenberg, B.; Madden, P. A.; Daffos, B.; Taberna, P. L.; Simon, P.; Salanne, M., Highly confined ions store charge more efficiently in supercapacitors. *Nat Commun* **2013,** *4*.

206. Ohba, T.; Kaneko, K., Competition of Desolvation and Stabilization of Organic Electrolytes in Extremely Narrow Nanopores. *The Journal of Physical Chemistry C* **2013,** *117* (33), 17092-17098.

207. Richey, F. W.; Dyatkin, B.; Gogotsi, Y.; Elabd, Y. A., Ion Dynamics in Porous Carbon Electrodes in Supercapacitors Using in Situ Infrared Spectroelectrochemistry. *Journal of the American Chemical Society* **2013,** *135* (34), 12818-12826.

208. Wang, H.; Forse, A. C.; Griffin, J. M.; Trease, N. M.; Trognko, L.; Taberna, P.-L.; Simon, P.; Grey, C. P., In Situ NMR Spectroscopy of Supercapacitors: Insight into the Charge Storage Mechanism. *Journal of the American Chemical Society* **2013,** *135* (50), 18968-18980.

209. Griffin, J. M.; Forse, A. C.; Wang, H.; Trease, N. M.; Taberna, P.-L.; Simon, P.; Grey, C. P., Ion Counting in Supercapacitor Electrodes using NMR Spectroscopy. *Faraday Discussions* **2014**.

210. Tsai, W.-Y.; Taberna, P.-L.; Simon, P., Electrochemical Quartz Crystal Microbalance (EQCM) Study of Ion Dynamics in Nanoporous Carbons. *Journal of the American Chemical Society* **2014,** *136* (24), 8722-8728.

211. Fedorov, M. V.; Kornyshev, A. A., Ionic liquid near a charged wall: Structure and capacitance of electrical double layer. *Journal of Physical Chemistry B* **2008,** *112* (38), 11868-11872.

212. Lee, A. A.; Vella, D.; Perkin, S.; Goriely, A., Unravelling nanoconfined films of ionic liquids. *The Journal of Chemical Physics* **2014,** *141* (9), -.

213. Kirchner, K.; Kirchner, T.; Ivaništšev, V.; Fedorov, M. V., Electrical double layer in ionic liquids: Structural transitions from multilayer to monolayer structure at the interface. *Electrochimica Acta* **2013,** *110* (0), 762-771.

214. Ivaništšev, V.; O'Connor, S.; Fedorov, M. V., Poly(a)morphic portrait of the electrical double layer in ionic liquids. *Electrochemistry Communications* **2014,** *48* (0), 61-64.

215. Jiang, D.-e.; Wu, J., Unusual effects of solvent polarity on capacitance for organic electrolytes in a nanoporous electrode. *Nanoscale* **2014,** *6* (10), 5545-5550.

216. Sweeney, J.; Hausen, F.; Hayes, R.; Webber, G. B.; Endres, F.; Rutland, M. W.; Bennewitz, R.; Atkin, R., Control of Nanoscale Friction on Gold in an Ionic Liquid by a Potential-Dependent Ionic Lubricant Layer. *Physical Review Letters* **2012,** *109* (15), 155502.

217. Werzer, O.; Cranston, E. D.; Warr, G. G.; Atkin, R.; Rutland, M. W., Ionic liquid nanotribology: mica-silica interactions in ethylammonium nitrate. *Physical Chemistry Chemical Physics* **2012**.

218. Elbourne, A.; Sweeney, J.; Webber, G. B.; Wanless, E. J.; Warr, G. G.; Rutland, M. W.; Atkin, R., Adsorbed and near-surface structure of ionic liquids determines nanoscale friction. *Chemical Communications* **2013**.

219. Israelachvili, J.; Chen, Y. L.; Yoshizawa, H., Relationship between adhesion and friction forces. *Journal of Adhesion Science and Technology* **1994,** *8* (11), 1231-1249.

220. Kumacheva, E.; Klein, J., Simple liquids confined to molecularly thin layers. II. Shear and frictional behaviour of solidified films. *Journal of Chemical Physics* **1998,** *108* (16), 7010-7022.

221. Thompson, P. A.; Robbins, M. O., Origin of stick-slip motion in boundary lubrication. *Science* **1990,** *250*, 792-794.

222. Schoen, M.; Rhykerd, C. L.; Diestler, D. J.; Cushman, J. H., Shear Forces in Molecularly Thin Films. *Science* **1989,** *245* (4923), 1223-1225.

223. Lei, Y.; Leng, Y., Stick-Slip Friction and Energy Dissipation in Boundary Lubrication. *Physical Review Letters* **2011,** *107* (14), 147801.

224. Espinosa-Marzal, R. M.; Arcifa, A.; Rossi, A.; Spencer, N. D., Ionic Liquids Confined in Hydrophilic Nanocontacts: Structure and Lubricity in the Presence of Water. *The Journal of Physical Chemistry C* **2014,** *118* (12), 6491-6503.

225. Raviv, U.; Klein, J., Fluidity of bound hydration layers. *Science* **2002,** *297*, 1540-1543.

226. Briscoe, W. H.; Titmuss, S.; Tiberg, F.; Thomas, R. K.; McGillivray, D.; Klein, J., Boundary lubrication under water. *Nature* **2006,** *444* (7116), 191.

227. Wood, M. H.; Welbourn, R. J. L.; Charlton, T.; Zarbakhsh, A.; Casford, M. T.; Clarke, S. M., Hexadecylamine Adsorption at the Iron Oxide–Oil Interface. *Langmuir* **2013,** *29* (45), 13735-13742.

228. Doig, M.; Camp, P. J., The structures of hexadecylamine films adsorbed on iron-oxide surfaces in dodecane and hexadecane. *Physical Chemistry Chemical Physics* **2015**.

229. Thompson, P. A.; Robbins, M. O., Origin of stick-slip motion in boundary lubrication. *Science* **1990,** *250* (4982), 792-794.

230. Merlet, C.; Limmer, D. T.; Salanne, M.; van Roij, R.; Madden, P. A.; Chandler, D.; Rotenberg, B., The Electric Double Layer Has a Life of Its Own. *The Journal of Physical Chemistry C* **2014,** *118* (32), 18291-18298.

231. Kornyshev, A. A.; Qiao, R., Three-Dimensional Double Layers. *The Journal of Physical Chemistry C* **2014,** *118* (32), 18285-18290.

232. Docherty, H.; Cummings, P. T., Direct evidence for fluid-solid transition of nanoconfined fluids. *Soft Matter* **2010,** *6* (8), 1640-1643.

233. Fajardo, O. Y.; Bresme, F.; Kornyshev, A. A.; Urbakh, M., Electrotunable Lubricity with Ionic Liquid Nanoscale Films. *Sci. Rep.* **2015,** *5*.

234. Péan, C.; Merlet, C.; Rotenberg, B.; Madden, P. A.; Taberna, P.-L.; Daffos, B.; Salanne, M.; Simon, P., On the Dynamics of Charging in Nanoporous Carbon-Based Supercapacitors. *ACS Nano* **2014,** *8* (2), 1576-1583.

235. Kondrat, S.; Wu, P.; Qiao, R.; Kornyshev, A. A., Accelerating charging dynamics in subnanometre pores. *Nature Materials* **2014,** *13* (4), 387-393.

236. Du, Q.; Xiao, X. d.; Charych, D.; Wolf, F.; Frantz, P.; Shen, Y. R.; Salmeron, M., Nonlinear optical studies of monomolecular films under pressure. *Physical Review B* **1995,** *51* (12), 7456-7463.

237. Koltover, I.; Idziak, S. H. J.; Davidson, P.; Li, Y.; Safinya, C. R.; Ruths, M.; Steinberg, S.; Israelachvili, J. N., Alignment of Complex Fluids under Confinement and Flow. *J. Phys. II France* **1996,** *6* (6), 893-907.

238. Mukhopadhyay, A.; Zhao, J.; Bae, S. C.; Granick, S., Contrasting Friction and Diffusion in Molecularly Thin Confined Films. *Physical Review Letters* **2002,** *89* (13), 136103.